Cross-layer Design for Multi-hop Two-way Relay Network

by

Haoyuan Zhang
B. Eng., Harbin Institute of Technology, China, 2010
M. Eng., Harbin Institute of Technology, China, 2012

A Dissertation Submitted in Partial Fulfillment of the
Requirements for the Degree of

DOCTOR OF PHILOSOPHY

in the Department of Electrical and Computer Engineering

Cross-layer Design for Multi-hop Two-way Relay Network

by

Haoyuan Zhang
B. Eng., Harbin Institute of Technology, China, 2010
M. Eng., Harbin Institute of Technology, China, 2012

Supervisory Committee

Dr. Lin Cai, Supervisor
(Department of Electrical and Computer Engineering)

Dr. T. Aaron Gulliver, Departmental Member
(Department of Electrical and Computer Engineering)

Dr. Hongchuan Yang, Departmental Member
(Department of Electrical and Computer Engineering)

Dr. Sudhakar Ganti, Outside Member
(Department of Computer Science)

Abstract

Physical layer network coding (PNC) was proposed under the two-way relay channel (TWRC) scenario, where two sources exchange information aided by a relay. PNC allows the two sources to transmit to the relay simultaneously, where superimposed signals at the relay can be mapped to network-coded symbols and then be broadcast to both sources instead of being treated as interference. Concurrent transmissions using PNC achieve a higher spectrum efficiency compared to time division and network coding solutions. Existing research mainly focused on the symmetric PNC designs, where the same channel coding and modulation configurations are applied by both sources. When the channel conditions of the two source-relay links are asymmetric or unequal amount of data are exchanged, heterogeneous modulation PNC designs are necessary. In additional, the design and optimization of multi-hop PNC, where multiple relays forming a multi-hop path between the two sources, remains an open issue. The above issues motivate the study of this dissertation.

This dissertation investigates the design of heterogeneous modulation physical layer network coding (HePNC), the integration of channel error control coding into HePNC, the combination of HePNC with hierarchical modulation, and the design and generalization of multi-hop PNC. The contributions of this dissertation are four-fold.

First, under the asymmetric TWRC scenario, where the channel conditions of the two source-relay links are asymmetric, we designed a HePNC protocol, including the optimization of the adaptive mapping functions and the bit-symbol labeling, to minimize the end-to-end BER. In addition, we developed an analytical framework to derive the BER of HePNC. HePNC can substantially enhance the throughput compared to the existing symmetric PNC under the asymmetric TWRC scenario.

Second, we investigated channel coded HePNC and integrated the channel error control coding into HePNC in a link-to-link coding, where the relay tries to decode the superimposed codewords in the multi-access stage. A full-state sum-product decoding algorithm is proposed at the relay based on the repeat-accumulate codes to guarantee reliable end-to-end communication.

Third, we proposed hierarchical modulation PNC (H-PNC) under asymmetric TWRC, where additional data exchange between the relay and the source with the relatively better channel condition is achieved in addition to that between the two end sources, benefiting from superimposing the additional data flow on the PNC transmission. When the relay also has the data exchange requirement with the source

with a better source-relay channel, H-PNC outperforms HePNC and PNC in terms of the system sum throughput.

Fourth, we designed and generalized multi-hop PNC, where multiple relays located in a linear topology are scheduled to support the data exchange between two end sources. The impact of error propagation and mutual interference among the nodes are addressed and optimized. The proposed designs outperform the existing ones in terms of end-to-end BER and end-to-end throughout.

Contents

List of Tables

List of Figures

Acknowledgments

I would like to express my special appreciation and thanks to my supervisor Dr. Cai, who has been a mentor for both of my research and my life. You have taught me how to well schedule multi-task and improve the ability to deal with pressure, which I believe are so important not only in research but also in society. I cannot imagine whether I can have an intensive study on my research if without your enlighten. I would also like to thank my committee member, Dr. Gulliver, who has read my dissertation carefully and patiently, and raised many inspiring questions. I would also like to thank Dr. Yang, Dr. Ganti and Dr. Jun Cai for serving as my committee members.

I would especially like to thank my wife, who has stayed in Victoria for more than three years during most of my Ph.D study. You have helped me to overcome the loneless in a foreign country. I cannot forget how many nights you have accompanied me in our lab without any regrets. A special thanks to my parents for all of the sacrifices that you have made on my behalf.

Last but not least, I would like to thank all my friends in Victoria. We have shared happiness and sadness during the past four years. Thanks Dr. Cai and Dr. Zhang to help to proofread my dissertation.

Haoyuan Zhang, Victoria, BC, Canada

Dedication

To My Dear Family, Mentors, and Motherland.

Chapter 1

Introduction

1.1 Background

The two-relay relay channel (TWRC) is a fundamental network structure of much interest to the wireless communications research community. Physical layer network coding (PNC) was proposed in 2006 by Zhang *et al.* [1] and Popovski *et al.* [2], independently, and was mainly researched in the TWRC scenarios, where two sources exchange information with the help of a relay node as the sources are out of each other's transmission range. In the wireless communication network, when a receiver receives multiple signals from multiple transmitters, signals from other transmitters except that from the respective transmitter are typically considered as negative interference. In TWRC, PNC allows concurrent signal transmissions from the sources to the relay. The 'interference' between the two sources' signals at the relay can be positively utilized, as the electromagnetic waves from the sources superimpose at the relay by nature in a form of network coding, and the sources can obtain each other's information by utilizing the network-coded information and the original information transmitted by themselves. Thus, PNC achieves a higher spectrum efficiency compared to time-division and digital network coding solutions, where the sources need to transmit to the relay sequentially. A comprehensive survey of PNC can be found in [3].

Generally speaking, the transmission procedure of PNC protocol includes two stages, multiple-access (MA) stage and broadcast (BC) stage. In the MA stage, PNC allows the sources to transmit their signals to the relay simultaneously. A network-coded symbol, which contains the necessary information of both sources' symbols,

is obtained from the superimposed signals at the relay instead of obtaining each of the symbols explicitly. In the BC stage, the network-coded symbol is broadcast back to the sources, and each source can obtain the target information from the other source by utilizing the knowledge of the network-coded symbol and the original symbol transmitted by itself. Depending on whether the range of the network-coded symbol is in a finite or an infinite set, PNC can be classified into two categories, finite-set PNC and infinite-set PNC [3]. Examples of finite-set PNC are the denoise-and-forward schemes [1, 4, 5], where the relay demodulates or decodes at least part of the transmitted message. A variant is the compute-and-forward scheme [6], where the relay decodes the linear equations of the transmitted messages based on the nested lattice codes. Examples of the infinite-set PNC are analog network coding (ANC) [7–12], where the weighted sum is amplified and forwarded in an amplify-and-forward manner. A general comparison between the finite-set PNC and the infinite-set PNC is highly dependent on the uplink channel conditions in the MA stage. In [3], it showed that for non-channel-coded schemes, generally speaking, finite-set PNC outperforms infinite-set PNC when the uplinks are good, and infinite-set PNC outperforms finite-set PNC when the uplinks are bad. Because for the finite-set PNC, when the noise at the MA stage is large, to obtain the network-coded symbol is error-prone. However, for channel-coded schemes, finite-set PNC outperforms infinite-set PNC as the noise in the MA stage can be managed by the channel codes. In this dissertation, we study the finite-set PNC schemes in a denoise-and-forward manner, where the relay tries to remove the noise in the superimposed signals.

We present a BPSK-BPSK PNC example, where both sources use BPSK modulation and the relay operates in a denoise-and-forward manner. Consider that sources A and B need to exchange two binary data $S_a = 0$ and $S_b = 1$, respectively. In the MA stage, source A transmits the BPSK symbol $X_a = 1 - 2S_a = 1$ and source B transmits the BPSK symbol $X_b = 1 - 2S_b = -1$ to the relay simultaneously. At the relay, instead of obtaining the superimposed symbols X_a and X_b explicitly, it demodulates and obtains the network-coded symbol 1, i.e., the binary result of S_a XOR S_b, and then broadcasts the network-coded symbol back to the sources in the BC stage. Finally, source A can obtain source B's original data with the knowledge of the network-coded symbol and the original symbol transmitted by itself. Note that the sum throughput of the system is 1 bit per symbol duration without considering the transmission errors. If the traditional network-coded solution or the TDMA solution are applied, the sum throughput of system is $\frac{2}{3}$ bit per symbol duration and $\frac{1}{2}$ bit per symbol

duration, respectively. Thus, PNC achieves a substantial throughput gain.

One important issue in the PNC design is the synchronization issue [13–16], including the symbol alignment and the carrier frequency synchronization. Perfect symbol alignment denotes that the symbols from two sources arrive at the relay with symbol boundaries aligned exactly. Carrier frequency synchronization determines that whether a relative phase offset for the two superimposed signals are required. How to align the symbols from multiple transmitters at a common receiver is a fundamental issue for many communication systems [17]. In this dissertation, perfect symbol alignment is assumed. The carrier frequency synchronization is much harder to achieve in a practical system due to the frequency mismatch at the transmitter and the receiver oscillators and the existence of Doppler shift. Thus, carrier frequency synchronization is not assumed. In addition, each node is equipped with a single antenna and works in a half-duplex mode in this dissertation. Combining PNC with MIMO [18–32] and full-duplex [33–36] are possible but beyond the scope of this dissertation.

1.2 Research Objectives and Contributions

1.2.1 Design and analysis of heterogeneous modulation physical layer network coding

Most existing PNC designs are studied in the symmetric TWRC scenario, where the channel conditions of the two source-relay links are similar and the same channel coding and modulation can be applied by the sources. Although PNC can boost the system throughput substantially, using homogeneous modulation becomes inefficient in the asymmetric TWRC scenario where the two source-relay links have asymmetric channel conditions[1] or two source nodes have different amount of data to exchange. The heterogeneity in the asymmetric TWRC motivates us to develop heterogeneous PNC (HePNC) where the sources use heterogeneous modulation.

Similar to traditional PNC, the HePNC procedure has two stages: multiple-access (MA) stage and broadcast (BC) stage. In the MA stage, the relay receives the superimposed signals transmitted simultaneously from the sources, and then maps the received signals to a network-coded symbol by a mapping function. The optimization of the mapping functions is a critical issue in the PNC design. In the original design of

[1]It may not be easily to compensate by power control due to the maximum transmission power limit.

PNC in [1], XOR mapping was adopted. However, with different channel conditions of the two source-relay links, the amplitude attenuations and phase shifts of the two received signals from the sources are different at the relay, which directly affects the received constellation map, and further affects the demodulation success rate and the system performance. Thus, adapting the mapping function according to the channel conditions is necessary, which is known as adaptive mapping [37]. To ensure the sources can abstract the other's information from the network-coded symbol, a fundamental criterion for the mapping function design is that the Latin square constraint should be satisfied [37, 38]. A new challenge of HePNC is how to design and optimize the mapping function. In HePNC, adaptive mapping functions should be designed and optimized jointly considering the channel conditions, the Latin square constraint and the configurations of different modulation.

This dissertation proposes the HePNC design, which enhances the communication efficiency in scenarios with asymmetric source-relay channel conditions and unequal traffic loads from the sources. Several HePNC sample designs, including QPSK-BPSK, 8PSK-BPSK and 16QAM-BPSK HePNC are presented. The design and optimization of the mapping functions following the Latin square constraint are investigated. An analytical framework is developed to derive the error performance of QPSK-BPSK HePNC under AWGN channels, and the performance bound under Rayleigh fading channels.

1.2.2 Channel coded heterogeneous modulation physical layer network coding

How to integrate the channel error control coding into PNC to guarantee the communication reliability is an important issue. Depending on whether the relay decodes the codewords from the sources in the superimposed signals or not, channel coded PNC can take two approaches, end-to-end coding and link-to-link coding [3]. With end-to-end coding, the relay processes the superimposed signals at the symbol-level instead of decoding the superimposed codewords at the bit-level. Thus, end-to-end coding suffers from noise accumulation at the relay, which further affects the end-to-end bit error rate (BER) in the BC stage. Link-to-link coding [5, 39–49] outperforms end-to-end coding in terms of end-to-end BER as the relay tries to correct errors in the MA stage using channel codes.

Several schemes of heterogeneous modulation PNC in asymmetric TWRC were

proposed in [5,39–49], where two different modulation-order symbols from the sources can be applied and an unequal data exchange between the two sources can be supported. However, all of them operate on the symbol-level, which can only integrate with channel coding in an end-to-end coding. How to integrate the channel error control coding into HePNC in a link-to-link coding is an open issue.

This dissertation proposes and designs channel coded heterogeneous modulation physical layer network coding (CoHePNC), which integrates the channel error control coding into HePNC in a link-to-link coding. Based on repeat-accumulate (RA) codes applied to the sources, a full-state sum-product decoding algorithm is proposed at the relay with the bit-level adaptive mapping function design. The proposed decoding algorithm outperforms the existing decoding solutions in terms of relay error rate (RER) and end-to-end BER under the asymmetric TWRC scenario.

1.2.3 Hierarchical modulation physical layer network coding

Although heterogeneous modulation PNC try to maximize the system throughput under the asymmetric TWRC scenario, the system throughput is subject to the channel conditions of the bottleneck link [50–52]. In an asymmetric TWRC scenario, to guarantee a BER threshold, the relay may need to decrease the modulation order of the network-coded symbol from a higher-order one into several lower-order ones and broadcast them in multiple slots subject to the bottleneck link. Thus, the channel of the source-relay link with the better channel quality cannot be fully utilized. For example, consider QPSK-BPSK heterogeneous modulation PNC, where links between A-R and B-R support QPSK and BPSK, respectively, determined by the source-relay channel conditions given the BER threshold. The network-coded symbol obtained at the relay is a QPSK symbol subject to the Latin square constraint [38]. Heterogeneous modulation PNC designs benefit from the asymmetric data exchange between sources A and B, e.g., 2:1 for QPSK-BPSK heterogeneous modulation PNC. However, because the bottleneck link between source B and relay R can only support BPSK, the QPSK network-coded symbol needs two slots to be broadcast back to the sources. Thus, the system throughput is 1 bit/slot only.

Thus, it is worthy to develop new schemes that can fully utilize the channel of the source-relay link with the better channel condition. Also, the majority of the previous PNC research considered the designs that only bidirectional information exchange between the sources can be achieved, and the relay cannot be a source or

a destination [53]. In the scenarios that the relay also needs to exchange information with the source node, the traditional PNC solutions are far from optimal.

This dissertation proposes a new transmission solution, hierarchical modulation PNC (H-PNC), which achieves data exchange not only between the two sources nodes, but also between the relay and the source node with a relatively better channel condition by taking advantage of hierarchical modulation. H-PNC outperforms traditional heterogeneous modulation PNC and symmetric PNC solutions under the asymmetric TWRC scenario in terms of system throughput. Three H-PNC sample designs are presented, and the optimization criteria are investigated. The design of H-PNC jointly considers the optimization of bit-symbol labeling, hierarchical modulation constellation design and the H-PNC mapping constraint. In addition, the error performance of QPSK-BPSK H-PNC under both AWGN and Rayleigh fading channels are also provided.

1.2.4 Multi-hop physical layer network coding

PNC was originally proposed and further investigated considering a single relay scenario [3, 5, 13, 37, 54–56]. Inspired from the extension of network coding [57–61], researchers focused on extending traditional PNC under TWRC to more generalized network topologies such as scenarios with multiple sources and one relay [62, 63]. However, multi-hop PNC design where multiple relays help the information exchange between two end sources has not been well researched. The existing work [4, 64–66] either provided the designs with a specified number of relays or only achieved an end-to-end throughput upper bound lower than that of the traditional PNC with a single relay. An inspiring generalization of multi-hop PNC was proposed in [1]. However, an error propagation problem exists, which may result in excessive end-to-end estimation errors. Also, the impact of the mutual-interference from other transmit nodes was not well addressed in the existing multi-hop PNC designs [1, 4, 34, 64–66].

It is challenging to design and generalize multi-hop PNC. The first important issue is the error propagation effect. Different from the traditional PNC with a single relay, where the transmission period is two slots and different periods are independent, in the multi-hop PNC, one error at any of the relay may impact on the correctness of other nodes in the following several or even endless slots. The second issue is that the received information in previous slots can be positively applied by the sources and the relays [1] in the multi-hop PNC. However, the options to apply this information

at any node go to infinity with the increase of the transmission slots and improperly applying this information may result in serious error propagation problem. The third issue is that, different from the traditional PNC with a single relay, a receiver in multi-hop PNC may not only receive useful information from neighboring nodes, but also interfering signals from other transmit nodes. The impact of the mutual-interference cannot be neglected in multi-hop PNC and given the end-to-end SNR, the SINR of any two neighboring nodes are upper bounded determined by the hop-distance. The design and generalization of multi-hop PNC transmission protocol should jointly consider the impact of the error propagation and the mutual-interference in order to minimize the end-to-end BER and maximize the end-to-end throughput.

This dissertation investigates the key issues in multi-hop PNC design, including the impact of the error propagation and mutual interference, and provides guidelines of how to properly utilize the previously received information. By carefully addressing the key issues, this dissertation proposes two multi-hop PNC designs, including direct multi-hop PNC (D-MPNC) and stored multi-hop PNC (S-MPNC). D-MPNC benefits from the simple implementation as the relay operations are the same as that of the traditional PNC with a single relay. S-MPNC outperforms D-MPNC in terms of end-to-end BER by enabling the relays to properly utilize the previously received information. Both D-MPNC and S-MPNC can achieve a maximum throughput upper bound of 1 symbol per symbol duration. The theoretical analysis of the end-to-end BER bounds of D-MPNC and S-MPNC are provided, which approaches exact end-to-end BER when the per-hop error rate is sufficiently low. The impact of the relay locations in multi-hop PNC is further studied.

1.3 Dissertation Organization

The remainder of the dissertation is organized as follows.

In Chapter 2, we investigate the design of HePNC under asymmetric TWRC. The adaptive mapping functions for QPSK-BPSK, 8PSK-BPSK and 16QAM-BPSK HePNC are presented. The theoretical BER analysis of QPSK-BPSK HePNC is provided under both AWGN and Rayleigh fading channels.

In Chapter 3, we integrate repeat accumulate codes into HePNC using link-to-link coding, where a full-state sum-product decoding algorithm is proposed at the relay followed by a bit-level mapping function design.

In Chapter 4, we present the design of hierarchical modulation physical layer

network coding (H-PNC) under asymmetric TWRC, which achieves the data exchange not only between the two sources but also between the relay and the source with the relatively better source-relay link. The theoretical BER analysis of QPSK-BPSK H-PNC is provided under both AWGN and Rayleigh fading channels.

In Chapter 5, we generalize the design of multi-hop physical layer network coding, where multiple relays are located in a linear topology and help to exchange the message of two end sources. The impact of mutual-interference and error propagation are addressed. Two multi-hop PNC schemes, D-MPNC and S-MPNC are provided, which target simple implementation and optimal end-to-end BER, respectively.

Chapter 6 concludes the dissertation.

1.4 Bibliographic Notes

The work in Chapter 2 was published in [67, 68], and the work in Chapter 4 was published in [69].

Chapter 2

Heterogeneous Modulation Physical Layer Network Coding

2.1 Overview

In this chapter, we provide the design and analysis of heterogeneous modulation physical layer network coding (HePNC) under the asymmetric TWRC scenario, where an unequal amount of data is exchanged between two sources. The proposed HePNC is operated in a symbol-level and end-to-end channel coding can be integrated directly. We propose adaptive mapping functions in HePNC, which map the superimposed signals to the network-coded symbols adaptively according to the channel conditions of two source-relay links. The theoretical analysis for the proposed QPSK-BPSK HePNC is provided. The performance evaluation is conducted by considering relay mapping error rate in the multiple-access stage and end-to-end BER in the broadcast stage under both AWGN and Rayleigh fading channels.

2.2 Related Work

PNC [1, 2] extended the operation of network coding [70–74] using a PHY layer approach. Two key issues in a PNC system are how to design the mapping function and how to represent the network-coded symbol to guarantee that the sources can abstract each other's information accurately and effectively. In dynamic mapping function design, i.e., adaptive mapping [37, 75], the selection of mapping function varies with the channel conditions, which benefits system performance at a cost of

higher complexity and overheads.

In the literature, PNC was mainly investigated in a symmetric TWRC scenario, where the channel conditions of the two source-relay links are similar, and the sources select the same coding and modulation [5, 7, 37, 57, 76–83]. When the channel conditions of the two source-relay links are quite different, the scenario is specified as asymmetric TWRC. In [84], the impact of the asymmetric channels on PNC was studied, where both sources still use BPSK modulation. Sources can also select different modulation according to the channel conditions in asymmetric TWRC [85–87]. In [85], adaptive modulation and network coding (AMNC) was proposed. Sources select modulation according to the amplitude ratio of two source-relay channel gains, however, the influence of the random phase shift difference was not addressed. [86,87] focused on how to design the network-coded symbol at the relay. Consider 2^{q_1}-ary and 2^{q_2}-ary constellations for the two sources' signals, respectively. In [86], decode-and-forward joint-modulation (DF-JM) was proposed, where the network-coded symbol was represented by a $2^{q_1+q_2}$-ary constellation, which is composed of the direct combinations of the two source symbols. In [87], two joint modulation and relaying solutions were proposed, JMR1 (a variant of DF-JM) and JMR2. In JMR2, the relay uses a many-to-one mapping function to obtain a $2^{\max(q_1,q_2)}$-ary network-coded symbol, while the impact of phase shift difference between the superimposed symbols at the relay was not addressed. In [37], a method to design the many-to-one mapping function known as adaptive mapping was proposed under symmetric TWRC, where the relay can design and select different many-to-one functions according to the channel conditions. The many-to-one mapping design should follow the Latin square constraint [38], also known as the exclusive law [37].

In this dissertation, we propose HePNC and investigate how to design and optimize the mapping function and the network-coded symbol by jointly considering the channel conditions, the Latin square constraint and the combination of heterogeneous modulation with a random phase shift between the two received signals at the relay in an asymmetric TWRC scenario. The proposed HePNC design is within compute-and-forward (CF) framework, which was proposed in [6] and extended in [88,89] with the lattice network coding schemes, from the information theoretic perspective. [90, 91] followed the CF framework, where the pulse amplitude modulation (PAM) was considered and linear mapping functions were designed. Different from [90,91], PSK/QAM modulation is considered, and the relay computes the channel conditions of the two source-relay links and maps the estimated sources' symbols with the designed map-

ping functions.

2.3 HePNC in Asymmetric TWRC

2.3.1 System model

Consider an asymmetric TWRC scenario, where source nodes A and B exchange information through a relay, R, because the source nodes are out of each other's transmission range. Each node is equipped with one antenna[1]. We consider a block fading channel, and the channel conditions of the link A–R, L_{ar}, and that of the link B–R, L_{br}, are different. Without loss of generality, we assume that L_{ar} is better than L_{br}, and L_{ar} can support a higher-order modulation. We assume symbol-level synchronization at the relay and perfect channel estimation at the receivers, i.e., the relay node in the MA stage and the source nodes in the BC stage. Synchronization problems in multi-hop networks have been extensively studied [93]. The feasibility study for the symbol-level synchronization can be found in [55,56,79]. To be practical, in HePNC the carrier-phase synchronization is not required at the relay and global full CSI is not required at the transmitters.

Similar to traditional PNC, the HePNC procedure has two stages: MA and BC stages. In the MA stage, the two source nodes transmit the signals to relay R simultaneously, and relay R demodulates and maps the received superimposed signals to a network-coded symbol. In the BC stage, the network-coded symbol is broadcast back to the source nodes. Different from symmetric PNC, heterogeneous modulation can be selected by the sources according to L_{ar} and L_{br} in the MA stage, and more transmission slots may be required to broadcast the network-coded symbol in the BC stage subject to the bottleneck link L_{br}. We also consider that the data exchanged between the sources may be unequal. In this chapter, the HePNC design is only considered in a symbol-level. How to combine channel codes and modulation is studied in Chapter 3.

2.3.2 HePNC procedure

Let $\mathcal{M}_m$ be 2^m-PSK modulation with the modulation order of m and $\mathbb{Z}_{2^m}$ be a non-negative integer set, which denotes the finite set with unity energy E_s and Gray

[1]An extension of HePNC to multiple-antenna scenario can be found in [92].

constellation mapping, $\mathbb{Z}_{2^m} = \{0,\ 1,\ \ldots,\ 2^m - 1\}$. Assume that S_a and S_b are the source symbols to be exchanged. Denote m_a and m_b as the modulation orders for sources A and B, respectively. Thus, we have $S_a \in \mathbb{Z}_{2^{m_a}}$, $S_b \in \mathbb{Z}_{2^{m_b}}$ and $m_a > m_b$.

Multiple access (MA) stage

In the MA stage, the received signal at relay R, Y_r can be expressed as

$$Y_r = H_a \mathcal{M}_{m_a}(S_a) + H_b \mathcal{M}_{m_b}(S_b) + N_r, \tag{2.1}$$

where H_a and H_b are the channel gains of L_{ar} and L_{br}, respectively, and N_r is complex Gaussian noise with variance of $2\sigma^2$. Denote $H_b/H_a = \gamma \exp(j\theta)$, where γ and θ stand for amplitude ratio and phase difference of the two received signals, respectively.

Define $(S_a,\ S_b)$ as a symbol pair, which denotes that two sources' symbols S_a and S_b are superimposed at relay R. The symbol pair $(S_a,\ S_b)$ can also be represented by one constellation point on the received constellation map at relay R. The maximum likelihood (ML) detection is proceeded by relay R to jointly demodulate $(S_a,\ S_b)$ from Y_r, and we have

$$(\hat{S}_a,\ \hat{S}_b) = \underset{(s_1,\ s_2) \in \mathbb{Z}_{2^{m_a}} \times \mathbb{Z}_{2^{m_b}}}{\operatorname{argmin}} |Y_r - H_a \mathcal{M}_{m_a}(s_1) - H_b \mathcal{M}_{m_b}(s_2)|^2, \tag{2.2}$$

where $(\hat{S}_a,\ \hat{S}_b)$ is the estimation of $(S_a,\ S_b)$.

Afterwards, relay R uses a mapping function $\mathcal{C}$ to map $(\hat{S}_a,\ \hat{S}_b)$ to a network-coded symbol $S_r = \mathcal{C}(\hat{S}_a,\ \hat{S}_b)$; $S_r \in \mathbb{Z}_{2^{m_a}}$. The mapping function $\mathcal{C}$ applied by relay R is known by all nodes, and is subject to the Latin square constraint [38] (also known as the exclusive law [37]), which requires

$$\begin{aligned} &\mathcal{C}(s_1,\ s_2) \neq \mathcal{C}(s_1',\ s_2) \text{ for any } s_1 \neq s_1' \in \mathbb{Z}_{2^{m_a}} \text{ and } s_2 \in \mathbb{Z}_{2^{m_b}}, \\ &\mathcal{C}(s_1,\ s_2) \neq \mathcal{C}(s_1,\ s_2') \text{ for any } s_2 \neq s_2' \in \mathbb{Z}_{2^{m_b}} \text{ and } s_1 \in \mathbb{Z}_{2^{m_a}}. \end{aligned} \tag{2.3}$$

Although the superimposed signals at relay R is $2^{(m_a \times m_b)}$-ary, the mapping function $\mathcal{C}$ can decrease the network-coded symbol to 2^{m_a}-ary. The process of mapping $(\hat{S}_a, \hat{S}_b)$ to symbol S_r includes two steps, many-to-one mapping and relay labeling. The details of the many-to-one mapping and relay labeling will be discussed in Sec. 2.4.1 and Sec. 2.4.2, respectively.

Broadcast (BC) stage

The bottleneck link L_{br} can only support a lower-order modulation 2^{m_b}. The relay reduces the modulation order of the network-coded symbol S_r from m_a to m_b to guarantee reliable transmissions in the BC stage. Thus, HePNC applies a multiple-slot scheme to broadcast the network-coded symbol in the BC stage. Relay R uses modulation $\mathcal{M}_{m_b}$ to broadcast S_r back to the source nodes by $\lceil \frac{m_a}{m_b} \rceil$ transmission slots in the BC stage[2]. In each transmission slot, a part of S_r denoted by $S'_r \in \mathbb{Z}_{2^{m_b}}$ is transmitted. An estimation of S_r is conducted at each source node by concatenating all the estimated S'_r. We use an example to explain the multiple-slot design in the BC stage. Considering QPSK-BPSK HePNC, in order to ensure that the bit error rate from the relay to source B is below 10^{-3} in the BC stage, the bottleneck link L_{br} with $\text{SNR}_{br} = 7$ dB can only support BPSK. The network-coded symbol S_r is a QPSK symbol, and thus, the relay uses two BC slots to broadcast one BPSK symbol in each BC slot to guarantee the BER threshold. SNR is defined as the received signal to noise power ratio. For AWGN channels, it can be calculated by $\text{SNR(dB)} = 10\log_{10}\frac{E_r}{N_0}$, where E_r denotes received symbol energy, and N_0 is noise spectral density. For fading channels, SNR denotes average received SNR.

For each transmission slot in the BC stage, source A receives $Y_a = H_a\mathcal{M}_{m_b}(S'_r) + N_a$ from relay R, where N_a is complex Gaussian noise with variance of $2\sigma^2$. Source A estimates S'_r as $\hat{S}'_r$ by the ML decision

$$\hat{S}'_r = \underset{s'_r \in \mathbb{Z}_{2^{m_b}}}{\operatorname{argmin}} |Y_a - H_a\mathcal{M}_{m_b}(s'_r)|^2. \tag{2.4}$$

Then, an estimate of S_r denoted as $\hat{S}_r$ is obtained by concatenating all the $\hat{S}'_r$. Finally, source A estimates S_b by

$$\hat{S}'_b = \underset{s_b \in \mathbb{Z}_{2^{m_b}}}{\operatorname{argmin}} |\hat{S}_r - \mathcal{C}(S_a,\ s_b)|^2. \tag{2.5}$$

Note that in (2.5), source A decodes source B's information by using both the original information transmitted by itself in the MA stage and the mapping function $\mathcal{C}$. Similarly, source B obtains the estimation of S_a.

[2]If $\frac{m_a}{m_b}$ is not an integer, relay R can schedule several BC stages to transmit the least common multiple of m_a and m_b bits.

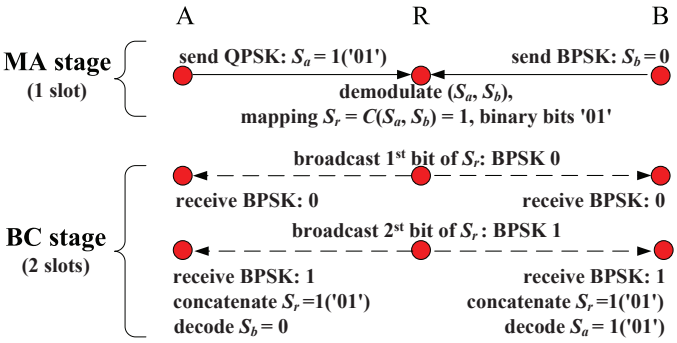

(a) MA and BC Stages for QPSK-BPSK HePNC.

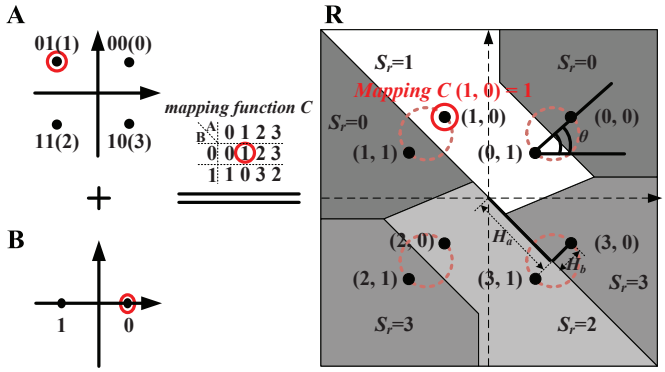

(b) Constellation maps at sources and relay with $\gamma = 0.3$ and $\theta = \frac{\pi}{4}$, the colored blocks represent decision regions for the ML decision in (2.2) and mapping results of S_r.

Figure 2.1: An example of QPSK-BPSK HePNC.

2.3.3 QPSK-BPSK HePNC example

Fig. 2.1 shows a sample design of QPSK-BPSK HePNC. Fig. 2.1(a) shows QPSK-BPSK HePNC procedure literally, and Fig. 2.1(b) considers the procedure from the constellation map perspective. In the MA stage, source A uses QPSK to send symbol $S_a = 1$ to relay R, meanwhile source B uses BPSK to send $S_b = 0$ to relay R. Note that the QPSK symbol $S_a = 1$ can also be represented as '01' by two binary bits. In this chapter, we use ' ' to present the binary bits that compose one symbol. The bit-symbol labeling method applied for QPSK constellation is shown in Fig. 2.1(b). Relay R demodulates a symbol pair $(S_a, S_b) = (1, 0)$, and then uses a mapping function $\mathcal{C}$ as shown in Fig. 2.1(b) to obtain a network-coded symbol $S_r = \mathcal{C}(1, 0) = 1$, which can be represented by binary bits '01'. Since the bottleneck link L_{br} can only support BPSK, S_r is split into two BPSK symbols, 0 and 1, which are broadcast in two transmission slots in the BC stage. After receiving S_r, sources A and B can decode each other's

information with the same mapping function $\mathcal{C}$ and the original symbol transmitted by itself in the MA stage.

Fig. 2.1(b) shows the constellation maps at the sources and relay. In the received constellation map at relay R, four dotted circles are resulted from superimposing the expected received BPSK symbols $-H_b \exp(j\theta)$ and $H_b \exp(j\theta)$ on the expected received QPSK symbol $H_a\mathcal{M}_2(S_a)$ with phase difference θ. We specify the circles as BPSK circles. Each center of the BPSK circles is the expected received QPSK symbol $H_a\mathcal{M}_2(S_a)$, and the radius of each BPSK circle equals $|H_b|$. We observe that, the structure of the received constellation map is determined by parameters γ and θ, and the size of the received constellation maps is determined by both $|H_a|$ and $|H_b|$, which is a useful conclusion for designing the mapping function $\mathcal{C}$ discussed in the following section.

2.4 HePNC Design and Analysis

A critical issue of HePNC is the mapping function $\mathcal{C}$ design including many-to-one mapping $\mathcal{F}$ design and relay labeling design. We begin with QPSK-BPSK HePNC as a sample design to elaborate the design criterion, which presents the insights for designing higher-order modulation HePNC. Then we discuss 8PSK-BPSK HePNC and 16QAM-BPSK HePNC designs.

2.4.1 Many-to-one mapping design

The many-to-one mapping $\mathcal{F}$ is a $2^{\min(m_a, m_b)}$-to-one mapping. One feature of the mapping scheme is that the superimposed signals at the relay are reduced from $2^{m_a \times m_b}$-ary to $2^{\max(m_a, m_b)}$-ary. Another feature is that part of the demodulation errors in the process of obtaining $(\hat{S}_a, \hat{S}_b)$ can be corrected, e.g., considering the example in Fig. 2.1, we have $(S_a, S_b) = (1,0)$, and even if relay R demodulates $(\hat{S}_a, \hat{S}_b) = (0,1)$ by mistake, the many-to-one mapping result is still correct if $\mathcal{F}(0,1) = \mathcal{F}(1,0)$. We discuss how to design the many-to-one mapping in the following.

Define the error rate of $S_r \neq \mathcal{C}(S_a, S_b)$ as relay mapping error rate (RER). RER is an important performance index, which determines whether the network-coded symbol is correctly obtained before the BC stage or not. More details of the RER error performance estimation for QPSK-BPSK HePNC is analyzed in Sec. 2.5.1. A proper many-to-one mapping design aims to minimize RER under the Latin square

constraint. The RER performance is dominated by the smallest Euclidean distance between two symbol pairs, e.g., the Euclidean distance between symbol pairs (1,0) and $(1,1)$ as shown in Fig. 2.1(b). However, $(1,0)$ and $(1,1)$ cannot be grouped together, because they violate the Latin square constraint. Given γ and θ, the optimal many-to-one mapping can be obtained by a *Closest Neighbor Clustering* (CNC) algorithm [37], which selects symbol pairs with the smallest Euclidean distance under the condition that these two symbol pairs satisfy the Latin square constraint. The influence of two source-relay channel conditions on the received constellation map can be reflected by parameters γ and θ, and the optimal many-to-one mapping varies with γ and θ. Relay R can select the optimal many-to-one mapping according to the channel conditions referred to parameters γ and θ [37]. Although obtaining the optimal mapping functions by the CNC method is of high complexity [38], they can be done offline, so the approach is feasible as the relay only needs to store the designed optimal mapping functions and looks up the labeling tables.

The *Closest Neighbor Clustering* algorithm can determine the many-to-one mapping, e.g., for QPSK-BPSK HePNC, when $\theta \in (0,\ \frac{\pi}{4})$ and $\gamma < 0.5$[3], the optimal many-to-one mapping $\mathcal{F}_1$ can be expressed as

$$\begin{aligned} &\mathcal{F}_1(0,\,0) = \mathcal{F}_1(1,\,1),\ \mathcal{F}_1(0,\,1) = \mathcal{F}_1(1,\,0), \\ &\mathcal{F}_1(2,\,0) = \mathcal{F}_1(3,\,1),\ \mathcal{F}_1(2,\,1) = \mathcal{F}_1(3,\,0). \end{aligned} \tag{2.6}$$

How to label the many-to-one mapping results by $S_r \in \mathbb{Z}_{2^{m_a}}$ is defined as relay labeling, and it will be discussed in the following subsection.

2.4.2 Relay labeling design

First, we clarify the differences between the bit-symbol labeling at each source and the relay labeling at the relay. In this chapter, each source applies Gray mapping as the bit-symbol labeling, e.g., the bit-symbol labeling for QPSK as shown in Fig. 2.1(b). The relay labeling aims to label the many-to-one mapping results as shown in (2.6), which can be labeled by QPSK symbols, and in the following we target to design and optimize the relay labeling.

Even relay R can correctly obtains $S_r = \mathcal{C}(S_a,\ S_b)$ in the MA stage, the source nodes may not successfully decode each other's information if there are errors in the

[3]The threshold $\gamma = 0.5$ will be explained in Sec. 2.4.3.

broadcast stage. The link from relay R to source B , L_{br}[4], is the bottleneck link in the BC stage, which limits the throughput of the BC stage. We can optimize the relay labeling process by maximizing the successful transmission bits under the condition that at most one error happens in one transmission slot over link L_{br} in the BC stage. Note that if an error happens in any transmission slot over link L_{ar} in the BC stage[5], source A cannot decode the information from source B.

We use an example to illustrate the design criterion of the relay labeling. Consider the QPSK-BPSK HePNC example as shown in Fig. 2.1, where the source symbol pair is $(S_a, S_b) = (1, 0)$, which can also be expressed as $(S_a, S_b) = (\text{'01'}, 0)$ with the Gray mapping as shown in Fig. 2.1(b). Consider the many-to-one mapping $\mathcal{F}_1$ in (2.6) and suppose that $(\hat{S}_a, \hat{S}_b)$ is correctly estimated by relay R in the MA stage. Considering a worst case example of a random relay labeling, e.g., relay labels $\mathcal{F}_1(1, 0) = \mathcal{F}_1(0, 1)$ to '00', $\mathcal{F}_1(3, 0) = \mathcal{F}_1(2, 1)$ to '01', and then $S_r = \mathcal{F}_1(1, 0)$ to '00' in bits. In the BC stage, when an error happens in the second transmission slot over link L_{br}, source B estimates the network-coded symbol as $\hat{S}_r =$ '01' in error, and source B finally decodes $\hat{S}'_a = 3$ in QPSK symbol, i.e., '10' in bits, by using the mapping function $\mathcal{F}_1(3, 0)$. Thus, two bits are incorrect by decoding the expected $S_a =$ '01' as $\hat{S}'_a =$ '10'. When $S_b = 0$, one way to reduce the probability of the worst case is to label $\mathcal{F}_1(1, 0)$ and $\mathcal{F}_1(3, 0)$ according to Gray mapping, e.g., label $\mathcal{F}_1(1, 0)$ and $\mathcal{F}_1(3, 0)$ to be '01' and '10', respectively, and the same strategy is applied for $\mathcal{F}_1(0, 0)$ and $\mathcal{F}_1(2, 0)$, i.e., to label $\mathcal{F}_1(0, 0)$ and $\mathcal{F}_1(2, 0)$ to be '00' and '11'. In this way, the worst case, i.e., two bits in error in the above example, only occurs when errors happen in both of the L_{br} transmissions.

The labeling design that only considers $S_b = 0$ may not be suitable for $S_b = 1$, so the relay labeling for $\mathcal{F}(s_a, 0)$ and $\mathcal{F}(s_a, 1)$ ($s_a \in \mathbb{Z}_4$) should be jointly optimized. With an exhaustive search, we find that for QPSK-BPSK HePNC, the optimal relay labeling can simply label $\mathcal{F}(s_a, 0) = s_a$, and then label $\mathcal{F}(s_a, 1)$ according to the selected many-to-one mapping $\mathcal{F}$. To generalize the bit-symbol labeling for QPSK-BPSK HePNC, there are three types of bit-symbol labeling for the QPSK modulation, please refer to Fig. 1 in [86], and with any type of QPSK bit-symbol labeling in QPSK-BPSK HePNC, the optimal relay labeling conclusion above is still valid. Note that the

[4]We denote both links from source B to relay R and from relay R to source B as L_{br}; however, the channel conditions can be different for the transmission from source B to relay R in the MA stage and that from relay R to source B in the BC stage.

[5]As L_{ar} has a relatively better channel condition compared to L_{br}, this error probability can be neglected at high SNR.

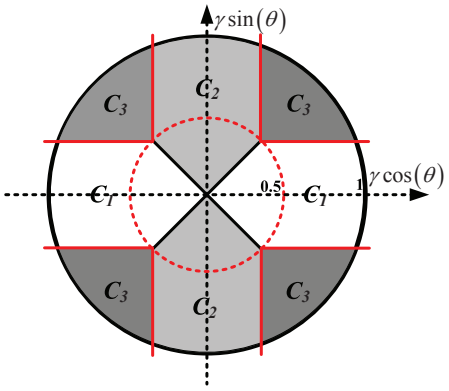

Figure 2.2: QPSK-BPSK HePNC adaptive mapping functions.

optimal relay labeling is not unique.

2.4.3 Mapping function of QPSK-BPSK HePNC

The mapping function $\mathcal{C}$ design includes the many-to-one mapping $\mathcal{F}$ design and the relay labeling design, which are analyzed in the above two subsections. Thus, the optimal mapping function for QPSK-BPSK HePNC can be designed and shown in Fig. 2.2, and the details of the many-to-one mapping and relay labeling are shown in Table 2.2. Depending on the two source-relay channel conditions, i.e., γ and θ, the mapping functions can be adaptively selected by the relay according to Fig. 2.2. When γ is small, e.g., $\gamma \in (0, 0.5)$, the region is only divided into two parts labeled by $\mathcal{C}_1$ and $\mathcal{C}_2$; when $\gamma \in (0, 1)$[6], the region can be divided into three parts, labeled by $\mathcal{C}_1$, $\mathcal{C}_2$ and $\mathcal{C}_3$, respectively. A general explanation is that with the increase of γ, the BPSK circles on the received constellation map at the relay shown in Fig. 2.1(b) become larger, which changes the smallest Euclidean distance between constellation points with different θ, and thus $\mathcal{C}_3$ occurs when $\gamma \in (0.5, 1)$.

Define η as the boundary of different adaptive mapping functions C_1, C_2 and C_3 when $\theta \in (0, \frac{\pi}{2})$ as shown in Fig. 2.2, and we have

$$\eta = \begin{cases} \dfrac{\pi}{4}, & \text{when } \gamma < 0.5; \\ \arcsin \dfrac{\sqrt{2}}{4\gamma}, & \text{when } 0.5 < \gamma < 1. \end{cases} \tag{2.7}$$

[6]We consider the asymmetric TWRC, where the channel condition of L_{ar} is better than that of L_{br}, and thus we have $\gamma \in (0, 1)$.

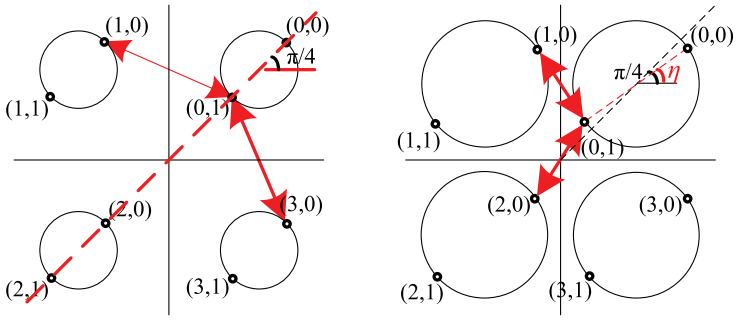

(a) $\gamma < 0.5$. (b) $\gamma > 0.5$.

Figure 2.3: An example of the mapping function boundary.

We use Fig. 2.3 to explain how to obtain (2.7), and the threshold $\gamma = 0.5$ is indirectly explained. When $\gamma < 0.5$, the received constellation at the relay is shown in Fig. 2.3(a). When $\theta \in (0, \frac{\pi}{4})$, the smallest Euclidean distance is that between (1,0) and (0,1), and also the distance between (2,0) and (3,1). Thus, (1,0) and (0,1) are mapped to the same cluster, and the same for (2,0) and (3,1). Then, we can obtain mapping function $\mathcal{C}_1$. When $\theta = \frac{\pi}{4}$, the distance between (1,0) and (0,1) equals the distance between (0,1) and (3,0); when $\theta \in (\frac{\pi}{4}, \frac{\pi}{2})$, the smallest Euclidean distance is that between (1,1) and (2,0), and also that between (3,0) and (0,1), which results in mapping function $\mathcal{C}_2$. Thus, $\eta = \frac{\pi}{4}$ is the boundary of mapping functions $\mathcal{C}_1$ and $\mathcal{C}_2$ for $\gamma < 0.5$. Fig. 2.3(b) shows the received constellation map when $\gamma > 0.5$. With the increase of θ from 0 to $\frac{\pi}{4}$, these exists a θ where the Euclidean distance between (1,0) and (0,1) equals that between (0,1) and (2,0). This value of θ is the boundary, η, of the mapping functions $\mathcal{C}_1$ and $\mathcal{C}_3$. Note that with the increase of γ from 0 to 1, this situation happens first when $\gamma = 0.5$ and $\theta = \frac{\pi}{4}$, and thus $\gamma = 0.5$ is the threshold. By letting the Euclidean distance between (1,0) and (0,1) equal that between (0,1) and (2,0), we can easily obtain $\eta = \arcsin \frac{\sqrt{2}}{4\gamma}$. Another method to obtain the threshold $\gamma = 0.5$ is to let $\eta = \frac{\pi}{4}$, and then we have $\gamma = 0.5$ according to $\eta = \arcsin \frac{\sqrt{2}}{4\gamma}$, which indicates the situation that the first time $\mathcal{C}_3$ occurs with the increase of γ from 0 to 1.

The CNC method is applied to design the adaptive mapping functions in this chapter, another well known mapping function design method targets to remove the singular fade state (SFS) of the received constellations at the relay [38]. SFS denotes the case when the minimum distance of the received constellation points at the relay

Table 2.1: Singular fade state points of QPSK-BPSK HePNC

SFS points	P_1	P_2	P_3	P_4	P_5
γ	$\frac{\sqrt{2}}{2}$	$\frac{\sqrt{2}}{2}$	$\frac{\sqrt{2}}{2}$	$\frac{\sqrt{2}}{2}$	1
θ	0 or π	$\frac{\pi}{2}$ or $\frac{3\pi}{2}$	0 or π	$\frac{\pi}{2}$ or $\frac{3\pi}{2}$	$\frac{\pi}{4}$ or $\frac{3\pi}{4}$ or $\frac{5\pi}{4}$ or $\frac{7\pi}{4}$

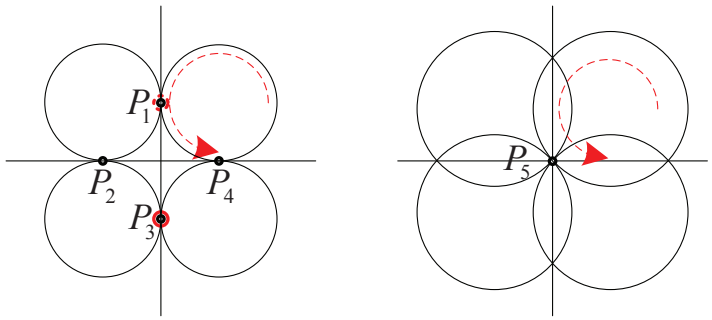

(a) $\gamma = \frac{\sqrt{2}}{2}$. (b) $\gamma = 1$.

Figure 2.4: Singular fade state points of QPSK-BPSK HePNC constellations.

becomes zero, which results in large error probabilities if without suitable mapping function designs. We use an example to show that the SFS points of QPSK-BPSK HePNC constellations at the relay can be removed by the designed mapping functions as shown in Fig. 2.3. For QPSK-BPSK HePNC, the SFS points on the received constellation map at the relay are shown in Fig. 2.4 and summarized in Table 2.1, labeled from P_1 to P_5[7]. The SFS points P_1 and P_3 can be removed by mapping function $\mathcal{C}_1$, and P_2 and P_4 can be removed by $\mathcal{C}_2$, and P_5 can be removed by $\mathcal{C}_3$. For example, considering the case shown in Fig. 2.4(a), when $\gamma = \frac{\sqrt{2}}{2}$ and $\theta = 0$, symbol pairs (0,1) and (1,0) overlap on the received constellation resulting in the SFS point P_1, which is marked by the red dotted circle, and (2,0) and (3,1) overlap to be another SFS point P_3 marked by the lined circle. By $\mathcal{C}_1$, (0,1) and (1,0) are mapped to the same network-coded symbol, and the same for (2,0) and (3,1). Thus, P_1 and P_3 can be removed. The other SFS points can also be removed by the designed mapping functions similarly.

In the MA stage, the relay obtains two source-relay channel conditions H_a and H_b by channel estimation, where H_a and H_b are complex numbers. By definition

[7]Note that, $\gamma = 0$ and $\gamma = \infty$ can be considered as two special cases resulting in non-removable singular fade state points, which also exist in other PNC schemes.

Table 2.2: Details of the optimal mapping functions for QPSK-BPSK HePNC

	0	1	2	3
0	0	1	2	3
$1(\mathcal{C}_1)$	1	0	3	2
$1(\mathcal{C}_2)$	3	2	1	0
$1(\mathcal{C}_3)$	2	3	0	1

$H_b/H_a = \gamma \exp(j\theta)$, γ and θ can be obtained. Then the relay can select the optimal mapping function $\mathcal{C}$ according to Fig. 2.2 referring to γ and θ, and find details of the mapping function $\mathcal{C}$ including the many-to-one mapping and relay labeling by Table 2.2. For example, when $\gamma < 0.5$, $\theta \in (0, \frac{\pi}{4})$ and $(\frac{7\pi}{4}, 2\pi)$, the optimal mapping function $\mathcal{C}_1$ should be applied, and the details of $\mathcal{C}_1$ can be found according to Table 2.2, which is the same as the mapping function used in Fig. 2.1(b). If $\mathcal{C}_2$ or $\mathcal{C}_3$ is found to be optimal, the first row of the mapping function is not changed, i.e., $\mathcal{F}(s_a, 0) = s_a$, and only the second row is changed accordingly. Note that, the mapping functions $\mathcal{C}_1$ and $\mathcal{C}_2$ are non-linear, but $\mathcal{C}_3$ is linear [90]. In other words, HePNC can be possibly applied for both non-linear and linear PNC mapping. Please refer to [90] for more discussions about optimization of linear PNC design.

2.4.4 Further discussion on higher-order modulation HePNC

For other higher-order modulation HePNC, such as 8PSK-BPSK and 16QAM-BPSK HePNC, the optimal many-to-one mapping and relay labeling can also be obtained by the *Closest Neighbor Clustering* algorithm and exhaustive search as discussed above. However, as the set size of superimposed signals increases for higher-order modulation HePNC, the number of optimal mapping functions increases especially when γ is large, which increases the complexity of mapping function selection, and the relay needs to change mapping function frequently.

Simplified mapping function $\mathcal{C}$ designs for 8PSK-BPSK and 16QAM-BPSK HePNC are shown in Figs. 2.5(a) and 2.5(b), respectively. Table 2.3 shows the details of 8PSK-BPSK HePNC mapping function design. The mapping details of 16QAM-BPSK HePNC is omitted due to space limit. The procedure of obtaining Fig. 2.5(a) and Table 2.3 is summarized as follows:

1) When $\gamma < 0.5$, obtain the optimal many-to-one mapping set $\mathcal{F} = \{\mathcal{F}_1, \cdots, \mathcal{F}_8\}$ by the *Closest Neighbor Clustering* algorithm.[8]

[8]The threshold $\gamma = 0.5$ for 8PSK-BPSK HePNC is obtained by exhaustive searching using the

2) When $\gamma > 0.5$, given γ and θ, find all of the pairwise symbol pairs $(s_1,\ s_2)$ and $(s_1',\ s_2')$ satisfying the conditions that they have the smallest Euclidean distance and satisfy the Latin square constraint, i.e., $s_1 \neq s_1'$ and $s_2 \neq s_2'$. Note that several symbol pairs may satisfy the above two conditions.
3) Generate a temporary mapping way $\mathcal{F}_{temp}(s_1,\ s_2) = \mathcal{F}_{temp}(s_1',\ s_2')$, $\mathcal{F}_{temp}$ contains the mapping ways for all the pairwise symbol pairs obtained in step 2.
4) Check whether $\mathcal{F}_{temp}(s_1,\ s_2) = \mathcal{F}_{temp}(s_1',\ s_2')$ can be included by the existing many-to-one mapping in set $\mathcal{F}$.
5) If any many-to-one mapping $\mathcal{F}_i$ ($\mathcal{F}_i \in \mathcal{F}$) includes $\mathcal{F}_{temp}$, update $\mathcal{F}_{temp} = \mathcal{F}_i$; if none of the existing many-to-one mapping includes $\mathcal{F}_{temp}$, generate a new many-to-one mapping $\mathcal{F}_9$, update $\mathcal{F}_9 = F_{temp}$, and put $\mathcal{F}_9$ into set $\mathcal{F}$.
6) Repeat steps 2, 3, 4, 5, and obtain the many-to-one mapping $\mathcal{F} = \{\mathcal{F}_1,\ \cdots,\ \mathcal{F}_{10}\}$[9].
7) For all $\mathcal{F} = \{\mathcal{F}_1,\ \cdots,\ \mathcal{F}_{10}\}$, label the mapping results by $\mathcal{F}(s_a, 0) = s_a$, label $\mathcal{F}(s_a, 1)$ according to the determined $\mathcal{F}$, and obtain mapping functions $\{\mathcal{C}_1,\ \cdots,\ \mathcal{C}_{10}\}$.

Similarly, the mapping functions for 16QAM-BPSK HePNC as shown in Fig. 2.5(b) can be obtained. For 8PSK-BPSK and 16QAM-BPSK HePNC, for each many-to-one mapping, we can use exhaustive search to find the optimal relay labeling $\mathcal{F}(s_a,\ 0) = s_a,\ s_a \in \mathbb{Z}_{2^{m_a}}$.

With the increase of γ, the size of BPSK circles would go larger, and the constellation points on the received constellation map at the relay can superimpose on each other which leads to more errors. Higher-order modulation HePNC can only be supported when γ is small. To initialize the HePNC transmission, a HePNC scheme should be selected first according to the SNR of the two source-relay links and the data exchange ratio requirements, which is similar to the concept of adaptive modulation. In the initialization of HePNC, the source nodes report the requirements of data needed to be exchanged individually, and then the relay estimates two source-relay channel conditions and determines the modulation applied by the sources by jointly considering the two source-relay channel conditions and the data exchange requirements, and feedbacks the modulation configuration to the sources. Generally speaking, the source node who wants to exchange a larger amount of data should have a source-relay link with the relatively better channel condition, which can be satisfied when an appropriate relay node is selected for the sources.

Closest Neighbor Clustering algorithm, and the theoretical proof is similar to that analyzed in Sec. 2.4.3 to obtain the threshold $\gamma = 0.5$ for QPSK-BPSK HePNC.

[9] $\mathcal{F}_9$ and $\mathcal{F}_{10}$ are generated because they cannot be included by the existing many-to-one mapping in set $\mathcal{F}$.

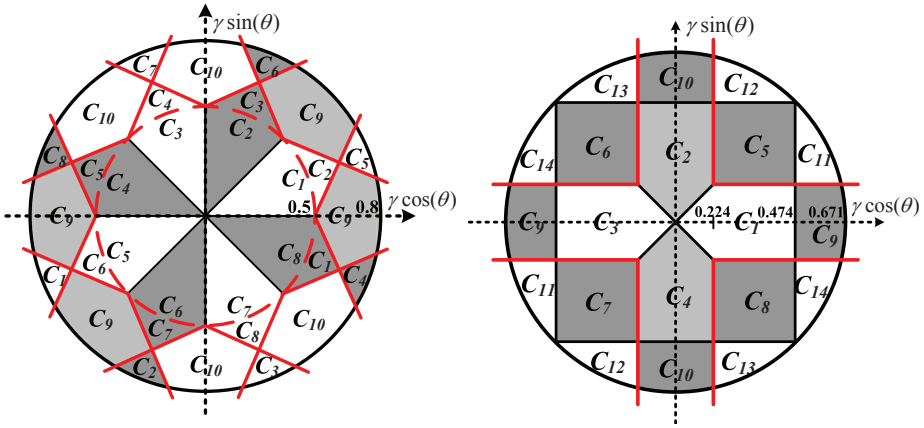

(a) 8PSK-BPSK HePNC. (b) 16QAM-BPSK HePNC.

Figure 2.5: Mapping functions for 8PSK-BPSK and 16QAM-BPSK HePNC.

Table 2.3: Details of the optimal mapping functions for 8PSK-BPSK HePNC

	0	1	2	3	4	5	6	7
0	0	1	2	3	4	5	6	7
$1(\mathcal{C}_1)$	1	2	7	6	3	4	5	0
$1(\mathcal{C}_2)$	1	2	3	0	7	4	5	6
$1(\mathcal{C}_3)$	7	2	3	4	1	0	5	6
$1(\mathcal{C}_4)$	7	0	3	4	5	2	1	6
$1(\mathcal{C}_5)$	7	0	1	4	5	6	3	2
$1(\mathcal{C}_6)$	3	0	1	2	5	6	7	4
$1(\mathcal{C}_7)$	5	4	1	2	3	6	7	0
$1(\mathcal{C}_8)$	1	6	5	2	3	4	7	0
$1(\mathcal{C}_9)$	2	7	0	5	6	3	4	1
$1(\mathcal{C}_{10})$	6	3	4	1	2	7	0	5

2.5 Error Probability Analysis

In this section, we analyze the error performance of QPSK-BPSK HePNC[10]. We use the techniques introduced in [94–97] and calculate the RER and BER of QPSK-BPSK HePNC under AWGN channels, and obtain a performance bound under Rayleigh fading channels.

[10]For higher-order modulation HePNC, the received constellation map at the relay contains more symbol pairs, i.e., $2^{m_1+m_2}$, which introduces more complexity to error performance analysis by the technique in [94–97].

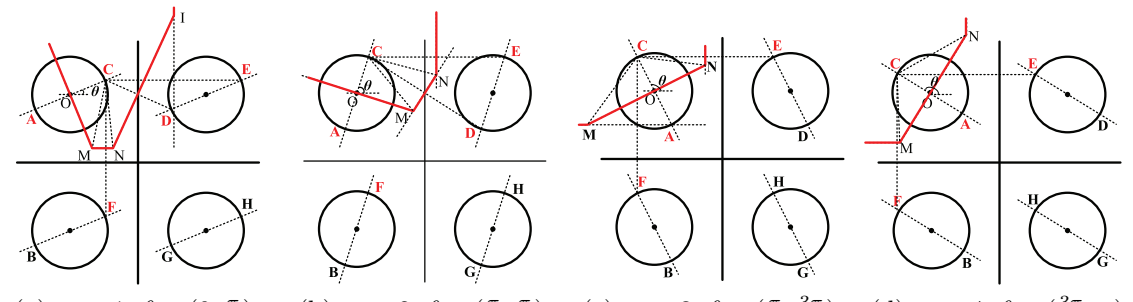

(a) case 1, $\theta \in (0, \frac{\pi}{4})$. (b) case 2, $\theta \in (\frac{\pi}{4}, \frac{\pi}{2})$. (c) case 3, $\theta \in (\frac{\pi}{2}, \frac{3\pi}{4})$. (d) case 4, $\theta \in (\frac{3\pi}{4}, \pi)$.

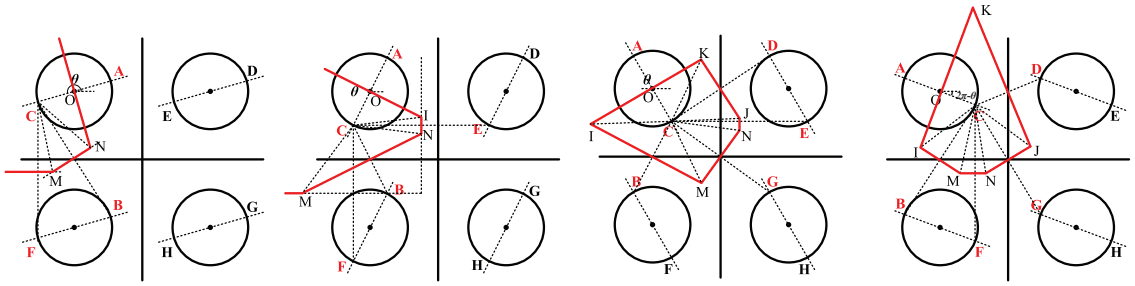

(e) case 5, $\theta \in (\pi, \frac{5\pi}{4})$. (f) case 6, $\theta \in (\frac{5\pi}{4}, \frac{3\pi}{2})$. (g) case 7, $\theta \in (\frac{3\pi}{2}, \frac{7\pi}{4})$. (h) case 8, $\theta \in (\frac{7\pi}{4}, 2\pi)$.

Figure 2.6: Decision boundaries for $\gamma \in (0, \frac{\sqrt{2}}{2})$ and $\theta \in (0, 2\pi)$.

2.5.1 Relay mapping error analysis

We study RER performance of the QPSK-BPSK HePNC system under AWGN channels first. We consider that sources have the same transmission power. Denote the SNR for link L_{ar} and L_{br} as SNR_{ar} and SNR_{br}, respectively. Denote $\Delta\text{SNR(dB)} = \text{SNR}_{ar}\text{(dB)} - \text{SNR}_{br}\text{(dB)}$. Considering path loss, the average received SNR of all links are inversely proportional to the link distance to the power of, α, the path loss exponent. By derivation, we have

$$\gamma = |H_b|/|H_a| = 10^{(-\Delta\text{SNR(dB)}/20)}. \tag{2.8}$$

Considering a complex plane, Fig. 2.6 shows the received constellation map at the relay and decision boundaries for constellation point C when $\gamma \in (0, \frac{\sqrt{2}}{2})$ and $\theta \in (0, 2\pi)$. Note that C represents symbol pair $(S_a, S_b) = (1, 0)$, which is also used in the example introduced in Fig. 2.1. For all $\gamma \in (0, \frac{\sqrt{2}}{2})$, BPSK circles always lie in each quadrant. When $\gamma > \frac{\sqrt{2}}{2}$, BPSK circles would cross X and Y axes; thus, new decision boundaries are needed. According to (2.8), when $\Delta\text{SNR} = 3$ dB, $\gamma \approx \frac{\sqrt{2}}{2}$, so $\gamma \in (0, \frac{\sqrt{2}}{2})$ covers the range $\Delta\text{SNR} \geq 3$ dB, which is suitable for QPSK-BPSK

HePNC, as the SNR difference between QPSK and BPSK modulation to maintain a symbol error rate (SER) lower than 10^{-3} is about 3 dB.

Each symbol pair $(S_a,\ S_b)$, $S_a \in \mathbb{Z}_4$ and $S_b \in \mathbb{Z}_2$, has the same transmitting probability $\frac{1}{8}$, and the expected received constellation map has a symmetric feature considering $\theta \in [0,\ 2\pi)$ with a uniform distribution. Thus, the RER performance can be calculated by considering one symbol pair only, e.g., constellation point C. Then by calculating all $\theta \in [0,\ 2\pi)$, all cases are considered. We use Fig. 2.6(a) as an example to illustrate. C is the expected received constellation point, and relay R may demodulate $(S_a,\ S_b)$ as A, D, E and F falsely due to the noise. The coordinates of the constellation points from A to H are obtained by

$$H_a\mathcal{M}_{m_a}(s_1)+H_b\mathcal{M}_{m_b}(s_2),\ \text{for all } s_1\in\mathbb{Z}_4,\ s_2\in\mathbb{Z}_2. \tag{2.9}$$

Points M, N and I are used for auxiliary calculation, so they are not practical constellation points. The coordinates of points M, N and I are

$$\begin{cases} M = [-|H_b|\frac{\sin^2(\theta)}{\cos(\theta)} + \frac{\sqrt{2}}{2}|H_a|(\frac{\sin(\theta)}{\cos(\theta)} - 1)] + j[|H_b|\sin(\theta)], \\ N = [-|H_b|\sin(\theta)] + j[|H_b|\sin(\theta)], \\ I = [|H_b|\cos(\theta)] + j[\frac{\sqrt{2}}{2}|H_a|(\frac{\sin(\theta)}{\cos(\theta)} + 1) - |H_b|\frac{\cos^2(\theta)}{\sin(\theta)}]. \end{cases}$$

Denote the error probability of mapping the desired constellation x_1 to an error constellation point x_2 as $P_{x_1x_2}$, and denote the Euclidean distance between x_1 and x_2 as $D_{x_1x_2}$. We obtain the error probabilities by

$$\begin{cases} P_{CA} = \frac{1}{2\pi}\int_0^{\angle ACM+\frac{\pi}{2}} \exp(\frac{-(D_{CA}/2)^2}{2\sigma^2\sin^2(\theta')})\mathrm{d}\theta', \\ P_{CF} = \frac{1}{2\pi}\int_0^{\angle MCN} \exp(\frac{-(D_{CF}/2)^2}{2\sigma^2\sin^2(\theta'+\angle CMN)})\mathrm{d}\theta', \\ P_{CD} = \frac{1}{2\pi}\int_0^{\angle NCI} \exp(\frac{-(D_{CD}/2)^2}{2\sigma^2\sin^2(\theta'+\angle CNI)})\mathrm{d}\theta', \\ P_{CE} = \frac{1}{2\pi}\int_0^{\frac{\pi}{2}-\angle ICE} \exp(\frac{-(D_{CE}/2)^2}{2\sigma^2\sin^2(\theta'+\frac{\pi}{2}+\angle ICE)})\mathrm{d}\theta'. \end{cases}$$

The RER calculation also needs to consider positive influence of the adaptive mapping functions, as partial demodulation errors can be corrected by the many-to-one mapping scheme discussed in Sec. 2.4.1. Errors of P_{CD}, P_{CB} and P_{CG} can be corrected by the mapping functions $\mathcal{C}_1$, $\mathcal{C}_2$ and $\mathcal{C}_3$, respectively.

Denote RER_i, $i \in \{1, \cdots, 8\}$, as the relay mapping error for case i. RER_1 can be

calculated by

$$\mathrm{RER}_1 = \frac{1}{2\pi}[\int_{\theta\in(0,\frac{\pi}{4})} (P_{CA}+P_{CF}+P_{CE})\,\mathrm{d}\theta + \int_{\theta\in(\frac{\pi}{4}-\eta,\frac{\pi}{4})} P_{CD}\,\mathrm{d}\theta]. \tag{2.10}$$

Summing all RER_i obtains the overall $\mathrm{RER} = \sum_{i=1}^{8} \mathrm{RER}_i$. Note that for different RER_i, the decision boundaries and adaptive mapping functions should be jointly considered.

The error probability of P_{CA} exists in all RER_i, and P_{CA} indicates rate of errors within the BPSK circle, which is

$$P_{CA} = \Pr\{S_r = C(S_a, 1 - S_b)\}. \tag{2.11}$$

When $\gamma \in (0,\, \frac{\sqrt{2}}{2})$, $D_{CA} = |H_b|$ is always the smallest Euclidean distance between two symbols in the received constellation map that contributes to most errors, as other symbol errors due to smaller symbol Euclidean distances than D_{CA} can be corrected by the adaptive mapping function $\mathcal{C}$. Thus, according to the minimum distance criterion, the overall RER can be estimated by considering the error probability $P_{CA} = Q[\frac{|H_b|}{\sigma}] = Q[\sqrt{2 \cdot \mathrm{SNR}_{br}}]$ only when γ is small enough, where $Q[.]$ is the Q function.

2.5.2 System end-to-end BER analysis

Denote BER_{ab} and BER_{ba} as the end-to-end BER from source A to source B and source B to source A, respectively. Denote BER_{all} as the overall BER. For QPSK-BPSK HePNC, we have $\mathrm{BER}_{all} = (2 \cdot \mathrm{BER}_{ab} + \mathrm{BER}_{ba})/3$.

For simplicity, let $\alpha_1 = (1 - Q[\sqrt{2 \cdot \mathrm{SNR}_{ar}}])^2$ and $\alpha_2 = (1 - Q[\sqrt{2 \cdot \mathrm{SNR}_{br}}])^2$, which denote probabilities that there is no error in transmissions over L_{ar} and L_{br} respectively in the BC stage. The probability that relay R obtains a correct network-coded symbol $S_r = \mathcal{C}(S_a,\, S_b)$ equals $1 - \mathrm{RER}$. If $S_r \neq \mathcal{C}(S_a,\, S_b)$, it is counted as an error event. BER_{ba} and BER_{ab} can be estimated by

$$\mathrm{BER}_{ba} \approx \begin{cases} (1 - \mathrm{RER})(1 - \alpha_1), & \text{when } S_r = \mathcal{C}(S_a,\, S_b), \\ \mathrm{RER}, & \text{when } S_r \neq \mathcal{C}(S_a,\, S_b), \end{cases} \tag{2.12}$$

$$\mathrm{BER}_{ab} \approx \begin{cases} (1 - \mathrm{RER})(1 - \alpha_2)/2, & \text{when } S_r = \mathcal{C}(S_a,\, S_b), \\ \mathrm{RER}/2, & \text{when } S_r \neq \mathcal{C}(S_a,\, S_b). \end{cases} \tag{2.13}$$

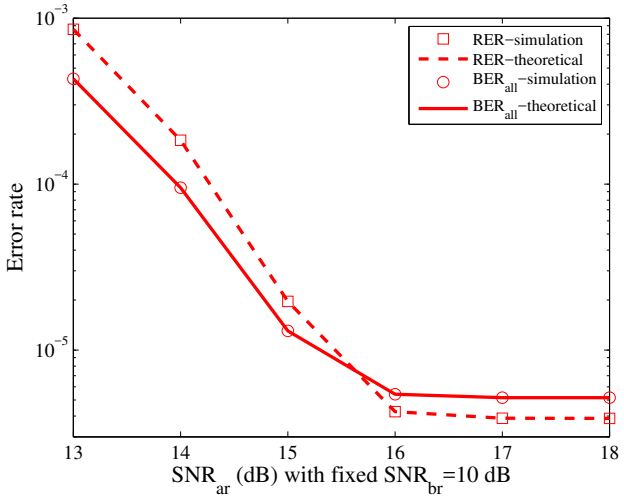

Figure 2.7: Simulation and theoretical results under AWGN channels.

Then we can estimate BER_{all} by

$$\mathrm{BER}_{all} \approx \frac{2 \cdot \mathrm{RER} + 2 \cdot Q[\sqrt{2 \cdot \mathrm{SNR}_{br}}]}{3}, \tag{2.14}$$

where $Q[\sqrt{2 \cdot \mathrm{SNR}_{ar}}] \ll Q[\sqrt{2 \cdot \mathrm{SNR}_{br}}]$ and it is omitted.

Note that in (2.13), when $S_r = \mathcal{C}(S_a, S_b)$, we apply the conclusion from the relay labeling design, i.e., source B can still successfully receive one bit from source A if an error happens in any of two transmissions over L_{br} in the BC stage. Fig. 2.7 shows the theoretical and simulation results for QPSK-BPSK HePNC under AWGN channels, with fixed $\mathrm{SNR}_{br} = 10$ dB. When SNR_{ar} is small, the BPSK circles are relatively large which leads to a larger RER; when SNR_{ar} is large, the RER performance is mainly determined by $Q[\sqrt{2 \cdot \mathrm{SNR}_{br}}]$, and errors in the bottleneck link L_{br} dominate the performance of the BC stage.

2.5.3 Rayleigh fading channels

We analyze the RER performance under Rayleigh fading channels in this subsection. Denote the probability density function (PDF) of Rayleigh distribution as $f(x, \delta) = \frac{x}{\delta^2} \exp\left(\frac{-x^2}{2\delta^2}\right)$, with mean $E(x) = \delta\sqrt{\frac{\pi}{2}}$. Denote the PDF of channel gains $|H_a|$ and $|H_b|$ as $f(|H_a|, \delta_2)$ and $f(|H_b|, \delta_1)$, respectively. The PDF of γ can be calculated by

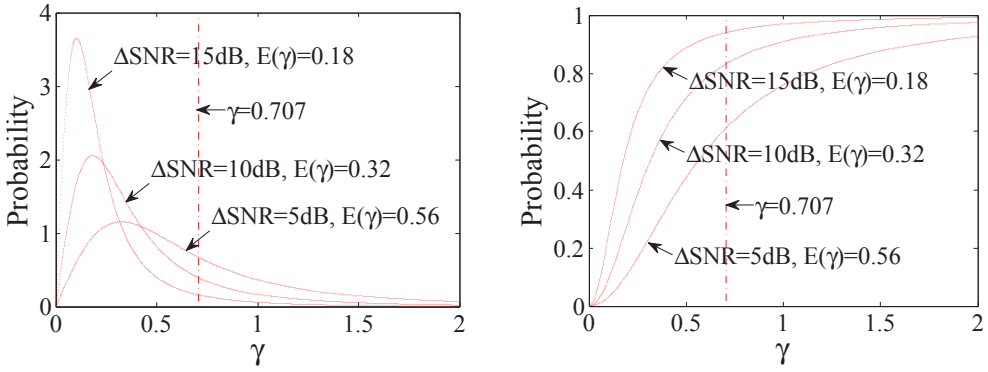

(a) PDF(γ). (b) CDF(γ).

Figure 2.8: PDF and CDF of γ.

$$\text{PDF}(\gamma) = \int_0^\infty |H_a| f(|H_a|\gamma, \delta_1) \mathrm{d}|H_a| = \frac{2\gamma {\delta_1}^2 {\delta_2}^2}{({\delta_1}^2 + {\delta_2}^2\gamma^2)^2}. \tag{2.15}$$

PDF(γ) and cumulative distribution function (CDF) of γ, CDF(γ), are shown in Fig. 2.8. When ΔSNR is large, γ is within the range of $(0, \frac{\sqrt{2}}{2})$ with a higher probability, e.g., when $\Delta\text{SNR} = 15$ dB, $\text{CDF}(\gamma = \frac{\sqrt{2}}{2}) = 94.04\%$. We can conclude that, in the Rayleigh fading channels, the RER of QPSK-BPSK HePNC is upper bounded by

$$\int_0^\infty f(|H_b|, \delta_2) Q\left[\frac{|H_b|}{\sigma}\right] \mathrm{d}|H_b|, \tag{2.16}$$

which is derived as follows. Under Rayleigh fading channels, RER can be expressed as

$$\int_0^\infty \int_0^\infty f(|H_b|, \delta_2) \text{PDF}(\gamma) f_{rer}(|H_b|, \gamma) \mathrm{d}|H_b| \mathrm{d}\gamma,$$

where $f_{rer}(|H_b|, \gamma)$ denotes the RER expression related to parameters $|H_b|$ and γ. When $\gamma \in (0, \frac{\sqrt{2}}{2})$, with the minimum distance criterion and the analysis for (2.11), we have

$$\int_0^\infty \int_0^{\sqrt{2}/2} f(|H_b|, \delta_2) \text{PDF}(\gamma) Q\left[\frac{|H_b|}{\sigma}\right] \mathrm{d}|H_b| \mathrm{d}\gamma < \text{RER};$$

when $\gamma > \frac{\sqrt{2}}{2}$, D_{CA} is not the smallest Euclidean distance and P_{CA} no longer dominates system performance, so we have

$$\int_0^\infty \int_{\sqrt{2}/2}^\infty f(|H_b|, \delta_2) \text{PDF}(\gamma) Q\left[\frac{|H_b|}{\sigma}\right] \mathrm{d}|H_b| \mathrm{d}\gamma < \text{RER}.$$

Thus, we have $\int_0^{\infty} f(|H_b|, \delta_2) Q[\frac{|H_b|}{\sigma}] \mathrm{d}|H_b| < \mathrm{RER}$. Note that for other BPSK-based HePNC, the above performance upper bound also holds. For higher-order modulation HePNC, the Euclidean distance between the BPSK circles D_{CA} no longer dominates system performance when $\gamma < \frac{\sqrt{2}}{2}$. Thus, we can still obtain the same conclusion by the above analysis.

2.6 Performance Evaluation

In this section, the performance of HePNC under asymmetric TWRC is evaluated. In the simulations, the relay is located on the line segment between the two sources. We let all nodes transmit signals with the same symbol energy E_s and set the average received SNR of all links be proportional to $d^{-\alpha}$, where d is the link distance and the path loss exponent $\alpha = 3$. Phase shift difference θ is uniformly distributed between $[0,\ 2\pi)$.

In the following, we first study RER and system BER_{all} performance of the proposed HePNC and JMR2 under both AWGN and Rayleigh fading channels, where JMR2 [87] is the existing state-of-the-art solution, which does not use adaptive mapping. Then we study the optimal relay location issue. Further more, we discuss how to maximize the throughput[11] and minimize the energy consumption by jointly considering the modulation combination for the sources and ratio of source data loads.

2.6.1 Error performance with fixed SNR_{br}

Fig. 2.9 compares the error performance of HePNC and JMR2 under AWGN channels, where we fix $\mathrm{SNR}_{br} = 7$ dB and gradually increase SNR_{ar}. Fig. 2.9(a) shows the error performance of QPSK-BPSK HePNC and QPSK-BPSK JMR2. For QPSK-BPSK HePNC, RER and BER_{all} monotonously decrease with the increase of SNR_{ar}, and RER performance converges to $Q[\sqrt{2 \cdot \mathrm{SNR}_{br}}]$ as shown by the solid line. For QPSK-BPSK JMR2, RER and BER_{all} increase first and then decrease, because for different ΔSNR, the single mapping function may suffer a larger error probability for certain structures of the received constellation map. Adaptive mapping applied in HePNC can adjust the mapping functions suitable to the current received constellation map. From the figure, ensuring BER_{all} below 10^{-3}, the proposed HePNC achieves 3 to 5 dB gain compared to JMR2. For the RER and BER_{all} performance in QPSK-BPSK

[11] Throughput (bits/slot) is defined as the successfully received bits per slot by all the destinations.

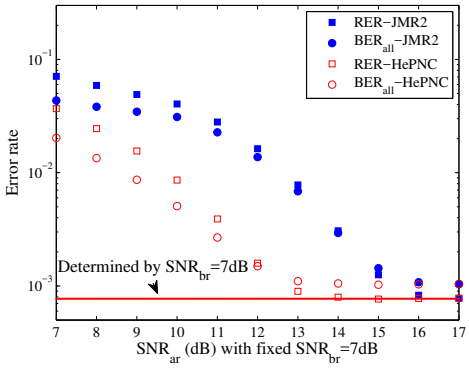

(a) QPSK-BPSK HePNC.

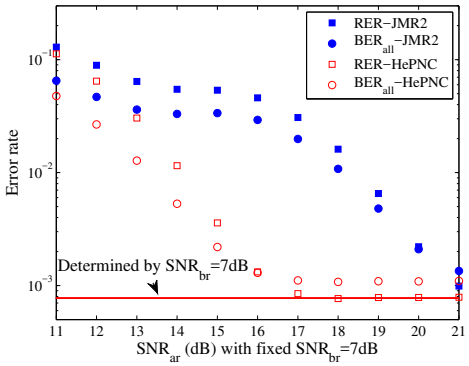

(b) 8PSK-BPSK HePNC.

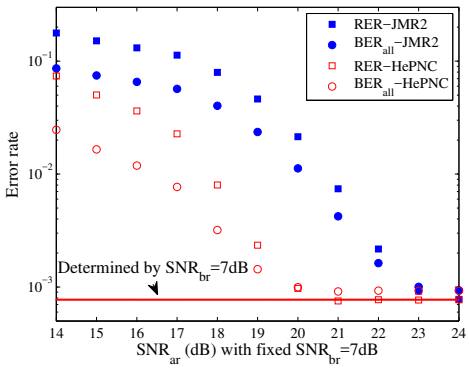

(c) 16QAM-BPSK HePNC.

Figure 2.9: Error rate with fixed SNR$_{br}$ under AWGN channels.

HePNC, when SNR$_{ar}$ is small, BER$_{all}$ is lower than RER; when SNR$_{ar}$ goes larger, RER is lower than BER$_{all}$. This is because when SNR$_{ar}$ is small, the BPSK circles on the received constellation map are relatively large, so the constellation points are close to or even overlap with each other, which leads to a higher BER. When SNR$_{ar}$

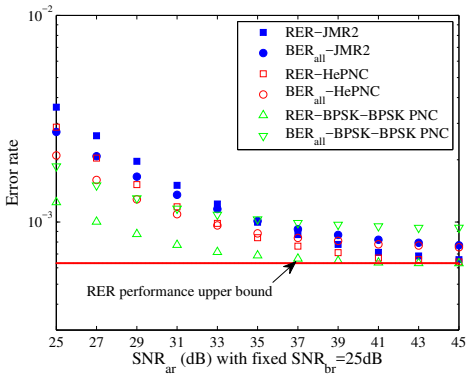

(a) QPSK-BPSK HePNC.

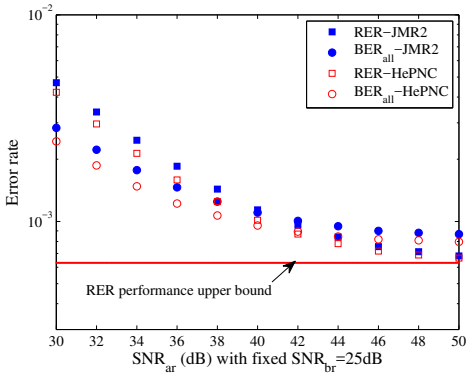

(b) 8PSK-BPSK HePNC.

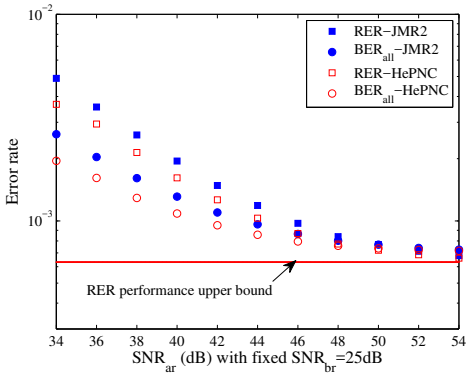

(c) 16QAM-BPSK HePNC.

Figure 2.10: Error rate with fixed SNR$_{br}$ in Rayleigh fading channels.

is large, the BPSK circles are relatively small, and errors in the bottleneck link L_{br} dominate the performance in the BC stage.

Figs. 2.9(b) and 2.9(c) compare the performance of HePNC and JMR2 with 8PSK-BPSK and 16QAM-BPSK. For a higher-order modulation HePNC, a larger

ΔSNR is needed to maintain the same BER and RER levels compared to the lower-order QPSK-BPSK HePNC. Given the same SNR_{br}, with the increase of SNR_{ar}, the RER performance of all the schemes converge to the error rate determined by $Q[\sqrt{2 \cdot \text{SNR}_{br}}]$, and BER_{all} is bounded by (2.14); however, the HePNC schemes converge monotonously and more quickly than JMR2.

Fig. 2.10 shows the performance of HePNC and JMR2 under Rayleigh fading channels. We fix $\text{SNR}_{br} = 25\,\text{dB}$ and gradually increase SNR_{ar}. When ΔSNR is large, the RERs of HePNC schemes converge to the error rate bounded by (2.16) as shown by the solid lines. However, HePNC does not have the same large performance gain over JMR2 as that in the AWGN case. Because under Rayleigh fading channels, $\gamma \in (0, \infty)$ with $\text{PDF}(\gamma)$ shown in (2.15), the channel condition of L_{ar} cannot be guaranteed to be always better than that of L_{br}, and the HePNC transmission may suffer a higher error rate for certain values of γ. Thus, if possible, the sources should apply adaptive modulation for HePNC according to the channel conditions. Fig. 2.10(a) also compares the error performance of QPSK-BPSK HePNC with BPSK-BPSK PNC. Under Rayleigh fading channel, the singular fade state affects the error performance of HePNC. Generally speaking, the error performance of higher-order modulation will result in worse error performance with the same value of SNR_{ar}. For example, when $\text{SNR}_{ar} = 34$ dB, the BER for BPSK-BPSK converges to the minimum, around 0.001, while that for 16QAM-BPSK is around 0.002. Furthermore, when SNR_{ar} is large enough, the RER performance of BPSK-BPSK PNC and that of HePNC converge to the same value (determined by SNR_{br}) because the error performance is dominated by the errors within one BPSK circle. Note that the BER performance of HePNC is slightly better than BPSK-BPSK PNC in the high SNR_{ar} region. This is because for HePNC, even if the relay broadcasts an erroneous network-coded symbol, source node B still has a probability to correctly obtain some bits of the higher-order modulation symbols.

From Figs. 2.9 and 2.10, it is observed that a proper HePNC scheme should be selected according to the channel conditions of both source-relay links. For example, in Fig. 2.9(a), SNR_{br} of the bottleneck link is 7 dB, which can support the single hop BPSK modulation with BER lower than 10^{-3} as shown by the red line. However, if SNR_{ar} equals or is close to 7 dB, the system BER performance of the QPSK-BPSK HePNC scheme is still much higher than 10^{-3}. Similar to the idea applied by the well known adaptive modulation, the HePNC system should consider both the two source-relay channel conditions and the data exchange ratio requirements to select

the HePNC schemes. In Sec. 2.6.2, the suitable relay locations for different HePNC schemes will be obtained, and Sec. 2.6.3 will study the throughput achieved for different data exchange ratio requirements.

2.6.2 Optimal relay with fixed SNR_{ab}

We study how the relay location influences the system error performance where the relay is located on the line segment between the two sources. We fix the distance between sources A and B as 600 m. Denote the distance between sources A and R as D_{ar}, and we gradually increase D_{ar} by moving the relay from sources A towards B. All channels are assumed AWGN ones. Note that, different from the scenario in Sec. 2.6.1, where error performance is studied by fixing SNR_{br}, here with the increase of D_{ar} by given SNR_{ab}, SNR_{ar} is reduced and SNR_{br} is increased.

Figs. 2.11(a) and 2.11(b) show the HePNC error performance with fixed $\mathrm{SNR}_{ab} =$ 0 dB and 3 dB, respectively. In Fig. 2.11(a), we consider BER_{all} as the system performance index, and there are optimal relay locations existing for QPSK-BPSK, 8PSK-BPSK and 16QAM-BPSK HePNC at $D_{ar} = 240$ m, 200 m and 170 m, respectively. To compare with the symmetric PNC scheme, the green curves show the performance of symmetric BPSK-BPSK PNC, for which the optimal relay locates in the middle of sources i.e., $D_{ar} = 300$ m. Note that for 8PSK-BPSK and 16QAM-BPSK HePNC, RERs are minimized when $D_{ar} = 200$ m and 150 m. Thus, at the optimal relay locations where the system performance is optimized in terms of BER_{all}, the RER performance may not be optimal. Before reaching the optimal relay locations, BER_{all} decreases first thanks to the improvement of the bottleneck link SNR_{br}. After the optimal relay location, BER_{all} becomes worse because SNR_{ar} cannot further support the higher-order modulation, and the BPSK circles become so large that they lead to more errors.

The underlying reason why the optimal relay locations exist can be observed from Fig. 2.1(b). D_{ar} determines the structure of the received constellation map at the relay, i.e., smaller D_{ar} leads to smaller BPSK circles, and larger D_{ar} leads to larger BPSK circles. When the BPSK circles are too small, the errors within one BPSK circle cause a higher RER; when the BPSK circles are too large, errors between different BPSK circles would cause a higher RER. Thus, there exists an optimal location of the relay to minimize the RER performance, which further affects the overall BER performance of the system. In summary, given the traffic load and the locations of

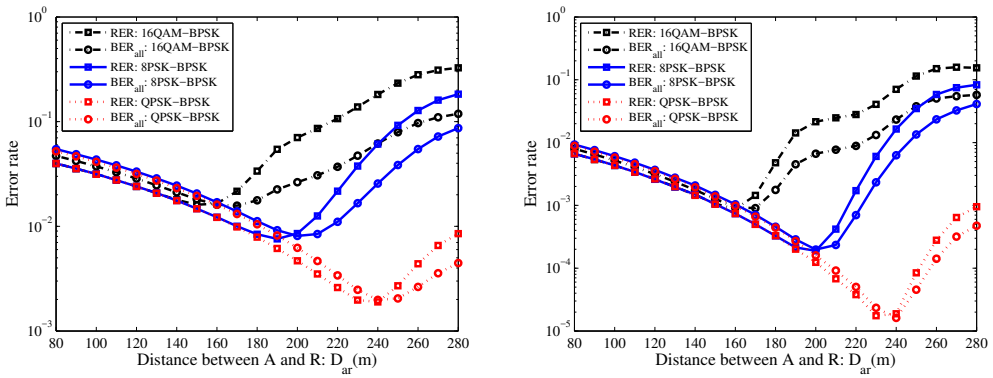

(a) $\mathrm{SNR}_{ab}=0$ dB. (b) $\mathrm{SNR}_{ab}=3$ dB.

Figure 2.11: HePNC performance with fixed SNR_{ab}.

the two source nodes, we can identify the optimal relay location and select the best relay. Then given the relay location under conditions of two source-relay channels, we can configure the modulation accordingly.

Comparing different HePNC schemes, the optimal relay locations of higher-order modulation HePNC have a smaller D_{ar} since a larger SNR_{ar} is needed to support the higher-order modulation. When D_{ar} is small, e.g., $D_{ar} \in$ (80 m, 140 m), the RER performance of different HePNC schemes including the symmetric BPSK-BPSK PNC scheme are the same, because RER is dominated by the bottleneck SNR_{br}, and it can be estimated by $Q[\sqrt{2 \cdot \mathrm{SNR}_{br}}]$. Thus, HePNC can support asymmetric data exchange ratio[12] with the same error performance compared to the symmetric BPSK-BPSK PNC scheme. In terms of BER_{all}, 8PSK-BPSK HePNC performs worst due to that a circle-shape constellation map has worse performance than a square-shape one. 16QAM-BPSK HePNC performs best in terms of BER_{all} because more bits can be successfully exchanged when errors happen in the BC stage thanks to Gray mapping.

Fig. 2.11(b) shows the performance of different HePNC schemes with $\mathrm{SNR}_{ab} =$ 3 dB. The relay locations where RER and BER_{all} are minimized change slightly, and the overall error performance is improved. Considering BER_{all}, the optimal relay locations for QPSK-BPSK and 8PSK-BPSK HePNC remain the same. For 16QAM-BPSK HePNC, the optimal relay location changes to $D_{ar}=160$ m. Thus, to optimize HePNC, both of the MA and BC stages should be considered, as errors in the BC stage also affect system performance.

[12]HePNC may support a higher throughput compared to the symmetric PNC for the asymmetric data exchange ratio as discussed in Sec. 2.6.3.

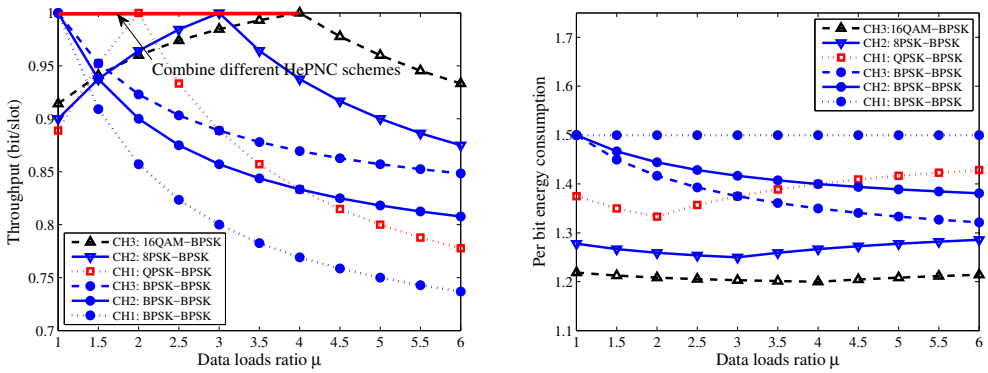

(a) Throughput upper bound. (b) Energy consumption.

Figure 2.12: Throughput upper bound and energy efficiency.

2.6.3 Throughput and energy efficiency

In this section, the throughput upper bound and energy efficiency of HePNC and symmetric BPSK-BPSK PNC are compared under the asymmetric TWRC scenario. We also consider asymmetric data loads of the sources. Let Sz_a denote the data load from source A to B, and Sz_b vice versa. $\mu = Sz_a/Sz_b$ indicates the degree of traffic asymmetry. In addition, it is also assumed that the source node with the better link to the relay always has more data to send[13]. For simplicity, we define one slot equal to symbol duration. Note that, in initialization of HePNC configuration, the relay needs to jointly consider two source-relay channel conditions and data exchange ratio requirements, which can be done by first transmitting requests from the sources to the relay individually including the data needed to be exchanged, and then the relay feedbacks the determined modulation scheme to the sources.

For a fair comparison, we consider three channel conditions: CH1, CH2 and CH3, in which link L_{ar} can support QPSK, 8PSK and 16QAM, respectively, with a negligible error rate, and link L_{br} can only support BPSK. In CH3, if not all the source A's (or source B's) bits can be transmitted by using the HePNC or BPSK-BPSK PNC, the leftover bits are sent to source B (source A) through relay R in two hops using 16QAM and BPSK over L_{ar} and L_{br}, respectively. Similarly, L_{ar} is assumed to support up to QPSK and 8PSK for CH1 and CH2, respectively, with negligible error rates. Note that for the symmetric PNC, both source nodes can only use BPSK

[13]For example, L_{ar} has a higher average SNR than L_{br} and $\mu \geq 1$. For case $\mu < 1$, HePNC can still be used but throughput and energy gains over the existing PNC are not as obvious.

modulation due to the bottleneck link L_{br}.

Fig. 2.12(a) shows throughput (bit/slot) upper bound of three HePNC schemes and BPSK-BPSK PNC under different traffic asymmetry μ. For BPSK-BPSK PNC, when $\mu = 1$, it achieves the highest throughput, 1 bit/slot; With the increase of μ, its throughput reduces, which indicates that BPSK-BPSK PNC is not suitable to support the asymmetric data loads exchange. For HePNC, all the throughput upper bound curves increase first till reaching the maximum, 1 bit/slot, and then reduce to stable levels. QPSK-BPSK, 8PSK-BPSK and 16QAM-BPSK reach their maximum when $\mu = 2$, $\mu = 3$ and $\mu = 4$, respectively. This is because all the bits can be exchanged using HePNC with a high efficiency when μ equals the optimal value and no bit has to be sent using the two-hop relay path.

To generalize how to choose HePNC suitable to various μ, under constraints of channel quality, it is most desirable to use 2^{μ}-PSK or QAM and BPSK modulation scheme for sources A and B, respectively. While μ is a non-integer, hybrid HePNC with different modulation over L_{ar} can be used. Assuming link L_{ar} can support $2^{\lceil \mu \rceil}$PSK–BPSK modulation (e.g., 16QAM), we can combine the HePNC using $2^{\lfloor \mu \rfloor}$PSK-BPSK and $2^{\lceil \mu \rceil}$PSK–BPSK to achieve a throughput of 1 bit/slot, e.g., when $\mu = 3.5$, 8PSK-BPSK HePNC and 16QAM-BPSK HePNC can be combined with the ratio of $1 : 1$. Note that when both source-relay links can support 2^m-PSK or QAM (for $m > 1$), the throughput can be higher than 1 bit/slot.

In Fig. 2.12(b), the energy efficiency is evaluated in terms of per bit end-to-end energy consumption, which measures the average energy consumption for each bit being delivered from the source to the destination. In the simulation, the symbol energy is assumed to be a constant E_s. As shown in Fig. 2.12(b), HePNC also achieves a higher energy efficiency than PNC. Obviously, for different modulation combinations, the highest energy efficiency of HePNC is achieved when $\mu = \max(m_a,\ m_b)$, e.g., $\mu = 4$ for 16QAM-BPSK HePNC.

Chapter 3

Design of Channel Coded Heterogeneous Modulation Physical Layer Network Coding

3.1 Overview

How to integrate the channel error control coding into PNC-based schemes is an important issue. In Chapter 2, we proposed the design of HePNC in symbol-level where only end-to-end channel coding can be integrated. Because the relay does not obtain individual bits of the superimposing symbols and the network-coded symbol may not be a valid codeword even if channel coding is applied to the sources. In this chapter, we investigate how to integrate channel coding into HePNC with link-to-link coding, where the relay tries to decode the superimposed codewords so noise in the multiple-access (MA) stage can be possibly cleared. We propose a channel coded HePNC (CoHePNC) and a full-state sum-product decoding algorithm at the relay, where full-state information from the superimposed signals are applied to the input of the decoding algorithm followed by a bit-level adaptive mapping process.

3.2 Related Work

The majority of work studying how to integrate channel error control coding into PNC refer to link-to-link coding. In the link-to-link coding [5, 39–49], the relay decodes codewords from two sources in the superimposed signals and tries to minimize trans-

mission errors in the MA stage. A primitive link-to-link coding PNC proposed in [39] utilized the property that, given a linear code, the XOR result of two linear codewords is still a valid codeword. Thus, the relay tries to decode the XOR result of the superimposed symbols. [5] integrated RA codes into symmetric PNC by re-designing the sum-product decoding algorithm at the relay. The essence in [5] is to upgrade message passing in decoding algorithm from traditional two-state[1] to three-state[2], where the state defines how many possibilities the decoding input have. [40] followed this idea and proposed a generalized sum-product decoding algorithm with four-state message, where carrier synchronization is not required. Other variants [41–43] studied combining low-density parity-check (LDPC) codes with PNC by modifying the sum-product decoding algorithm. [44] studied irregular repeat accumulate (IRA) code based on an extension of extrinsic information transfer (EXIT). [45–47] studied convolutional code with PNC and [46] studied convolutional and turbo codes under various channel conditions, and [47] further removed symbol-level synchronization requirement. Note that the above works only considered that BPSK modulation is applied by both sources, which simplifies the decoding design at the relay compared to higher-order modulation PNC. [48] studied that QPSK modulation is applied by both sources, followed by designing the network-coded sequence with XOR mapping. However, for higher-order modulation PNC design, XOR mapping is not optimal [37, 38, 68]. [49] integrated IRA with symmetric PNC where both sources apply QPSK or PAM, but they still considered symmetric link-to-link PNC only.

In practice, there may not exist a relay with symmetric two source-relay channel conditions and the data exchange requirement between two sources may be unequal. Thus, heterogeneous modulation PNC designs are desirable. [37, 38, 68, 85–87, 98] focused on the HePNC design in the symbol-level. In [37,38,68,85], the network-coded symbols are constructed adaptively according to two source-relay channel conditions. [86, 87, 98] focused on optimizing the modulation order of the network-coded symbol. However, the existing HePNC [37, 38, 68, 85–87, 98] can be combined with end-to-end coding only, and the design of link-to-link coding HePNC is still an open issue. In this chapter, we refer the designs in [37, 38, 68, 85–87, 98] as the symbol-level HePNC.

In this chapter, we study how to combine channel error control coding with

[1] In traditional hop-to-hop transmission, there are only two-state for the message passing in sum-product decoding algorithm when BPSK modulation is applied, i.e., either 0 or 1.

[2] As perfect symmetric source-relay channel conditions with carrier synchronization are assumed, three-state is maximal when BPSK is applied by both sources, which is further explained in Sec. 3.4.2

HePNC with link-to-link coding. We study RA codes and propose a full-state sum-product decoding algorithm containing full-state message passing jointly with bit-level adaptive mapping function designs, which are applied to construct the network-coded sequence in bit-level instead of symbol-level.

3.3 System Model and CoHePNC Procedure

3.3.1 System model

Consider an asymmetric TWRC scenario with the same setting as discussed in Chapter 2. In the following, we consider sources A and B use QPSK and BPSK modulation, respectively, subject to end-to-end BER requirement. Other higher-modulation CoHePNC can be similarly extended. We assume symbol-level synchronization at the relay and channel state information (CSI) is only available at the receivers. Note that, carrier-phase synchronization is not assumed.

The procedure of CoHePNC includes two stages, multiple access (MA) stage and broadcast (BC) stage. We focus on the MA stage design, because the main challenges when integrating channel coding into HePNC with link-to-link coding reside in the MA stage. To be more precise, the key issues are how to decode the superimposed codewords at the relay and how to construct the network-coded sequence, which contains the necessary information of the uncoded data in both sources, according to the decoding results. After the MA stage is properly designed, the upgrade of the BC stage from symbol-level HePNC to CoHePNC is straightforward.

3.3.2 CoHePNC procedure

In this subsection, we present the procedure of QPSK-BPSK CoHePNC with (K, N) channel coding. There are two key design differences between CoHePNC and symbol-level HePNC. The first one is that, in CoHePNC, source A with a higher-order modulation needs to re-organize two N-bit codewords into a new $2N$-bit sequence by intersecting their bits in sequence, and then modulates the $2N$-bit sequence by QPSK. The re-organizing process guarantees that codeword constructed only by the first bit (or second bit) of the QPSK symbols is a valid codeword related to source channel coding, which is a precondition for decoding algorithm design at the relay. The second one is that, in CoHePNC, the relay needs to construct a network-coded sequence in bit-

level as discussed in Sec. 3.4.4 instead of symbol-level in [37,38,68,85–87,98], i.e., the relay needs to construct the network-coded sequence from the decoding results of the superimposed codewords instead of directly from the demodulation results. Also, the network-coded sequence which contains necessary information of the uncoded source data needs to guarantee that each source can finally recover the other's information in the BC stage. We introduce CoHePNC procedure as follows.

Multiple access stage

A diagram of the CoHePNC procedure is shown in Fig. 3.1. We consider that the same (K, N) linear channel coding with coding efficiency $\frac{K}{N}$ is applied at both sources. Let $\mathbf{u}_{a1} = \{u_{a1}[1], \cdots, u_{a1}[K]\}$ and $\mathbf{u}_{a2} = \{u_{a2}[1], \cdots, u_{a2}[K]\}$ be two uncoded source data at A, and their codewords are $\mathbf{C}_{a1} = \{C_{a1}[1], \cdots, C_{a1}[N]\}$ and $\mathbf{C}_{a2} = \{C_{a2}[1], \cdots, C_{a2}[N]\}$, respectively, after encoding. Re-organize $\mathbf{C}_{a1}$ and $\mathbf{C}_{a2}$ to be a $2N$-bit sequence $\mathbf{C}_a = \{C_{a1}[1], C_{a2}[1], \cdots, C_{a1}[N], C_{a2}[N]\}$, i.e., to interleaver each bit of $\mathbf{C}_{a1}$ and $\mathbf{C}_{a2}$ in sequence. After that $\mathbf{C}_a$ is modulated by QPSK to be an N-symbol sequence $\mathbf{S}_a = \{S_a[1], \cdots, S_a[N]\}$. For the i-th element in $\mathbf{S}_a$, $S_a[i] = \langle C_{a1}[i], C_{a2}[i] \rangle$, where $\langle , \rangle$ denotes that two bits $C_{a1}[i]$ and $C_{a2}[i]$ are concatenated to be one QPSK symbol $S_a[i]$. At source B, uncoded source data $\mathbf{u}_b = \{u_b[1], \cdots, u_b[K]\}$ are encoded to $\mathbf{C}_b = \{C_b[1], \cdots, C_b[N]\}$, and then modulated to an N-symbol sequence $\mathbf{S}_b = \{S_b[1], \cdots, S_b[N]\}$ by BPSK. Let $\mathcal{M}_m$ be 2^m-QAM/PSK modulation with modulation order m. Let $\mathbf{X}_a$ and $\mathbf{X}_b$ be transmitted symbols from source A and B, respectively. We have $\mathbf{X}_a = \mathcal{M}_2(\mathbf{S}_a)$ and $\mathbf{X}_b = \mathcal{M}_1(\mathbf{S}_b)$, e.g., with BPSK, the i-th symbol $S_b[i] = 0$ and 1 is mapped to $X_b[i] = 1$ and -1, respectively.

Sources A and B use N symbol durations to transmit $\mathbf{X}_a$ and $\mathbf{X}_b$, respectively. At the i-th symbol duration, one QPSK symbol $X_a[i] = \mathcal{M}_2(S_a[i])$ and one BPSK symbol $X_b[i] = \mathcal{M}_1(S_b[i])$ are transmitted simultaneously and superimposed at the relay. The received signal $Y_r[i]$ at relay R is

$$Y_r[i] = H_a[i]X_a[i] + H_b[i]X_b[i] + N_0, \tag{3.1}$$

where $H_a[i]$ and $H_b[i]$ are channel gains over links L_{ar} and L_{br}, respectively[3], and N_0 is complex Gaussian noise with variance of $2\sigma^2$.

Different from symbol-level HePNC, where the relay can process demodulation in each symbol duration, in CoHePNC, the relay needs to obtain codewords $\mathbf{C}_a$

[3]We consider block fading channel, where H_a and H_b remain the same during N symbol durations.

and $\mathbf{C}_b$ in a period of N symbol durations and then processes the decoding input $\mathbf{Y}_r = \{Y_r[1], \cdots, Y_r[N]\}$. The final output after the decoding algorithm and mapping process is a well-designed network-coded sequence $\widehat{\mathbf{u}}_r = \{\widehat{u}_r[1], \cdots, \widehat{u}_r[K]\}$, $\widehat{u}_r[i] \in \{00, 01, 11, 10\}$ and $i \in \{1, \cdots, K\}$, where in this chapter we use wide-hat $\widehat{\cdot}$ to denote the estimation results. $\widehat{\mathbf{u}}_r$ contains necessary information of the uncoded source data $\widehat{\mathbf{u}}_{a1}$, $\widehat{\mathbf{u}}_{a2}$ and $\widehat{\mathbf{u}}_b$ so that each source can obtain the other source's information by recovering $\widehat{\mathbf{u}}_r$ in the BC stage. How to construct $\widehat{\mathbf{u}}_r$ is a critical issue. First, a basic requirement is that $\widehat{\mathbf{u}}_r$ contains necessary information of the uncoded source data. However, $\widehat{\mathbf{u}}_r$ should be constructed with as few bits as possible to reduce transmission load in the BC stage. Also, $\widehat{\mathbf{u}}_r$ should guarantee that transmission errors in the MA stage can be minimized. For 2^{m_a}QAM/PSK-2^{m_b}QAM/PSK CoHePNC, the minimum tuple of $\widehat{u}_r[i]$ is $\min(m_a, m_b)$. For QPSK-BPSK CoHePNC, which implies that $\widehat{u}_r[i] \in \{00, 01, 11, 10\}$, $i \in \{1, \cdots, K\}$. A brief explanation is that $u_r[i]$ at least needs two bits (four-tuple) to contain the information of $u_{a1}[i]$ and $u_{a2}[i]$ even if without considering the impact of $u_b[i]$. We show that $\min(m_a, m_b)$ is sufficient in Sec. 3.4.4.

One step before obtaining $\widehat{\mathbf{u}}_r$ is to obtain decoding results from the relay decoding algorithm, followed by mapping the decoding results to the network-coded sequence $\widehat{\mathbf{u}}_r$ according to mapping function $\mathcal{C}$. We discuss and compare several possible decoding and mapping solutions in Sec. 3.5, and then present the proposed full-state sum-product decoding algorithm which utilizes maximum-state information of $\mathbf{Y}_r$ as decoding input jointly mapping the output of the decoding algorithm with bit-level adaptive mapping functions to obtain network-coded sequence $\widehat{\mathbf{u}}_r$.

Broadcast stage

Let $\widehat{\mathbf{u}}_r = \langle \widehat{\mathbf{u}}_{r1}, \widehat{\mathbf{u}}_{r2} \rangle$, where $\widehat{\mathbf{u}}_{r1}$ and $\widehat{\mathbf{u}}_{r2}$ denote bit sequence composed of the first bit and second bit of $\widehat{u}_r[i]$, respectively. In the BC stage, the relay re-encodes $\widehat{\mathbf{u}}_{r1}$ and $\widehat{\mathbf{u}}_{r2}$ to be N-bit codewords $\mathbf{C}_{r1}$ and $\mathbf{C}_{r2}$, respectively[4], and then broadcasts the resulting codewords back to the sources. Due to the bottleneck link L_{br} can only support BPSK subject to the end-to-end BER requirement, the relay uses $2N$ symbol durations to broadcast $\mathbf{C}_{r1}$ and $\mathbf{C}_{r2}$ in sequence in the BC stage. Finally, each source decodes the estimated $\mathbf{C}_{r1}$ and $\mathbf{C}_{r2}$ as $\widehat{\widehat{\mathbf{u}}}_{r1}$ and $\widehat{\widehat{\mathbf{u}}}_{r2}$ by traditional decoding, respectively, and then

[4]Although theoretically the relay can use any channel coding to re-encode $\widehat{\mathbf{u}}_{r1}$ and $\widehat{\mathbf{u}}_{r2}$, for simplicity, we still consider the relay uses the same channel coding as applied in the source channel coding in the MA stage.

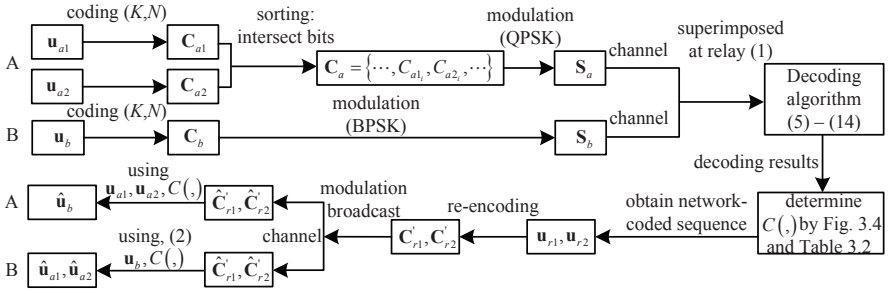

Figure 3.1: Diagram of integrating channel coding into HePNC in a link-to-link manner.

obtains each other's information by using the determined mapping function $\mathcal{C}$ and the original information transmitted by themselves. For example, at source A, the estimated i-th bit of $\mathbf{u}_b$ can be obtained by

$$\widehat{\widehat{u}}_b[i] = \underset{u_b[i]\in\{0,1\}}{\operatorname{argmin}} \left|\langle \widehat{\widehat{u}}_{r1}[i], \widehat{\widehat{u}}_{r2}[i]\rangle - \mathcal{C}(\langle u_{a1}[i], u_{a2}[i]\rangle, u_b[i])\right|^2. \tag{3.2}$$

Source B can obtain the estimations of $\mathbf{u}_{a1}$ and $\mathbf{u}_{a2}$, denoted as $\widehat{\widehat{\mathbf{u}}}_{a1}$ and $\widehat{\widehat{\mathbf{u}}}_{a1}$, in a similar way.

3.4 Design and Optimization Criteria

In this section, repeat-accumulate (RA) coding is studied as an example of linear channel coding integrated into HePNC. We analyze and compare several relay decoding and mapping solutions, and then elaborate the proposed full-state sum-product decoding algorithm for CoHePNC jointly with a bit-level adaptive mapping function design.

3.4.1 Repeat-accumulate encoding at the sources

RA coding can be considered as special LDPC codes with low complexity decoding operation, or special Turbo codes with linear complexity encoding operation. We refer the readers to [99–101] for more background of the RA codes and the sum-product decoding algorithm.

RA codes with repeat parameter $q = 3$ is applied by A and B. For two uncoded date sequences $\mathbf{u}_{a1} = \{u_{a1}[1], \cdots, u_{a1}[K]\}$ and $\mathbf{u}_{a2} = \{u_{a2}[1], \cdots, u_{a2}[K]\}$ at source

A, the codewords are $\mathbf{C}_{a1} = \{C_{a1}[1], \cdots, C_{a1}[N]\}$ and $\mathbf{C}_{a2} = \{C_{a2}[1], \cdots, C_{a2}[N]\}$, respectively. Let $\mathbf{u}'_{a1} = \{u_{a1}[1], u_{a1}[1], u_{a1}[1], \cdots, u_{a1}[K], u_{a1}[K], u_{a1}[K]\}$ be the duplication result of $\mathbf{u}_{a1}$ with duplication parameter $q=3$. Let $\mathbf{u}''_{a1}$ be interleaving[5] result of $\mathbf{u}'_{a1}$, and we have $u''_{a1}[i] = u'_{a1}[k]$, $i, k \in \{1, \cdots, N\}$, which denotes that the i-th element in $\mathbf{u}''_{a1}$ equals to the k-th element in $\mathbf{u}'_{a1}$. Similarly, let $\mathbf{u}'_{a2}$, $\mathbf{u}'_b$ and $\mathbf{u}''_{a2}$, $\mathbf{u}''_b$ be duplication and interleaving results for data flow $\mathbf{u}_{a2}$ and $\mathbf{u}_b$, respectively. For the i-th codeword, $i \in \{2, \cdots, N\}$, we have

$$\begin{aligned} C_{a1}[i] &= C_{a1}[i-1] \oplus u''_{a1}[i] = C_{a1}[i-1] \oplus u'_{a1}[k], \\ C_{a2}[i] &= C_{a2}[i-1] \oplus u''_{a2}[i] = C_{a2}[i-1] \oplus u'_{a2}[k], \\ C_b[i] &= C_b[i-1] \oplus u''_b[i] = C_b[i-1] \oplus u'_b[k], \end{aligned} \tag{3.3}$$

where $C_{a1}[1] = u''_{a1}[1]$, $C_{a2}[1] = u''_{a2}[1]$ and $C_b[1] = u''_b[1]$, and $\oplus$ denotes the XOR operation.

3.4.2 Relay decoding solutions extending from channel coded symmetric PNC

In this subsection, we present and compare the relay decoding and mapping options for channel coded HePNC by extending the decoding and mapping options from the existing channel coded symmetric PNC. For channel coded HePNC, according to whether the codewords $\mathbf{C}_{a1}$, $\mathbf{C}_{a2}$ and $\mathbf{C}_b$ are separately decoded or jointly decoded and how many states the message passing have in the re-designed sum-product decoding algorithm, solutions for channel coded HePNC at the relay can be summarized as follows.

Separately decode $\mathbf{C}_{a1}$, $\mathbf{C}_{a2}$ and $\mathbf{C}_b$

A straightforward solution extended from the symmetric channel coded PNC is to perform three traditional sum-product decoding processes to decode each of $\mathbf{C}_{a1}$, $\mathbf{C}_{a2}$ and $\mathbf{C}_b$ individually, and then obtain network-coded sequence $\widehat{\mathbf{u}}_r = \langle \widehat{\mathbf{u}}_{r1}, \widehat{\mathbf{u}}_{r2} \rangle$ by letting $\widehat{\mathbf{u}}_{r1} = \widehat{\mathbf{C}}_{a1}$ XOR $\widehat{\mathbf{C}}_b$ and $\widehat{\mathbf{u}}_{r2} = \widehat{\mathbf{C}}_{a2}$ XOR $\widehat{\mathbf{C}}_b$. In this method, the mapping process is included by the XOR operation obtaining $\widehat{\mathbf{u}}_{r1}$ and $\widehat{\mathbf{u}}_{r2}$. This method is not optimal due to over-decoding [5,102], as the relay only needs to obtain network-coded forms $\mathbf{u}_{r1}$ and $\mathbf{u}_{r2}$ instead of obtaining $\widehat{\mathbf{C}}_{a1}$, $\widehat{\mathbf{C}}_{a2}$ and $\widehat{\mathbf{C}}_b$ explicitly.

[5]The interleaving pattern is the same and known by all nodes.

Separately decode $\mathbf{C}_{a1}$ XOR $\mathbf{C}_b$ and $\mathbf{C}_{a2}$ XOR $\mathbf{C}_b$

By extending the decoding solutions for symmetric BPSK-BPSK channel coded PNC [39], we can decompose the QPSK-BPSK channel coded HePNC into two BPSK-BPSK channel coded PNC and perform two BPSK-BPSK symmetric channel coded PNC decoding individually. In other words, consider codewords $\mathbf{C}_{a1}$ and $\mathbf{C}_b$, and $\mathbf{C}_{a2}$ and $\mathbf{C}_b$ as separate flows with a solution of BPSK-BPSK channel coded PNC for each flow. We use one flow $\mathbf{C}_{a1}$ and $\mathbf{C}_b$ to explain, and the solution to the other flow is equivalent. For BPSK-BPSK channel coded PNC, when sources apply the same linear channel coding, the result of $\mathbf{C}_{a1}$ XOR $\mathbf{C}_b$ is still a valid codeword associated with the channel coding applied at sources [39]. To apply this property in the sum-product decoding algorithm, the i-th input of the evidence node, $i \in \{1, \cdots, N\}$ can be a two-state message $\Pr\{(\widehat{C}_{a1}[i], \widehat{C}_b[i]) = (0,0)\} + \Pr\{(\widehat{C}_{a1}[i], \widehat{C}_b[i]) = (1,1)\}$ and $\Pr\{(\widehat{C}_{a1}[i], \widehat{C}_b[i]) = (0,1)\} + \Pr\{(\widehat{C}_{a1}[i], \widehat{C}_b[i]) = (1,0)\}$, i.e., the binary results of $\widehat{\mathbf{C}}_{a1}$ XOR $\widehat{\mathbf{C}}_b$. Thus, traditional sum-product decoding algorithm can be directly applied.

It was found that for BPSK-BPSK channel coded PNC, the input of the sum-product decoding algorithm at the relay can be a three-state message [5, 44] instead of a two-state one, i.e., $\Pr\{(\widehat{C}_{a1}[i], \widehat{C}_b[i]) = (0,0)\}$, $\Pr\{(\widehat{C}_{a1}[i], \widehat{C}_b[i]) = (0,1)\} + \Pr\{(\widehat{C}_{a1}[i], \widehat{C}_b[i]) = (1,0)\}$ and $\Pr\{(\widehat{C}_{a1}[i], \widehat{C}_b[i]) = (1,1)\}$. However, it brings new challenges that traditional sum-product decoding algorithm needs to be re-designed to fit the PNC feature. [40,41] further generalized [5,44] and proposed a four-state message sum-product decoding algorithm, where the i-th input of the decoding algorithm at the relay are four-state message $\Pr\{(\widehat{C}_{a1}[i], \widehat{C}_b[i]) = (0,0)\}$, $\Pr\{(\widehat{C}_{a1}[i], \widehat{C}_b[i]) = (0,1)\}$, $\Pr\{(\widehat{C}_{a1}[i], \widehat{C}_b[i]) = (1,0)\}$ and $\Pr\{(\widehat{C}_{a1}[i], \widehat{C}_b[i]) = (1,1)\}$ and showed that the four-state sum-product decoding algorithm outperforms the two-state and three-state decoding algorithms.

Jointly decoding $\mathbf{C}_{a1}$, $\mathbf{C}_{a2}$ and $\mathbf{C}_b$

The decoding solutions [5, 39–41, 44] focused on channel coded PNC design under symmetric TWRC, where BPSK modulation and the same linear channel coding are applied at both sources. [48, 49] studied symmetric channel coded PNC with QPSK/PAM modulations with XOR mapping. An upgrade from [48, 49] for QPSK-BPSK channel coded HePNC is to pass the message with four-state results of $\mathbf{C}_{a1}$

XOR $\mathbf{C}_b$ and $\mathbf{C}_{a2}$ XOR $\mathbf{C}_b$, i.e.,

$$\begin{aligned}
&\Pr\{(\widehat{C}_{a1}[i], \widehat{C}_{a2}[i], \widehat{C}_b[i]) = (0,0,0) \cup (1,1,1)\},\\
&\Pr\{(\widehat{C}_{a1}[i], \widehat{C}_{a2}[i], C_b[i]) = (0,1,0) \cup (1,0,1)\},\\
&\Pr\{(\widehat{C}_{a1}[i], \widehat{C}_{a2}[i], \widehat{C}_b[i]) = (1,1,0) \cup (0,0,1)\},\\
&\Pr\{(\widehat{C}_{a1}[i], \widehat{C}_{a2}[i], \widehat{C}_b[i]) = (1,0,0) \cup (0,1,1)\},
\end{aligned} \tag{3.4}$$

followed by using the four-state message decoding algorithm in [40,41] with the above four-state message as the decoding input.

For higher-order modulation HePNC, e.g., QPSK-BPSK channel coded HePNC, $\mathbf{C}_{a1}$ and $\mathbf{C}_{a2}$ can be jointly decoded together with $\mathbf{C}_b$. In this chapter, we propose a full-state sum-product decoding algorithm for QPSK-BPSK CoHePNC under asymmetric TWRC jointly with a bit-level adaptive mapping function design. The new contributions of the decoding algorithm proposed include two parts: first, we design the message updating rules for QPSK-BPSK CoHePNC with full-state message passing, which are different from updating rules of the existing symmetric channel coded PNC; second, we further show that the bit-level adaptive mapping design should be applied to obtain the network-coded sequence instead of symbol-level mapping. The proposed adaptive mapping design can also be applied to optimize the symmetric channel coded PNC under symmetric TWRC scenario.

3.4.3 Full-state sum-product decoding algorithm

In this subsection, we elaborate the proposed full-state decoding algorithm at the relay. The first is to obtain the eight-ary estimation results of $\widehat{\mathbf{u}}_{a1}$, $\widehat{\mathbf{u}}_{a2}$ and $\widehat{\mathbf{u}}_b$ from the received superimposed signals $\mathbf{Y}_r$. For QPSK-BPSK link-to-link channel coded HePNC, the maximum number of states at the relay is eight. Thus, in the following, we use eight-state and full-state interchangeably. The second step, which is discussed in Sec. 3.4.4, is to obtain the four-ary network-coded sequence $\widehat{\mathbf{u}}_r$ from the eight-ary decoding results.

The same interleaver is applied by both sources. We virtually combine uncoded data sequences $\mathbf{u}_{a1}$, $\mathbf{u}_{a2}$ and $\mathbf{u}_b$ as an ensemble $\mathbf{u}_{a1}\mathbf{u}_{a2}\mathbf{u}_b$ for concise, where the i-th element $u_{a1}[i]u_{a2}[i]u_b[i] \in \{000, 001, 010, 011, 110, 111, 100, 101\}$, $i \in \{1, \cdots, K\}$. Equivalently, we can obtain duplication result $\mathbf{u}'_{a1}\mathbf{u}'_{a1}\mathbf{u}'_b$, interleaving result $\mathbf{u}''_{a1}\mathbf{u}''_{a1}\mathbf{u}''_b$ and codeword $\mathbf{C}_{a1}\mathbf{C}_{a2}\mathbf{C}_b$, where $u'_{a1}[i]u'_{a2}[i]u'_b[i] = u''_{a1}[k]u''_{a2}[k]u''_b[k]$ and $i, k \in \{1, \cdots, N\}$.

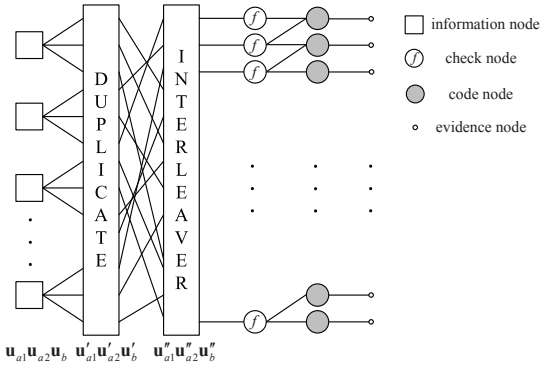

Figure 3.2: Tanner graph.

The corresponding Tanner graph [101] is shown in Fig. 3.2. The square nodes denote information nodes, where the i-th information node stores $\Pr\{\widehat{u}_{a1}[i]\widehat{u}_{a2}[i]\widehat{u}_b[i]\}$, $i \in \{1, \cdots, K\}$. The blocks of duplicate and interleaver store the probabilities of $\widehat{\mathbf{u}}'_{a1}\widehat{\mathbf{u}}'_{a2}\widehat{\mathbf{u}}'_b$ and $\widehat{\mathbf{u}}''_{a1}\widehat{\mathbf{u}}''_{a2}\widehat{\mathbf{u}}''_b$, respectively. The round nodes with function $f(.)$ are the check nodes, which denote that the edges connected to the same check nodes need to satisfy constraint $f(.)$. The dark circles are the code nodes, which store the probabilities of $\widehat{\mathbf{C}}_{a1}\widehat{\mathbf{C}}_{a2}\widehat{\mathbf{C}}_b$. The small circles are evidence nodes, which denote the input of the decoding algorithm.

The encoding process can be considered as reading the Tanner graph shown in Fig. 3.2 from left to right [99–101]. The decoding process starts from adding input into the evidence nodes on the rightmost and then passes the eight-state message iteratively between the information nodes and code nodes. The message are the probabilities of $\Pr\{\widehat{C}_{a1}[i]\widehat{C}_{a2}[i]\widehat{C}_b[i]\}$, $\Pr\{\widehat{u}'_{a1}[i]\widehat{u}'_{a2}[i]\widehat{u}'_b[i]\}$, $\Pr\{\widehat{u}''_{a1}[i]\widehat{u}''_{a2}[i]\widehat{u}''_b[i]\}$ and $\Pr\{\widehat{u}_{a1}[i]\widehat{u}_{a2}[i]\widehat{u}_b[i]\}$ depending on the type of nodes that the messages are associated with. We present the decoding algorithm of CoHePNC as follows, where steps 1) and 2) are the decoding settings, and steps 3) and 4) are the iteration bodies. Step 5) denotes the termination condition.

Step 1: Initialization

Let $\mathbf{P} = (p_1, p_2, p_3, p_4, p_5, p_6, p_7, p_8)$ and $\mathbf{Q} = (q_1, q_2, q_3, q_4, q_5, q_6, q_7, q_8)$ be the message input from two different nodes. All the messages associated with the edges are set to be $(\frac{1}{8}, \frac{1}{8}, \frac{1}{8}, \frac{1}{8}, \frac{1}{8}, \frac{1}{8}, \frac{1}{8}, \frac{1}{8})$ initially except for the messages on the edges connected to the evidence nodes.

Step 2: Input of the evidence nodes

The input of the decoding algorithm is the message from evidence nodes, which contains eight-state probabilities of $\widehat{\mathbf{C}}_{a1}\widehat{\mathbf{C}}_{a2}\widehat{\mathbf{C}}_b$ obtained from the superimposed signals $\mathbf{Y}_r$ in (3.1). Denote the input of the i-th evidence node as

$$p_{input}[i] = (p_1, p_2, p_3, p_4, p_5, p_6, p_7, p_8). \tag{3.5}$$

Define function $g(.)$ as

$$g(x_a, x_b) = \frac{1}{\beta}\exp(\frac{-|Y_k[i] - H_a x_a - H_b x_b|^2}{2\sigma^2}). \tag{3.6}$$

Specify $p_1 = g(\frac{\sqrt{2}+\sqrt{2}j}{2}, 1)$, $p_2 = g(\frac{\sqrt{2}+\sqrt{2}j}{2}, -1)$, $p_3 = g(\frac{-\sqrt{2}+\sqrt{2}j}{2}, 1)$, $p_4 = g(\frac{-\sqrt{2}+\sqrt{2}j}{2}, -1)$, $p_5 = g(\frac{-\sqrt{2}-\sqrt{2}j}{2}, 1)$, $p_6 = g(\frac{-\sqrt{2}-\sqrt{2}j}{2}, -1)$, $p_7 = g(\frac{\sqrt{2}-\sqrt{2}j}{2}, 1)$ and $p_8 = g(\frac{\sqrt{2}-\sqrt{2}j}{2}, -1)$, where j is the imaginary part and β is a normalization parameter to satisfy that $\sum_{i=1}^{8} p_i = 1$. We can find that $p_i, i \in \{1, \cdots, 8\}$ in $p_{input}[i]$ denotes one of the probabilities of $X_a[i] \in \{\frac{\sqrt{2}+\sqrt{2}j}{2}, \frac{-\sqrt{2}+\sqrt{2}j}{2}, \frac{-\sqrt{2}-\sqrt{2}j}{2}, \frac{\sqrt{2}-\sqrt{2}j}{2}\}$ and $X_b[i] \in \{1, -1\}$.

Step 3: Message updating for the variable nodes

Both code nodes and information nodes are variable nodes. Each variable node is connected to three other nodes (except for the code node at the bottom). Denote the output message of the variable node as $\mathrm{VAR}(\mathbf{P}, \mathbf{Q})$, where $\mathbf{P}$ and $\mathbf{Q}$ denote the message input from two connected edges and the output is the updated message on the rest edge. From [5, 44], we can obtain that the output message for variable node is

$$\mathrm{VAR}(\mathbf{P}, \mathbf{Q}) = \frac{(p_1 q_1, p_2 q_2, p_3 q_3, p_4 q_4, p_5 q_5, p_6 q_6, p_7 q_7, p_8 q_8)}{\alpha}, \tag{3.7}$$

where α is a normalization parameter which satisfies that $\sum_{i=1}^{8} \frac{1}{\alpha} p_i q_i = 1$.

Step 4: Message updating for the check nodes

One of the key issues in the sum-product decoding algorithm applied in PNC is how to design the message updating rules for check nodes. Each check node is connected to three edges (except for the check node at the top). Denote the output message of the check node as $\mathrm{CHK}(\mathbf{P}, \mathbf{Q})$, where $\mathbf{P}$ and $\mathbf{Q}$ denote the message input from two connected edges and the output is the updated message on the rest edge. As Gray

mapping is applied at source A, i.e., $\langle \mathbf{C}_{a1}, \mathbf{C}_{a2} \rangle \in \{00, 01, 11, 10\}$ are modulated as $\mathbf{X}_a \in \{\frac{\sqrt{2}+\sqrt{2}j}{2}, \frac{-\sqrt{2}+\sqrt{2}j}{2}, \frac{-\sqrt{2}-\sqrt{2}j}{2}, \frac{\sqrt{2}-\sqrt{2}j}{2}\}$ in the constellation map, respectively, for the i-th symbol duration, rewrite (3.1) as

$$\begin{aligned} Y_r[i] =& H_a[i]\{\frac{\sqrt{2}}{2}j(1-2C_{a1}[i]) + \frac{\sqrt{2}}{2}(1-2C_{a2}[i])\} \\ &+ H_b[i](1-2C_b[i]) + N_0, \end{aligned} \tag{3.8}$$

where $C_{a1}[i], C_{a2}[i], C_b[i] \in \{0, 1\}$. From (3.3) and (3.8), we have $C_{a1}[i] = C_{a1}[i-1] \oplus u'_{a1}[k]$, $C_{a2}[i] = C_{a2}[i-1] \oplus u'_{a2}[k]$ and $C_b[i] = C_b[i-1] \oplus u'_b[k]$. Note that, we have substituted $u''_{a1}[i]u''_{a2}[i]u''_b[i]$ with $u'_{a1}[k]u'_{a2}[k]u'_b[k]$.

Consider that two input messages $\mathbf{P}$ and $\mathbf{Q}$ defined in (3.7) are from code nodes and the output is the edge connected to interleaver. To obtain the function $f(.)$ processed in the check node, we target to obtain

$$\Pr\{\widehat{u}'_{a1}[k]\widehat{u}'_{a2}[k]\widehat{u}'_b[k]\} = f(\Pr\{\widehat{C}_{a1}[i]\widehat{C}_{a2}[i]\widehat{C}_b[i]\}, \Pr\{\widehat{C}_{a1}[i-1]\widehat{C}_{a2}[i-1]\widehat{C}_b[i-1]\}). \tag{3.9}$$

From (3.9), we have

$$\begin{aligned} &\Pr(\widehat{u}'_{a1}[k]\widehat{u}'_{a2}[k]\widehat{u}'_b[k] = 000|\mathbf{P}, \mathbf{Q}) \\ &= \sum_{i=1}^{8} \Pr(\widehat{C}_{a1}[i]\widehat{C}_{a2}[i]\widehat{C}_b[i] = \widehat{C}_{a1}[i-1]\widehat{C}_{a2}[i-1]\widehat{C}_b[i-1]) = \sum_{i=1}^{8} p_i q_i \triangleq \lambda_1. \end{aligned} \tag{3.10}$$

Similar to (3.10), we have

$$\begin{bmatrix} \lambda_2 \\ \lambda_3 \\ \lambda_4 \\ \lambda_5 \\ \lambda_6 \\ \lambda_7 \\ \lambda_8 \end{bmatrix} \triangleq \begin{bmatrix} \Pr(\widehat{u}'_{a1}[k]\widehat{u}'_{a2}[k]\widehat{u}'_b[k] = 001|\mathbf{P}, \mathbf{Q}) \\ \Pr(\widehat{u}'_{a1}[k]\widehat{u}'_{a2}[k]\widehat{u}'_b[k] = 010|\mathbf{P}, \mathbf{Q}) \\ \Pr(\widehat{u}'_{a1}[k]\widehat{u}'_{a2}[k]\widehat{u}'_b[k] = 011|\mathbf{P}, \mathbf{Q}) \\ \Pr(\widehat{u}'_{a1}[k]\widehat{u}'_{a2}[k]\widehat{u}'_b[k] = 110|\mathbf{P}, \mathbf{Q}) \\ \Pr(\widehat{u}'_{a1}[k]\widehat{u}'_{a2}[k]\widehat{u}'_b[k] = 111|\mathbf{P}, \mathbf{Q}) \\ \Pr(\widehat{u}'_{a1}[k]\widehat{u}'_{a2}[k]\widehat{u}'_b[k] = 100|\mathbf{P}, \mathbf{Q}) \\ \Pr(\widehat{u}'_{a1}[k]\widehat{u}'_{a2}[k]\widehat{u}'_b[k] = 101|\mathbf{P}, \mathbf{Q}) \end{bmatrix} = \begin{bmatrix} q_2 & q_1 & q_4 & q_3 & q_6 & q_5 & q_8 & q_7 \\ q_3 & q_4 & q_1 & q_2 & q_7 & q_8 & q_5 & q_6 \\ q_4 & q_3 & q_2 & q_1 & q_8 & q_7 & q_6 & q_5 \\ q_5 & q_6 & q_7 & q_8 & q_1 & q_2 & q_3 & q_4 \\ q_6 & q_5 & q_8 & q_7 & q_2 & q_1 & q_4 & q_3 \\ q_7 & q_8 & q_5 & q_6 & q_3 & q_4 & q_1 & q_2 \\ q_8 & q_7 & q_6 & q_5 & q_4 & q_3 & q_2 & q_1 \end{bmatrix} \begin{bmatrix} p_1 \\ p_2 \\ p_3 \\ p_4 \\ p_5 \\ p_6 \\ p_7 \\ p_8 \end{bmatrix} \tag{3.11}$$

Thus, the function $f(.)$ at the check node for the case that the input message are from two code nodes can be summarized in (3.10) and (3.11). The other two

cases are that the input message are from $\widehat{u}'_{a1}[k]\widehat{u}'_{a2}[k]\widehat{u}'_{b}[k]$ $(u''_{a1}[i]u''_{a2}[i]u''_{b}[i])$ and $\widehat{C}_{a1}[i]\widehat{C}_{a2}[i]\widehat{C}_{b}[i]$ or from $\widehat{u}'_{a1}[k]\widehat{u}'_{a2}[k]\widehat{u}'_{b}[k]$ $(u''_{a1}[i]u''_{a2}[i]u''_{b}[i])$ and $\widehat{C}_{a1}[i–1]\widehat{C}_{a2}[i–1]\widehat{C}_{b}[i–1]$, and the corresponding outputs are $\widehat{C}_{a1}[i-1]\widehat{C}_{a2}[i-1]\widehat{C}_{b}[i-1]$ and $\widehat{C}_{a1}[i]\widehat{C}_{a2}[i]\widehat{C}_{b}[i]$, respectively. For these two cases, the same update rules shown in (3.10) and (3.11) can be obtained similarly. Thus, the updating rules for the check nodes can be summarized as

$$\mathrm{CHK}(\mathbf{P},\mathbf{Q}) = (\lambda_1,\lambda_2,\lambda_3,\lambda_4,\lambda_5,\lambda_6,\lambda_7,\lambda_8). \tag{3.12}$$

Step 5: Iteration termination

The message is passed iteratively between code nodes and information nodes with the updating rules summarized in (3.7) and (3.12) starting from input of the evidence nodes summarized in (3.5) and (3.6). The output of the i-th information node is

$$p_{output}[i] = \mathrm{VAR}(\mathrm{VAR}(\mathbf{P}_1,\mathbf{P}_2),\mathbf{P}_3), \tag{3.13}$$

where $\mathbf{P}_1$, $\mathbf{P}_2$ and $\mathbf{P}_3$ denote the input message on the three edges connected to the i-th information node. Thus, decoding result $\widehat{u}_{a1}[i]\widehat{u}_{a2}[i]\widehat{u}_{b}[i]$ can be obtain by selecting the maximum probabilities in $p_{output}[i]$. The iteration terminates either with a fixed number of iterations or when achieving a BER threshold. In our work, the iteration terminates with a fixed number of iterations.

3.4.4 Bit-level mapping function design

Although the estimations of the uncoded source data is $2^{m_a+m_b}$-ary, the relay only needs to construct a $2^{\max(m_a,m_b)}$-ary network-coded sequence benefiting from the network coding. Each source can recover the other's information after obtaining the network-coded sequence using the mapping function $\mathcal{C}$ and the original information transmitted by itself as (3.2). In this subsection, we discuss how to map the $2^{m_a+m_b}$-ary decoding result $\widehat{\mathbf{u}}_{a1}\widehat{\mathbf{u}}_{a2}\widehat{\mathbf{u}}_{b}$ to the $2^{\max\{m_a,m_b\}}$-ary network-coded sequence $\widehat{\mathbf{u}}_{r}$. With traditional XOR mapping [5, 39, 40, 44], the i-th symbol $\widehat{u}_r[i]$ can be obtained as $\widehat{u}_r[i] = \langle \widehat{u}_{r1}[i], \widehat{u}_{r2}[i]\rangle = \langle \widehat{u}_{a1}[i] \oplus \widehat{u}_{b}[i], \widehat{u}_{a2}[i] \oplus \widehat{u}_{b}[i]\rangle$. In the following, we show that traditional XOR mapping is not optimal, and bit-level adaptive mapping functions should be designed and applied according to source-relay channel conditions. Note that, the bit-level mapping function design proposed in CoHePNC is different from the symbol-level mapping function design in symbol-level HePNC [37,38,68,85–87,98]. In

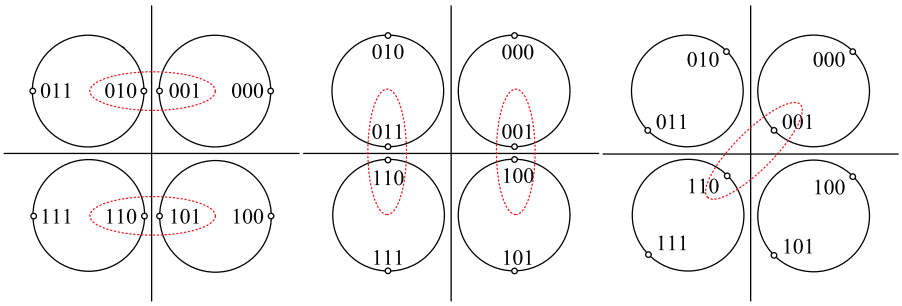

(a) $\theta = 0$. (b) $\theta = \frac{\pi}{2}$. (c) $\theta = \frac{\pi}{4}$.

Figure 3.3: Constellation maps with different phase shift θ.

Table 3.1: Constraints between $C_{a1}[i]C_{a2}[i]C_b[i]$, $C_{a1}[i-1]C_{a2}[i-1]C_b[i-1]$ and $u''_{a1}[i]u''_{a2}[i]u''_b[i]$

$C_{a1}[i-1]C_{a2}[i-1]C_b[i-1]$	000	001	010	011	110	111	100	101
$\widehat{u}''_{a1}[i]\widehat{u}''_{a2}[i]\widehat{u}''_b[i], C_{a1}[i]C_{a2}[i]C_b[i]=001$	001	000	011	010	111	110	101	100
$\widehat{u}''_{a1}[i]\widehat{u}''_{a2}[i]\widehat{u}''_b[i], C_{a1}[i]C_{a2}[i]C_b[i]=010$	010	011	000	001	100	101	110	111

the symbol-level HePNC, the relay tries to map the demodulation results $\widehat{\mathbf{C}}_{a1}\widehat{\mathbf{C}}_{a2}\widehat{\mathbf{C}}_b$ to the network-coded symbols $\widehat{\mathbf{u}}_r$ directly. However, in CoHePNC, $\widehat{\mathbf{C}}_{a1}\widehat{\mathbf{C}}_{a2}\widehat{\mathbf{C}}_b$ are first decoded to $\widehat{\mathbf{u}}_{a1}\widehat{\mathbf{u}}_{a2}\widehat{\mathbf{u}}_b$, and then the network-coded sequence is obtained from mapping $\widehat{\mathbf{u}}_{a1}\widehat{\mathbf{u}}_{a2}\widehat{\mathbf{u}}_b$ to $\widehat{\mathbf{u}}_r$. Thus, the bit-level mapping function design needs to consider the impact of decoding algorithm.

We use an example to show why the bit-level adaptive mapping design is necessary. Define γ and θ as amplitude ratio and phase shift difference of two source-relay channels, we have $H_b/H_a = \gamma \exp(j\theta)$. Consider the received constellation map at the relay in the i-th symbol duration shown in Fig. 3.3(a), where $\gamma = |\frac{H_b}{H_a}| \approx \frac{\sqrt{2}}{2}$ and $\theta = 0$. The Euclidean distance between constellation points $C_{a1}[i]C_{a2}[i]C_b[i] = 000$ and 001 is small, so is that between $C_{a1}[i]C_{a2}[i]C_b[i] = 110$ and 101. Assume that $C_{a1}[i]C_{a2}[i]C_b[i] = 010$ is correct. If without noise, the input of the i-th evidence node is $p_{input}[i] = (0,0,1,0,0,0,0,0,0,0)$, i.e., $\Pr\{C_{a1}[i]C_{a2}[i]C_b[i] = 010\} = 1$. However, with noise, due to the small Euclidean distance between constellation points 010 and 001, there is a large error probability that $\Pr\{\widehat{C}_{a1}[i]\widehat{C}_{a2}[i]\widehat{C}_b[i] = 001\}$ in error instead of $\Pr\{\widehat{C}_{a1}[i]\widehat{C}_{a2}[i]\widehat{C}_b[i] = 010\}$, i.e., the input of the i-th evidence node implies that the codeword $C_{a1}[i]C_a[i]C_b[i]$ is 001 in error instead of 010. This error probability increases when the Euclidean distance between 010 and 001 decreases.

We analyze the cast that if the input of the i-th evidence code, $\Pr\{\widehat{C}_{a1}[i]\widehat{C}_{a2}[i]\widehat{C}_b[i]\}$

Table 3.2: Mapping functions

	00	01	11	10
0	00	01	11	10
$1(\mathcal{C}_1)$	01	00	10	11
$1(\mathcal{C}_2)$	10	11	01	00
$1(\mathcal{C}_3)$	11	10	00	01

equals 001 is largest in error instead of $\Pr\{\widehat{C}_{a1}[i]\widehat{C}_{a2}[i]\widehat{C}_b[i] = 010\}$. For simplicity, we consider that the input of the i-th evidence node is 001 instead of 010 to stand for that $\Pr\{\widehat{C}_{a1}[i]\widehat{C}_{a2}[i]\widehat{C}_b[i] = 001\}$ has the highest probability. During each iteration, to update the i-th check node, the input messages $\Pr\{\widehat{C}_{a1}[i-1]\widehat{C}_{a2}[i-1]\widehat{C}_b[i-1]\}$ and $\Pr\{\widehat{C}_{a1}[i]\widehat{C}_{a2}[i]\widehat{C}_b[i]\}$ are from the i-th code node and the $(i-1)$-th code node, respectively. As $C_{a1}[i–1]C_{a2}[i–1]C_b[i–1]$ and $C_{a1}[i]C_{a2}[i]C_b[i]$ are independent [5], the output of the i-th code node $u''_{a1}[i]u''_{a2}[i]u''_b[i]$ is summarized in Table 3.1 according to (3.12), where $\widehat{C}_{a1}[i]\widehat{C}_{a2}[i]\widehat{C}_b[i]$ equals 011 falsely or 010 correctly and $\widehat{C}_{a1}[i-1]\widehat{C}_{a2}[i-1]\widehat{C}_b[i-1]$ equals $\{000, 001, 010, 011, 110, 111, 100, 101\}$ with the same probability of $\frac{1}{8}$. The estimation $\widehat{u}''_{a1}[i]\widehat{u}''_{a2}[i]\widehat{u}''_b[i]$ directly impacts on $\widehat{u}_{a1}[k]\widehat{u}_{a2}[k]\widehat{u}_b[k]$, as $u''_{a1}[i]u''_{a2}[i]u''_b[i] = u'_{a1}[k]u'_{a2}[k]u'_b[k]$, and $u'_{a1}[k]u'_{a2}[k]u'_b[k]$ is a duplication of $u_{a1}[\lceil\frac{k}{3}\rceil]u_{a2}[\lceil\frac{k}{3}\rceil]u_b[\lceil\frac{k}{3}\rceil]$. According to Table 3.1, there is a higher error probability that $\widehat{u}''_{a1}[i]\widehat{u}''_{a2}[i]\widehat{u}''_b[i]$ is estimated to be $\{001, 000, 011, 010, 111, 110, 101, 100\}$ falsely instead of $\{010, 011, 000, 001, 100, 101, 110, 111\}$ correctly. Thus, to minimize the estimation error in the uncoded source data $u_{a1}[\lceil\frac{k}{3}\rceil]u_{a2}[\lceil\frac{k}{3}\rceil]u_b[\lceil\frac{k}{3}\rceil]$, each column of Table 3.1 should be mapped to the same $\widehat{u}_r[i]$. In this way, even if $\widehat{u}''_{a1}[i]\widehat{u}''_{a2}[i]\widehat{u}''_b[i]$ is falsely estimated, the resulting $\widehat{u}_r[i]$ is still correct. Thus, for the case of Fig. 3.3(a), after obtaining $p_{output}[i]$ in (3.13), we can obtain network-coded sequence $\widehat{u}_r[i]$ by the following mapping function

$$\widehat{u}_r[i] = \begin{cases} 00 & \text{when } \widehat{u}_{a1}[i]\widehat{u}_{a2}[i]\widehat{u}_b[i] = 000 \text{ and } 011, \\ 01 & \text{when } \widehat{u}_{a1}[i]\widehat{u}_{a2}[i]\widehat{u}_b[i] = 010 \text{ and } 001, \\ 11 & \text{when } \widehat{u}_{a1}[i]\widehat{u}_{a2}[i]\widehat{u}_b[i] = 110 \text{ and } 101, \\ 10 & \text{when } \widehat{u}_{a1}[i]\widehat{u}_{a2}[i]\widehat{u}_b[i] = 100 \text{ and } 111. \end{cases} \tag{3.14}$$

The above analysis shows that by properly designing the bit-level mapping function to map the eight-ary $\widehat{\mathbf{u}}_{a1}\widehat{\mathbf{u}}_{a1}\widehat{\mathbf{u}}_b$ to four-ary $\widehat{\mathbf{u}}_r$, we try to minimize the decoding errors caused from the smallest Euclidean distance between different constellation points. For $\gamma \in (0, 1)$ and $\theta \in [0, 2\pi)$, the two cases of the smallest Euclidean dis-

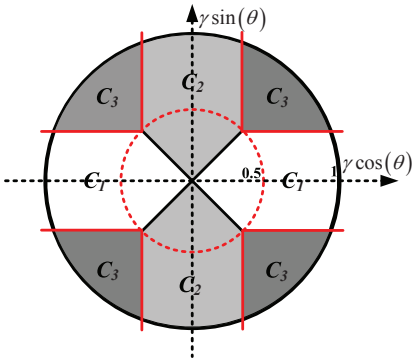

Figure 3.4: Bit-level adaptive mapping functions.

tance are shown in Figs. 3.3(b) and 3.3(c) denoted by the red circles. Thus, mapping functions $\mathcal{C}_2$ and $\mathcal{C}_3$ can be designed and summarized in Table 3.2 and Fig. 3.4. Given the source-relay channel conditions, i.e., γ and θ, the relay can adaptively select the mapping functions according to the source-relay channel conditions and then obtain the mapping function $\mathcal{C}$ from Table 3.2. In Table 3.2, the first row are the symbols from source A, and the first column are the symbols from source B, and $\mathcal{C}_1$, $\mathcal{C}_2$ and $\mathcal{C}_3$ are the bit-level mapping functions labelled in Fig. 3.4.

3.5 Performance Evaluation

In this section, the performance CoHePNC under the asymmetric TWRC scenario is studied. The existing solutions extending from the symmetric channel coded PNC are compared with the proposed CoHePNC under AWGN and Rayleigh fading channels. RA codes with duplication $q = 3$ are applied by both sources with a codeword length of 4096 bits. We let all the nodes transmit signals with the same symbol energy E_s and set the average received SNR of all links to be proportional to $d^{-\alpha}$, where d is the link distance and the path loss exponent $\alpha = 3$. The phase shift difference θ between the superimposed signals is uniformly distributed between $[0, 2\pi)$.

3.5.1 Comparisons of several decoding solutions

In this subsection, we compare the solutions extending from symmetric PNC to the proposed CoHePNC in terms of relay error rate (RER) as introduced in Sec. 3.4.2 under AWGN channels. Separate-two-state denotes the upgrade from [39], separate-

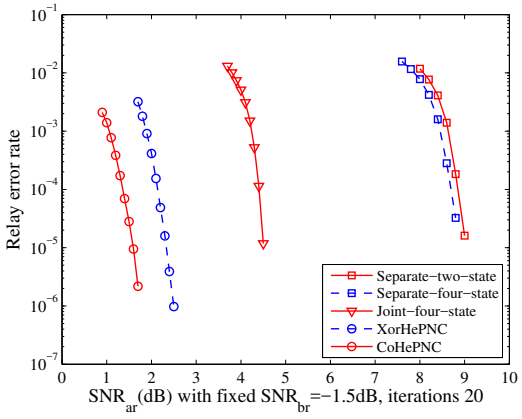

Figure 3.5: Comparison of several decoding algorithms.

four-state denotes the upgrade from [40,41,49], joint-four-state and XorHePNC denote the upgrade from [48, 49] with four-state or eight-state message passing with XOR mapping, and CoHePNC denotes the proposed decoding algorithm. In this chapter, SNR is defined as the received signal to noise ratio with the unit of dB. For AWGN channels, SNR can be calculated as $\text{SNR(dB)} = 10\log_{10}\frac{E_r}{N_0}$, where E_r denotes received symbol energy, and N_0 is noise spectral density. For Rayleigh fading channels, SNR denotes the average received SNR. RER is defined as $\text{RER} = \frac{\Pr\{\widehat{\mathbf{u}}_{r1} \neq \mathbf{u}_{r1}\} + \Pr\{\widehat{\mathbf{u}}_{r2} \neq \mathbf{u}_{r2}\}}{2}$. Note that in Fig. 3.5 we only compare error performance of the MA stage for these decoding algorithms as they share the same BC stage. A worse error performance in the MA stage directly results in a worse end-to-end BER.

In Fig. 3.5, the error performance RER improves with either a larger SNR_{ar} or SNR_{br}. For a fair comparison, we fixed $\text{SNR}_{br} = -1.5$ dB and gradually increase SNR_{ar} from 0 dB to 10 dB. We can observe that comparing separate-two-state and separate-four-state, increasing the state of the message passing improves RER with a cost of calculation complexity at the relay. Joint-four-state outperforms the separate decoding ones, because the full channel received information can be applied without being processed before the input of the decoding algorithm. In the three jointly decoding algorithms, increasing the state of the message passing from four to eight greatly improves the relay error performance. We further compare the two joint-eight-state algorithms, which both apply the full-state decoding with different mapping function design. It shows that the bit-level adaptive mapping function design can further improve the RER performance with a 1 dB gain as the fixed XOR mapping function design may suffer from the SFS effects resulting in a higher error rate. The

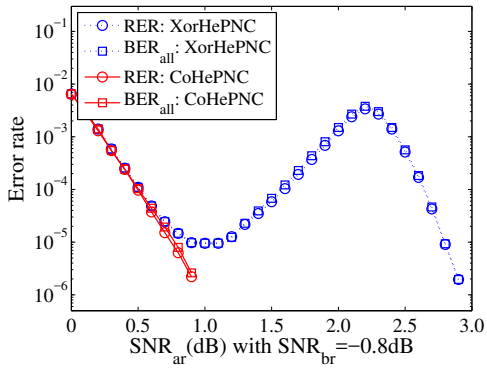

(a) $\mathrm{SNR}_{br} = -0.8$ dB

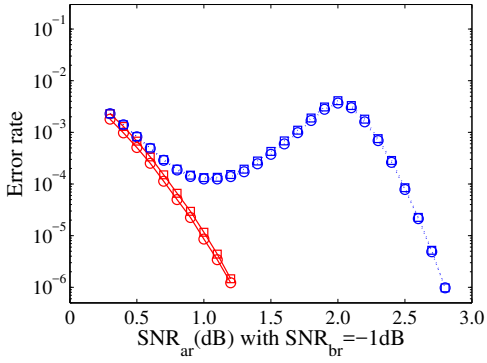

(b) $\mathrm{SNR}_{br} = -1.0$ dB

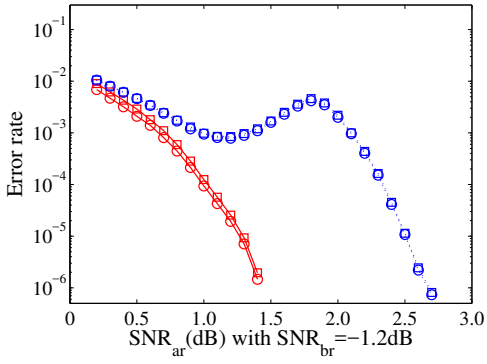

(c) $\mathrm{SNR}_{br} = -1.2$ dB

Figure 3.6: CoHePNC vs XOR HePNC with codeword length 4096 bits, iterations = 20 and duplicate $q = 3$ under AWGN channels.

adaptive mapping design tries to minimize RER by selecting the proper mapping functions according to two source-relay channel conditions.

3.5.2 Error performance under AWGN channels

We compare both the RER and end-to-end BER performance between CoHePNC and XorHePNC under AWGN channels in Fig. 3.6. The end-to-end BER is defined as $\mathrm{BER}_{all} = \frac{\Pr\{\widehat{\widehat{\mathbf{u}}}_{a1} \neq \mathbf{u}_{a1}\} + \Pr\{\widehat{\widehat{\mathbf{u}}}_{a2} \neq \mathbf{u}_{a2}\} + \Pr\{\widehat{\widehat{\mathbf{u}}}_{b} \neq \mathbf{u}_{b}\}}{3}$, where $\widehat{\widehat{\mathbf{u}}}_{a1}$, $\widehat{\widehat{\mathbf{u}}}_{a2}$ and $\widehat{\widehat{\mathbf{u}}}_{b}$ are final estimation results in the BC stage defined in (3.2). The number of iterations is set to be 20. The red and square curves show RER and BER_{all}, respectively. Note that increasing the number of iterations further improves the RER and BER performance. Fig. 3.6 shows the error performance of CoHePNC and XorHePNC with different SNR_{ar} and SNR_{br}. In Figs. 3.6(a), 3.6(b) and 3.6(c), SNR_{br} are fixed as -0.8 dB, -1.0 dB and -1.2 dB, respectively, and SNR_{ar} is gradually increasing. In Fig. 3.6(a), the error performance of CoHePNC is improved with the increase of SNR_{ar} monotonously. However, for XorHePNC, the error performance is improved with the increase of SNR_{ar} at first and then deteriorated and it reaches the worst at $\Delta\mathrm{SNR} = \mathrm{SNR}_{ar} - \mathrm{SNR}_{br} = 3$ dB. Because when ΔSNR equals 3 dB as explained in Fig. 3.3, the SFS effects greatly degrade the performance of relay decoding if without a proper mapping function design. CoHePNC can deal with the SFS effects with the bit-level adaptive mapping design as the relay selects an appropriate mapping function by minimizing the errors in the MA stage. Figs. 3.6(a), 3.6(b) and 3.6(c) show the trend with different SNR_{br} settings. We can observe that when $\Delta\mathrm{SNR} = 3$ dB, there are always inflexion points for XorHePNC due to the SFS effects.

3.5.3 Error performance under block Rayleigh fading channels

In this subsection, we study the error performance of CoHePNC and XorHePNC under block Rayleigh fading channels, where H_a and H_b remain the same during the codeword-length symbol durations. Figs. 3.7(a) and 3.7(b) show the RER and end-to-end BER performance, respectively. The codeword length is 4096 bits and the number of iterations is 20. We set SNR_{br} to be 15 dB, 20 dB and 25 dB, respectively, and SNR_{ar} is gradually increased. In Fig. 3.7, we can observe that the error performance converge with the increase of SNR_{ar} and converge value is determined by SNR_{br}. When SNR_{br} is small, e.g., $\mathrm{SNR}_{br} = 15$ dB, the improvement of CoHePNC is larger than that when $\mathrm{SNR}_{br} = 25$ dB, because the case of $\mathrm{SNR}_{br} = 15$ dB has a larger ΔSNR compared to the case $\mathrm{SNR}_{br} = 25$ dB, and CoHePNC outperforms XorHePNC more with a larger ΔSNR.

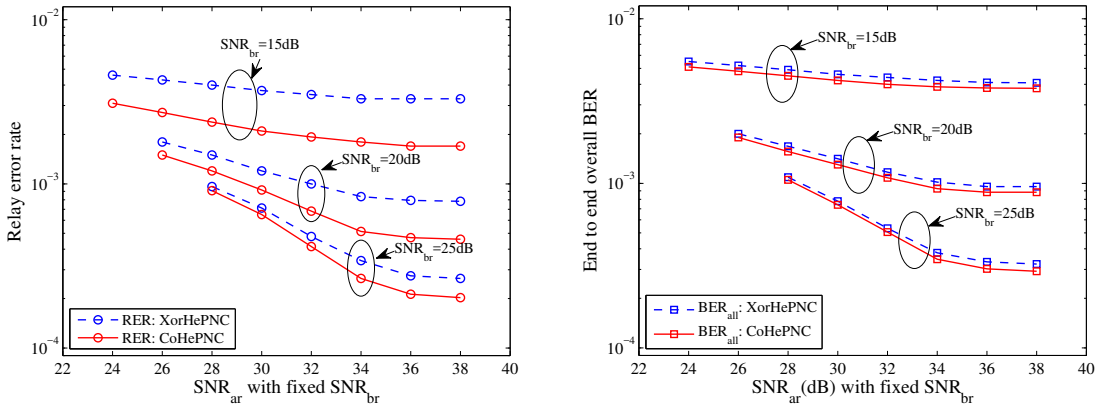

(a) Relay error rate.

(b) End-to-end BER.

Figure 3.7: Block fading channel with codeword length 4096 and iterations 20.

Chapter 4

Design and Analysis of Hierarchical Modulation Physical Layer Network Coding

4.1 Overview

In Chapters 2 and 3, the designs of symbol-level HePNC and link-to-link channel coded HePNC were given under the asymmetric TWRC scenario. One disadvantage of HePNC, also the other heterogeneous modulation PNC designs, is that the channel of the better source-relay link cannot be fully utilized in the broadcast stage, as the higher-order modulation network-coded symbol needs to be divided and broadcast in multiple slots subject to the bottleneck link given the BER threshold. In this chapter, we provide the design of hierarchical modulation physical layer network coding (H-PNC), which achieves an additional data exchange between the relay and the source with a relatively better source-relay channel condition by superimposing the additional data flow to the PNC transmission. The channel of the better source-relay link can be fully utilized in H-PNC by taking advantage of the hierarchical modulation. We provide several designs of H-PNC. The theoretical error performance of QPSK-BPSK H-PNC is also obtained.

4.2 Related Work

In asymmetric TWRC scenario, where the source-relay links have different channel conditions, the traditional symmetric PNC design cannot be directly applied or otherwise results in a low spectrum efficiency due to the bottleneck source-relay link, and also symmetric PNC design is unsuitable to support the asymmetric data exchange requirement [84–87, 91, 98]. In [84], the impact of the source-relay channels on PNC were studied, which demonstrated that the bottleneck link has a large impact on PNC error performance in asymmetric TWRC. In [85], adaptive modulation and network coding (AMNC) was proposed under the assumption that carrier-phase synchronization can be achieved at the relay. The authors in [86, 98] proposed and studied the decode-and-forward joint-modulation (DF-JM) scheme, where a higher-order modulation network-coded symbol is designed by directly combining two source symbols. However, a higher-order network-coded symbol reduces system throughput as more broadcast slots are needed in the BC stage subject to the bottleneck link. The authors in [67, 68, 87] proposed PNC without increasing modulation order of the network-coded symbol, and the authors in [67, 68] further studied adaptive mapping function design considering the impact of carrier-phase. The authors in [53] proposed a network-coded multiple access (NCMA) model, which combines PNC and multi-user decoding (MUD). The target is to deliver information from one source to another node instead of the simultaneously transmitted source. The authors in [91] studied various subtleties of applying linear PNC with q-level pulse amplitude modulation (q-PAM) under asymmetric TWRC to achieve the imbalanced data exchange between two sources.

Although the above proposed PNC designs for asymmetric TWRC tried to maximize system throughput, the overall throughput (bits per slot) taking both sources into account is still limited by the bottleneck link, also the channel of the source-relay link with the better channel condition is not fully utilized by broadcasting a lower-order modulation symbol. How to fully utilize the channel of the source-relay link with the better channel condition meanwhile achieving the information exchange between multiple sources is the main target in this work.

4.3 System Model and H-PNC Procedure

Consider the same asymmetric TWRC scenario with two source nodes A and B, and relay node R as that in Chapter 2. Without loss of generality, we assume that the channel condition between source A and relay R, L_{ar}, is better than that between source B and relay R, L_{br}. Sources A and B need to exchange information with the help of relay R. Meanwhile, source A also needs to exchange information with relay R. We assume perfect channel estimations at receivers only. Symbol-level synchronization is assumed at the relay and carrier-phase synchronization is not required. In this chapter, the H-PNC design is only considered in a symbol-level, and the combination of channel codes with H-PNC can be referred to Chapter 3.

Let $\mathcal{M}_m$ be 2^mQAM/PSK modulation with modulation order m. m_a and m_b are modulation orders for transmissions from sources A and B, respectively. One symbol transmitted from source A, S_a, consists of two sub-symbols: a symbol targeting to relay R, S_{ar}, and a symbol targeting to source B, S_{ab}, i.e., $S_a = [S_{ar}, S_{ab}]$, where $[,]$ denotes that sub-symbols S_{ar} and S_{ab} are concatenated to compose one symbol S_a. Denote S_{ba} as the symbol transmitted from source B targeting to source A. Let $\mathbb{Z}_{2^m}$ be a non-negative integer set, where $\mathbb{Z}_{2^m} = \{0, 1, \ldots, 2^m-1\}$, and we have $S_a \in \mathbb{Z}_{2^{m_a}}$, $S_{ba} \in \mathbb{Z}_{2^{m_b}}$. Note that each integer in $\mathbb{Z}_{2^m}$ can be expressed by an m-bit symbol. In this chapter, SNR is defined as the received symbol energy to noise power spectrum density ratio. For Rayleigh fading channels, SNR is the average received SNR.

4.3.1 H-PNC procedure

H-PNC takes the multiple access (MA) stage and the broadcast (BC) stage to achieve the two bidirectional information exchanges. H-PNC procedure is as follows.

Multiple Access Stage

In the MA stage, sources A and B transmit symbols, $X_a = \mathcal{M}_{m_a}(S_a)$ and $X_b = \mathcal{M}_{m_b}(S_{ba})$, to relay R simultaneously. The received signal at relay R is $Y_r = H_a X_a + H_b X_b + N_r$, where H_a and H_b are the channel gains of links L_{ar} and L_{br}, respectively, and N_r is Gaussian noise with variance of $2\sigma^2$. Denote $H_b/H_a = \gamma \exp(j\theta)$, where γ is the amplitude ratio and θ is the phase shift difference with a uniform distribution in $[0, 2\pi)$.

Denote (S_a, S_{ba}) as a symbol pair, i.e., symbols S_a and S_{ba} from the two source

nodes superimposed at relay R. One symbol pair (S_a, S_{ba}) is mapped to a unique constellation point at relay R, which can be expressed as

$$H_a\mathcal{M}_{m_a}(s_1)+H_b\mathcal{M}_{m_b}(s_2),\ \text{for all}\ s_1\in\mathbb{Z}_{2^{m_a}},\ s_2\in\mathbb{Z}_{2^{m_b}}. \tag{4.1}$$

Maximum likelihood (ML) detection is used to jointly decode symbols S_a and S_{ba} from Y_r. Denote the estimation of (S_a, S_{ba}) as $(\hat{S}_a, \hat{S}_{ba})$, we have

$$(\hat{S}_a, \hat{S}_{ba}) = \underset{(s_1,\, s_2)\in\mathbb{Z}_{2^{m_a}}\times\mathbb{Z}_{2^{m_b}}}{\operatorname{argmin}} |Y_r - H_a\mathcal{M}_{m_a}(s_1) - H_b\mathcal{M}_{m_b}(s_2)|^2. \tag{4.2}$$

Symbol $\hat{S}_a$ consists of the estimation of both S_{ar} and S_{ab}, i.e., $\hat{S}_a = [\hat{S}_{ar}, \hat{S}_{ab}]$. The information transmission from source A to relay R is achieved by extracting $\hat{S}_{ar}$ from $\hat{S}_a$. Then relay R uses a mapping function $\mathcal{C}$ to map the left sub-symbol pair $(\hat{S}_{ab}, \hat{S}_{ba})$ to a network-coded symbol $S_n = \mathcal{C}(\hat{S}_{ab}, \hat{S}_{ba})$. We have $S_n \in \mathbb{Z}_{2^{\max(m_{ab},\ m_b)}}$ subject to the Latin square constraint, where m_{ab} is the modulation order for sub-symbol S_{ab}. The mapping function $\mathcal{C}$ is known by all nodes. Its design is a key issue and is discussed in Sec. 4.3.2, 4.3.3 and 4.4.

Broadcast Stage

In the BC stage, the information transmission from relay R to source A, S_{ra}, can be achieved by superimposing S_{ra} onto the network coded symbol S_n on a hierarchical modulation constellation [103, 104]. S_n is modulated in the base layer to try to successfully broadcast S_n in the BC stage, and S_{ra} is modulated in the enhancement layer to fully utilize the channel of source-relay link L_{ar}. The broadcast symbol by relay R in the BC stage is $S_r = [S_n, S_{ra}]$. Finally, at source A, S_r is estimated by maximum likelihood (ML) detection, i.e., $\hat{S}_r = [\hat{S}_n, \hat{S}_{ra}]$, and the information from relay R to source A is obtained from $\hat{S}_{ra}$, and from source B to source A, S_{ba} is obtained from $\hat{S}_n$ together with the original transmitted symbol S_{ab} and the mapping function $\mathcal{C}$ used at relay R [87]. At source B, only symbol S_n is estimated, and S_{ab} is obtained in a similar way.

Note that, subject to the bottleneck link L_{br}, only a modulation order m_b can be supported given a BER threshold. When the modulation order of S_n, $\max(m_{ab}, m_b)$, is larger than m_b, relay R uses $\lceil \frac{m_{ab}}{m_b} \rceil$ slots to broadcast S_n to guarantee that in each BC slot the modulation order of base layer is no larger than m_b. An example of this case is 8QAM-BPSK H-PNC case 2, which is discussed in Sec. 4.4.3.

In the initialization of H-PNC, the data to be exchanged between A, B and R should be collected, and relay R estimates two source-relay channel conditions and determines modulation applied by the sources by jointly considering two source-relay channels and data exchange requirements, and then sends the modulation configuration to the sources.

4.3.2 Mapping function

The optimal mapping function varies with the two source-relay channel conditions [37, 67, 68]. Adaptive mapping is a mapping function design method, in which the relay dynamically selects a mapping function $\mathcal{C}$ according to two source-relay channel conditions. The relay needs to inform the sources the mapping functions applied, where the frequency is determined by the dynamic of the source-relay channels. Denote the error probability that $S_n \neq \mathcal{C}(S_{ab}, S_{ba})$ as relay mapping error rate (BER_r). Adaptive mapping design aims to minimize BER_r by the closest-neighbour clustering algorithm. We refer readers to [37, 67, 68] for the adaptive mapping designs of symmetric and asymmetric PNC.

For 2^{m_1}QAM/PSK-2^{m_2}QAM/PSK H-PNC, where m_1 and m_2 denote two integers, adaptive mapping can be applied as long as either S_{ab} or S_{ba} contains more than one bit; otherwise, exclusive or (XOR) is the unique mapping method. For example, as discussed in Sec. 4.4.3, for QPSK-BPSK H-PNC and 8QAM-BPSK H-PNC case 1 (S_{ab} contains 1 bit), XOR mapping is the unique mapping method; for 8QAM-BPSK H-PNC case 2 (S_{ab} contains 2 bits), adaptive mapping functions can be designed.

4.3.3 Mapping constraints

H-PNC mapping function design is more challenging compared to traditional PNC, which subjects to two constraints: one is the Latin square constraint [38] expressed in (4.3); the second is the H-PNC constraint expressed in (4.4).

$$\begin{aligned} &\mathcal{C}(s_1,\ s_2) \neq \mathcal{C}(s_1',\ s_2) \text{ for any } s_1 \neq s_1' \in \mathbb{Z}_{2^{m_{ab}}} \text{ and } s_2 \in \mathbb{Z}_{2^{m_b}}; \\ &\mathcal{C}(s_1,\ s_2) \neq \mathcal{C}(s_1,\ s_2') \text{ for any } s_2 \neq s_2' \in \mathbb{Z}_{2^{m_b}} \text{ and } s_1 \in \mathbb{Z}_{2^{m_{ab}}}. \end{aligned} \tag{4.3}$$

$$\mathcal{C}([s_1,\ s_2], s_3) = \mathcal{C}([s_1',\ s_2], s_3) \text{ for any } s_1 \neq s_1' \in \mathbb{Z}_{2^{m_{ar}}}, s_2 \in \mathbb{Z}_{2^{m_{ab}}} \text{ and } s_3 \in \mathbb{Z}_{2^{m_b}}. \tag{4.4}$$

The Latin square constraint implies that the minimum modulation order of the

network-coded symbol S_n is $\max(m_{ab}, m_b)$. The H-PNC constraint implies that on the expected received constellation map at the relay, given s_a and s_{ba}, $s_a \in \mathbb{Z}_{2^{m_a}}$ and $s_{ba} \in \mathbb{Z}_{2^{m_b}}$, symbol pair (s_a, s_{ba}) only appears once; however, sub-symbol pair (s_{ab}, s_{ba}), $s_{ab} \in \mathbb{Z}_{2^{m_{ab}}}$, appears $2^{m_{ar}}$ times, where m_{ar} is modulation order of sub-symbol S_{ar}. All the same sub-symbol pairs (s_{ab}, s_{ba}) should be mapped to the same network-coded symbol S_n.

We use an example to illustrate the H-PNC constraint. Consider QPSK-BPSK H-PNC, where $S_a = [S_{ar}, S_{ab}]$ is a QPSK symbol, and S_{ba} is a BPSK symbol. Two sub-symbol pairs (S_{ab}, S_{ba}) equal to $(0,1)$ and $(1,0)$, belong to $([0,0],1)$ and $([0,1],0)$, respectively, may be both mapped to a network-coded symbol $S_r = \mathcal{C}'(S_{ab}, S_{ba}) = 1$ by a mapping function $\mathcal{C}'$. By the H-PNC constraint, the mapping function $\mathcal{C}'$ further determines that other two sub-symbol pairs, i.e., $(0,1)$ and $(1,0)$ belong to $([1,0],1)$ and $([1,1],0)$, respectively, should also be mapped to the same network-coded symbol $S_r = 1$ by the mapping function $\mathcal{C}'$. The Latin square and H-PNC constraints impact on H-PNC design, which will be further discussed in Sec. 4.4.

4.4 H-PNC Sample Design

In this section, we first present the QPSK-BPSK H-PNC design in detail starting with an illustrative example. Then we present higher-order modulation H-PNC designs, including two cases of 8QAM-BPSK H-PNC.

4.4.1 QPSK-BPSK H-PNC example

Fig. 4.1(a) shows an example of QPSK-BPSK H-PNC procedure, where source A exchanges one unit of data with source B and relay R each. In the MA stage, source A transmits bit $S_{ar} = 0$ (targeting to relay R) and bit $S_{ab} = 1$ (targeting to source B) using a QPSK symbol $S_a = [S_{ar}, S_{ab}] = 01$. Source B transmits symbol $S_{ba} = 0$ (targeting to source A) by BPSK. Suppose relay R successfully demodulates the symbol pair $(\hat{S}_a, \hat{S}_{ba}) = (01, 0)$ by ML detection, and obtains $\hat{S}_{ar} = 0$ from source A by extracting $\hat{S}_{ar}$ from $\hat{S}_a$. Then relay R applies mapping function $\mathcal{C}$ (For QPSK-BPSK H-PNC, mapping function $\mathcal{C}$ can be XOR uniquely) to map $(\hat{S}_{ab}, \hat{S}_{ba})$ to a network-coded symbol $S_n = \mathcal{C}(\hat{S}_{ab}, \hat{S}_{ba}) = 1 \,\mathrm{XOR}\, 0 = 1$. In the BC stage, relay R transmits one unit of data $S_{ra} = 0$ to source A, which is superimposed on the network-coded symbol $S_n = 1$ using a hierarchical constellation. S_n is positioned on the base layer, and S_{ra}

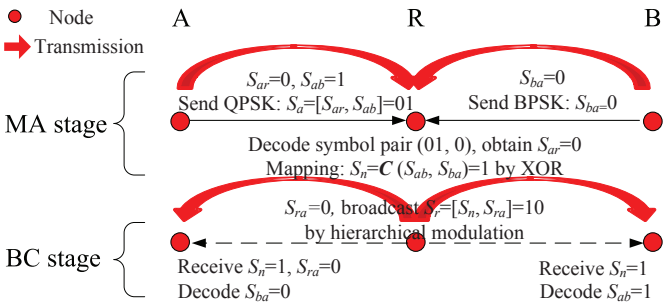

(a) MA and BC stages for QPSK-BPSK H-PNC.

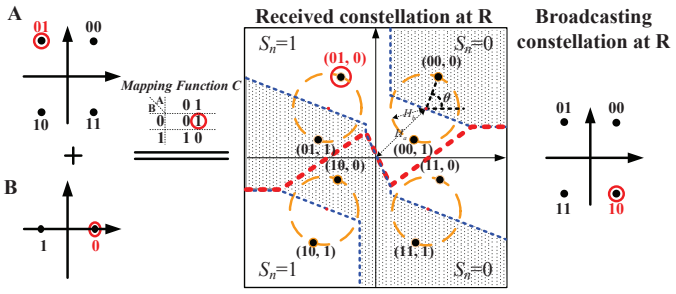

(b) Constellation maps.

Figure 4.1: QPSK-BPSK H-PNC with $\gamma = 0.5$ and $\theta = \frac{3\pi}{8}$.

is positioned on the enhancement layer. Thus, relay R broadcasts $S_r = [S_n, S_{ra}] = 10$. Finally, source A receives and obtains the estimations of both $\hat{S}_n = 1$ and $\hat{S}_{ra} = 0$ by ML detection. As source A already knows $S_{ab} = 1$, $S_{ba} = 0$ can be obtained by applying the mapping function $\mathcal{C}$ (XOR). Source B only needs to demodulate $\hat{S}_n = 1$, and obtains $S_{ab} = 1$ in a similar way.

Fig. 4.1(b) shows the constellation maps of QPSK-BPSK H-PNC. The left figures show transmit constellations at A and B, respectively. The right figure shows broadcast constellation at relay R in the BC stage. Note that, although both the transmit constellations applied at source A and the broadcast constellation at relay R use 2/4-QAM hierarchical constellation design, their bit-symbol labelings are different. The explanation is discussed in Sec. 4.4.2. The middle figure shows the expected received constellation map at relay R. The red dotted curves define decision boundaries for S_{ar}, and the blue curves define those for S_n. The shadowed regions are decision regions of $S_n = 0$. The four dashed circles are formed by BPSK symbols, $H_b\mathcal{M}_1(S_{ba})$, shifted with θ and superimposed to QPSK symbols $H_a\mathcal{M}_2(S_a)$, i.e., the center of each circle is the expected received QPSK symbol $H_a\mathcal{M}_2(S_a)$.

We can observe that modifying the transmit constellations at the sources impacts

the expected received constellation map at the relay. For example, given the symbol energy, enlarging the Euclidean distance between symbols 00 and 11 on the transmit constellation of source A would benefit the demodulation of S_{ar} thanks to a longer Euclidean distance, but the probability to obtain a correct $S_n = \mathcal{C}(S_{ab}, S_{ba})$ may be affected negatively as the distance of two BPSK circles horizontally would shrink. Another example is to consider the symbol pairs $(01, 1)$ and $(10, 0)$ on the expected received constellation at relay R in Fig. 4.1(b). Individually demodulating each bit of them would cause a larger error probability as the Euclidean distance between them is relatively small. However, only the first bit S_{ar} of the QPSK symbols are needed to be distinguished, because after S_{ar} is extracted from S_a, $(01, 1)$ and $(10, 0)$ shrink to $(1, 1)$ and $(0, 0)$, and are both mapped to $S_n = 0$ by XOR mapping. Thus, H-PNC design should jointly consider the transmit constellations and the positive effects of the mapping functions.

4.4.2 QPSK-BPSK H-PNC constellations

In this subsection, the design of the transmit constellation at source A in the MA stage, and the broadcast constellation at relay R in the BC stage will be studied. We observe that Gray mapping is not optimal for the transmit constellation of source A, and hierarchical modulation constellations should be designed for both constellations.

The transmit constellation at source A

Different from the broadcast constellation at relay R, transmit constellation design at source A also needs to consider the impact of the superimposed signals on the received constellation map at relay R. Denote BER_{ar} as the bit error rate (BER) of S_{ar}. For bit-symbol labeling of QPSK constellation, there are totally three methods to label the 2-bit symbols on the constellation map as shown in Figs. 4.2(a), 4.2(b) and 4.2(c), denoted as labeling-1, labeling-2 and labeling-3, respectively. For QPSK-BPSK H-PNC, labeling-1 is better than labeling-2, and labeling-2 is better than labeling-3, in terms of BER. The reasons are discussed in the following.

First, we compare labeling-2 and labeling-3. In the QPSK symbol, for the first bit S_{ar}, labeling-2 reduces the error probability in the horizontal direction, which can reduce BER_{ar}. For the second bit S_{ab}, given S_{ba}, labeling-2 and labeling-3 are mapped to the same S_n after S_{ar} is extracted from S_a, so they have the same BER_r performance. Thus, labeling-2 is better than labeling-3. Labeling-1 and labeling-2

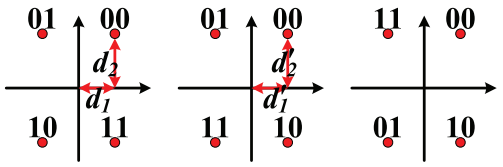

(a) Labeling-1.(b) Labeling-2.(c) Labeling-3.

Figure 4.2: QPSK labeling methods and hierarchical QPSK constellation maps.

have the same BER_{ar} performance. For the second bit S_{ab}, the impact of S_{ba} on the expected received constellation at relay R should be considered. One example of the worst-case is shown in Fig. 4.3, where $\theta = \frac{\pi}{2}$ and $\gamma = 0.5$. Note that $\theta = \frac{3\pi}{2}$ is another worst case of labeling-2. The red segment shows the smallest Euclidean distance between different constellation points. For labeling-2, the Euclidean distance between symbol pairs $(01, 1)$ and $(11, 0)$ is relatively small, and they are mapped to different S_n after extracting S_{ar}, i.e., $(01, 1)$ and $(11, 0)$ will be mapped to $\mathcal{C}(1, 1) = 0$ and $\mathcal{C}(1, 0) = 1$ by XOR, respectively, which leads to a higher BER_r. For labeling-1, $(01, 1)$ and $(10, 0)$ are both mapped to $S_n = 0$ by XOR after S_{ar} is extracted, and the smallest Euclidean distance for labeling-1 is always the diameter of BPSK circles whatever θ is. Therefore we concluded that for the transmit constellation at source A, labeling-1 is better than labeling-2, and labeling-2 is better than labeling-3 in terms of BER.

The above conclusion provides the insights to design an appropriate H-PNC transmit constellation at source A. The bit-symbol labeling criterion is summarized as follows: for symbol-set $S_a \in \mathbb{Z}_{2^{m_a}}$, $S_a = [S_{ar}, S_{ab}]$, symbols of S_a with the same S_{ar} should be grouped on the constellation to improve BER_{ar}, and symbols of S_a with the same S_{ab} should be separated on the constellation to guarantee BER_r. Note that BER_r further affects the error rate of S_{ab} and S_{ba} in the BC stage.

To have an optimal constellation design for H-PNC, an optimal bit-symbol labeling scheme is necessary but not sufficient. If labeling-1 is directly applied by source A with a symmetrical constellation, the BER_{ar} performance is much worse than that of BER_r because of the smallest Euclidean distance. Therefore, we propose to apply QPSK hierarchical modulation to further optimize the constellation map. Denote $\lambda_1 = \frac{d_2}{d_1}$ as shown in Fig. 4.2(a). Assume that all the symbols have unit energy $E_s = 1$, i.e., ${d_2}^2 + {d_1}^2 = 1$. It is easy to observe that enlarging d_2 reduces BER_{ar}. However, when $\lambda_1 = 1$, BER_r can be minimized thanks to the symmetrical features of the

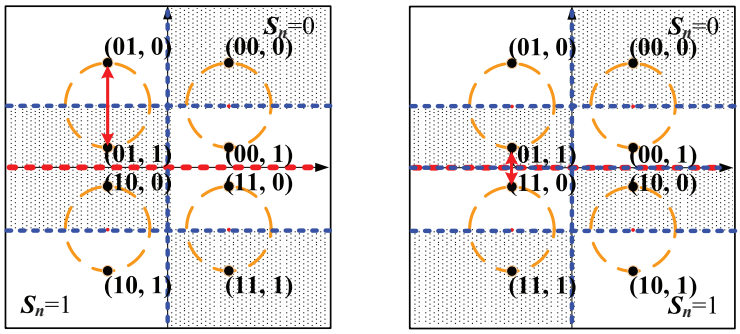

(a) Labeling-1. (b) Labeling-2.

Figure 4.3: Worst case comparison of labeling-1 and labeling-2.

constellation maps. Therefore there is a tradeoff to set λ_1.

The optimal λ_1 is obtained by maximizing the overall successful transmission rate in the MA stage. For QPSK-BPSK H-PNC, it can be simplified as

$$\min_{\lambda_1} \; 2 \cdot \mathrm{BER}_r + \mathrm{BER}_{ar}, \tag{4.5}$$

where the coefficient 2 before BER_r denotes that one unit of BER_r error may cause two units of final decoding errors, i.e., both S_{ab} and S_{ba} in the BC stage under the condition that the broadcast in the BC stage is correct. Note that the small probability that the network-coded symbol is erroneous but the end-to-end estimation at the BC stage is correct is neglected in (4.5) to simplify the analysis. The theoretical derivations of BER_r and BER_{ar} of QPSK-BPSK H-PNC are studied in Sec. 4.5.

Broadcast constellation at relay R

In the BC stage, relay R uses a hierarchical constellation to broadcast the superimposed symbol $S_r = [S_n, S_{ra}]$. For the bit-symbol labeling of the broadcast constellation, S_n is positioned on the base layer, and S_{ra} is positioned on the enhancement layer. It is easy to find that labeling-2 as shown in Fig. 4.2 is optimal. To maximize successful demodulation rate, i.e., to maximize the Euclidean distance between bits '0' and '1', labeling-1 and labeling-2 achieve the same performance which outperforms that of labeling-3 by considering the first bit of the QPSK symbol, and labeling-2 and labeling-3 achieve the same performance which outperforms that of labeling-1 by considering the second bit of the QPSK symbol. Thus, labeling-2 is optimal by considering both bits. Denote $\lambda_2 = d_2'/d_1'$, we have ${d_2'}^2 + {d_1'}^2 = 1$.

We mainly consider four-flow information exchange, including two flows between A and R and two flows between A and B. The BER of each flow is defined as BER_{ar}, BER_{ra}, BER_{ab} and BER_{ba}, respectively. The objective is to maximize the weighted sum throughput[1], which is equivalent to minimizing weighted BERs given by

$$\min_{\lambda_2} \sum_{i=1}^{4} w_i \mathrm{BER}_{jk}, \tag{4.6}$$

where the coefficient w_i refers to the data importance, and j, k denote the labels of nodes, $j, k \in (a, r, b)$, $j \neq k$. The scheduler may adjust w_i according to the importance of different flows.

In this chapter, we consider four flows have an equal importance, and w_i equals the number of bits in symbol S_{jk}, where S_{jk} is the symbol from node j to node k. For example, $w_i = 1$ in QPSK-BPSK H-PNC. The theoretical derivations of BER_{jk} are studied in Sec. 4.5.

4.4.3 8QAM-BPSK H-PNC

In this subsection, we present the 8QAM-BPSK H-PNC design. For 8QAM-BPSK H-PNC, there are two cases according to different demands of S_{ar}: case 1, source A transmits two units of data to relay R, and one unit to source B, i.e., S_{ar} consists of 2 bits and S_{ab} consists of 1 bit; case 2, source A transmits one unit of data to relay R, and two units to source B. The designs of these two cases are discussed in the following. Note that the designs for these two cases can be combined to support the non-integer data exchange ratio.

Case 1

The transmit constellation at source A in the MA stage and the broadcast constellation at relay R in the BC stage are shown in Figs. 4.4(a) and 4.4(b), labeled as constellation-1 and constellation-2, respectively. Constellation-1 and constellation-2 can be considered as 4/8-QAM and 2/8-QAM hierarchical constellations, respectively[2]. In Fig. 4.4(a), the eight red points are the transmit constellation points, and the circles are the BPSK circles on the received constellation map at the relay. The

[1]Throughput (bits/slot) is defined the successfully received bits per slot by all the destinations.

[2]The prototypes of constellation-1 and constellation-2 are from two typical 8QAM constellations, i.e., $d_1 = 0$ for constellation-1 and $d_1' = \frac{d_2'}{2}$ for constellation-2.

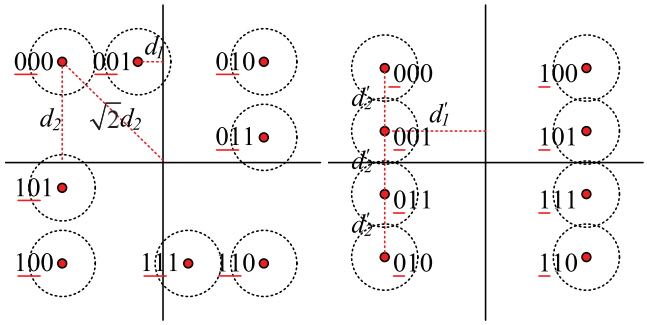

(a) Constellation-1. (b) Constellation-2.

Figure 4.4: Constellations for 8QAM-BPSK H-PNC.

first two bits of each symbol underlined are from S_{ar}, and the left one bit is S_{ab}. The bit-symbol labeling criterion is similar to that discussed in QPSK-BPSK H-PNC in Sec. 4.4.2, i.e., symbols with the same S_{ar} are grouped, and symbols with the same S_{ab} are separated. For example, symbols 000 and 001 are grouped as they have the same $S_{ar} = 00$, and different S_{ar} are separated and positioned in a Gray mapping pattern; after positioning symbols 000 and 001 clockwise, the neighboring symbol of 001 is 010 instead of 011 to minimize BER_r at relay R in the mapping process. Define coordinates of 001 and 000 as $-d_1 + d_2 j$ and $-d_2 + d_2 j$, respectively. We have $d_1^2 + 3d_2^2 = 2$ with the average symbol energy constraint $E_s = 1$. Similar to (4.5), we can obtain the optimal d_1 and d_2 by

$$\min_{d_1, d_2} \; 2 \cdot \text{BER}_r + \text{BER}_{ar}, \tag{4.7}$$

where coefficient 2 denotes that one incorrect $\hat{S}_{ar}$ may cause 1 bit error due to Gray mapping, and one incorrect $\hat{S}_n$ may cause 2 bit errors in the final demodulation of S_{ab} and S_{ba}.

The eight red points in Fig. 4.4(b) show the constellation points of the broadcast constellation at relay R. The first bit of each symbol underlined is the network-coded symbol S_n, and the left two bits are the superimposed bits S_{ra}. S_n is modulated in the base layer to guarantee the performance of the information exchange between source A and source B; S_{ra} is modulated in the enhancement layer in Gray mapping. Symbols starting with the same S_n are positioned with equal intervals to guarantee that different QPSK symbols S_{ra} have the similar error performance. We have energy constraint $4{d_1'}^2 + 5{d_2'}^2 = 4$. The optimal d_1' and d_2' are obtained according to (4.6).

For higher-order modulation H-PNC, the same estimation approaches introduced in Section 4.5 can be used but with a higher complexity. In this work, their optimal constellation settings are obtained by a searching algorithm summarized as follows:
1) For the transmit constellation at A, find a 4/8QAM prototype (constellation-1) and optimize the bit-symbol labeling according to the bit-symbol labeling criterion introduced in Sec. 4.4.2.
2) Minimize (7) by exhaustively searching d_1 and d_2 with the energy constraint $d_1^2 + 3d_2^2 = 2$.
3) For the broadcast constellation at R, find a 2/8QAM prototype (constellation-2) and optimize the bit-symbol labeling in priority of the network-coded symbol.
4) Minimize (6) by exhaustively searching d_1' and d_2' with the energy constraint $4{d_1'}^2 + 5{d_2'}^2 = 4$.

Case 2

For the bit-symbol labeling, both the transmit constellation at source A in the MA stage, and the broadcast constellation at relay R in the BC stage use the 2/8-QAM constellation-2 as shown in Fig. 4.4(b). For the transmit constellation at source A, S_{ar} is modulated as the first bit of each symbol, and S_{ab} are the left two bits modulated in Gray mapping with equal intervals. The equal interval design tries to guarantee different BPSK circles of the received constellation map at relay R would have a larger Euclidean distance on average. Due to the bottleneck link L_{br} which can support BPSK only given the BER threshold, two slots in the BC stage are needed to broadcast the QPSK network-coded symbol. In each BC slot, each bit of S_n is broadcast with the hierarchical constellation as shown in Fig. 4.4(b). The optimal constellation setting for the transmission constellation at source A is

$$\min_{d_1', d_2'} \; 3 \cdot \mathrm{BER}_r + \mathrm{BER}_{ar}, \tag{4.8}$$

where coefficient 3 denotes that one incorrect $\hat{S}_{ar}$ may cause 1 bit error, and one incorrect $\hat{S}_n$ may cause 3 end-to-end bits in error including 2 bits of S_{ab} and 1 bit of S_{ba}, as sources A and B cannot recover the correct information from an erroneous network-coded symbol. The optimal constellation setting of the broadcast constellation at relay R is obtained according to (4.6).

For case 2, adaptive mapping functions can be designed, i.e., the relay can select

Table 4.1: Adaptive mapping functions

	$(00,0)$	$(01,0)$	$(11,0)$	$(10,0)$	$(00,1)$	$(01,1)$	$(11,1)$	$(10,1)$
$\mathcal{C}_1$, $\theta \in (0,\pi)$	00	01	11	10	01	11	10	00
$\mathcal{C}_2$, $\theta \in (\pi,2\pi)$	00	01	11	10	10	00	01	11

the optimal mapping function according to the two source-relay channels. When γ is small enough[3], the optimal mapping functions are summarized in Table 4.1. Relay R estimates two source-relay channels, and obtains phase shift difference θ, and then selects the optimal mapping functions by looking up Table 4.1. For example, when $\theta \in (0,\pi)$, $\mathcal{C}_1$ is selected. If $\hat{S}_{ab} = 00$ and $\hat{S}_{ba} = 0$, relay R obtains $S_n = \mathcal{C}_1(\hat{S}_{ab}, \hat{S}_{ba}) = \mathcal{C}_1(00,0) = 00$ according to Table 4.1. Please refer to [37, 67, 68] and Chapter 2 for more details about the adaptive mapping design.

Note that, for both of 8QAM-BPSK H-PNC cases, in the BC stage, relay R can also superimpose one bit of S_{ra} instead of two bits on the network-coded symbol S_n to constitute a QPSK symbol instead of using 8QAM. The broadcast constellation can select the constellation as shown in Fig. 4.2(b). In this way, a better BER performance can be achieved in the BC stage at the cost of a lower system throughput. We can see that the H-PNC application is flexible to support different kinds of data exchange requirements and BER thresholds.

4.4.4 H-PNC generalization

Consider 2^mQAM-2^nQAM H-PNC under asymmetric TWRC, where 2^m-QAM and 2^n-QAM are applied by sources A and B, respectively. Assume $m > n$ without loss of generality. Consider that source A transmits k bits and $(m-k)$ bits to source B and relay R, respectively, where $k \in \{1, \cdots, m-1\}$. Source B transmits n bits to source A. The constellation map applied by source A and source B is an $(m-k)/m$-QAM hierarchical modulation constellation map and traditional 2^n-QAM constellation map, respectively. The network-coded symbol obtained at relay R has a modulation order of $\max(k,n)$ subject to the Latin square constraint. Relay R uses an n/m hierarchical modulation constellation map by $\lceil \frac{\max(n,k)}{n} \rceil$ slots to broadcast the $\max(k,n)$-bit

[3] γ may be larger due to the deep channel fading, which will result in a large BER_r due to the overlapping of the BPSK circles in Fig. 4.4(b). Thus, in order to guarantee the end-to-end BER, transmissions should be avoided in these deep fading slots using opportunistic scheduling solutions such as the Proportionally Fair Scheduling (PFS) used in the cellular systems, which is beyond the scope of this chapter.

network-coded symbol subject to the bottleneck link. In each slot, maximal $(m-n)$ bits targeting from relay R to source A can be superimposed on the n-bit base layer symbol.

In the MA stage, the received constellation map at relay R has 2^{m+n} constellation points, where 2^{m-k} constellation points for the data from source A to relay R are explicitly demodulated achieving by the $(m-k)/m$-QAM hierarchical modulation, and the leftover 2^{n+k} constellation points are mapped to the $\max(n,k)$-bit network-coded symbol. In the BC stage, source B uses $\lceil \frac{\max(n,k)}{n} \rceil$ slots to obtain a $\max(n,k)$-bit network-coded symbol by demodulating the n-bit on the base layer in each slot and then obtains the target information from source A by applying the information transmitted by itself and the mapping function reversely. Source A demodulates all of the m bits in each slot, where $(m–n)$ bits on the enhancement layer are the information from relay R to source A, and the n bits on the base layer are the information of the network-coded symbol. Note that the Euclidean distance between the constellation points on the hierarchical modulation constellation maps can be designed similarly to the algorithms in Sec. 4.4.3.

4.5 QPSK-BPSK H-PNC Error Performance Analysis

In this section, we use the techniques introduced in [105] and study the error performance of QPSK-BPSK H-PNC under AWGN and Rayleigh fading channels.[4] BER_{ar}, BER_{ra}, BER_{ab} and BER_{ba} are derived, receptively, so the problems of (4.5) and (4.6) can be directly solved.

4.5.1 Derivations of BER_{ar} and BER_{ra}

Given a modulation in any node, we consider that each symbol has an equivalent transmission probability. Denote $H_b/H_a = \gamma \exp(j\theta)$, where γ and θ are amplitude ratio and phase shift difference between two source-relay channel gains, and θ has a uniform distribution in $[0, 2\pi)$[5]. In Fig. 4.5, the decision boundaries of S_{ar} are shown

[4]It is challenging to systematically characterize the decision boundaries for higher-order modulation H-PNC due to the complexity of the received constellation map at the relay. However, the steps to analyze their performance are similar to the approach presented here.

[5]If in the future, more accurate synchronization can be achieved so the range of θ can be reduced, the performance gain of H-PNC can be even higher, while the analytical framework developed in

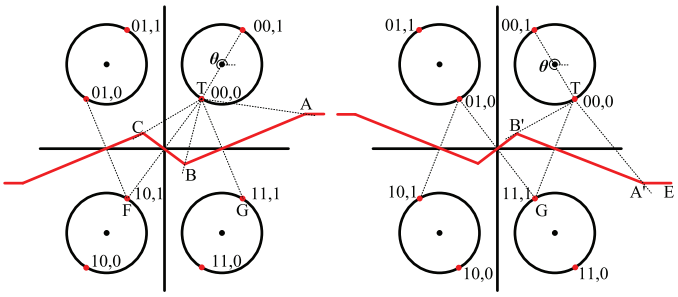

(a) $\theta \in (\pi, \frac{3\pi}{2})$. (b) $\theta \in (\frac{3\pi}{2}, 2\pi)$.

Figure 4.5: Decision boundaries of BER_{ar}.

by the red curves. The center of each circle is the target received symbol from source A. The four circles are obtained by superimposing two symbols from the sources with uniformed phase shift difference θ from $[0, 2\pi)$. The Euclidean distance between the original and each center of the circles is $|H_a|$, and the radius of each circle is $|H_b|$.

BER_{ar} denotes the bit transmission error rate from source A targeting to relay R in the MA stage. The error performance of BER_{ar} is obtained by considering symbol pair $(00, 0)$ traversing phase shift difference $\theta \in [0, 2\pi)$. The expected received constellation map at relay R is shown in Fig. 4.5, where the target symbol pair $(00, 0)$ is labeled as T.

The coordinate of the target symbol pair $(00, 0)$ is

$$[|H_a|\sqrt{\frac{1}{1+{\lambda_1}^2}} + |H_b|\cos(\theta)] + j[|H_a|\sqrt{\frac{{\lambda_1}^2}{1+{\lambda_1}^2}} + |H_b|\sin(\theta)],$$

where j is the imaginary unit.

For a target constellation point O, the error probability P_e that the received signal is located in the shadowed region R due to Gaussian noise with variance of $2\sigma^2$ can be calculated by

$$P_e = \frac{1}{2\pi}\int_0^{\theta_1} \exp(-\frac{L^2}{2\sigma^2\sin^2(\theta'+\theta_2)})\ \mathrm{d}\theta', \tag{4.9}$$

where L is the Euclidean distance between O and the decision boundary, and θ_1 and θ_2 are the angles in radians. Please find the detailed proof of (4.9) in [94].

Define $\Phi(\theta_1, \theta_2, L) = \frac{1}{2\pi}\int_0^{\theta_1} \exp(-\frac{L^2}{2\sigma^2\sin^2(\theta'+\theta_2)})\ \mathrm{d}\theta'$. For $\theta \in (\pi, \frac{3\pi}{2})$ shown in

this chapter is still applicable.

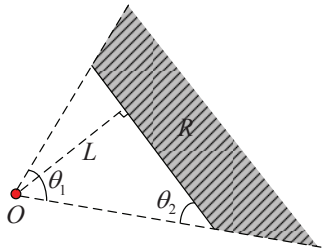

Figure 4.6: Error probability example.

Fig. 4.5(a), BER_{ar_1} can be estimated by

$$\mathrm{BER}_{ar_1} = \Phi(\angle\mathrm{BTA}, \angle\mathrm{ABT}, \frac{D_{TG}}{2}) + \Phi(\angle\mathrm{BTC}, \angle\mathrm{BCT}, \frac{D_{TF}}{2}), \tag{4.10}$$

where D_{ik} denotes the Euclidean distance between points i and k, and $\angle$ denotes angle. The coordinates of A, B, G in Fig. 4.5(a) are given by

$$\begin{cases} G = [|H_a|\sqrt{\frac{1}{1+{\lambda_1}^2}} - |H_b|\cos(\theta)] + j[-|H_a|\sqrt{\frac{{\lambda_1}^2}{1+{\lambda_1}^2}} - |H_b|\sin(\theta)], \\ B = [-|H_b|\cos(\theta)] + j[|H_b|\cos(\theta)\frac{|H_a|\sqrt{1/(1+{\lambda_1}^2)}+|H_b|\cos(\theta)}{|H_a|\sqrt{{\lambda_1}^2/(1+{\lambda_1}^2)}+|H_b|\sin(\theta)}], \\ A = [\frac{|H_b|\sin\theta}{\tan(\theta-\pi/2)} + |H_a|\sqrt{\frac{1}{1+{\lambda_1}^2}}(1 - \frac{\lambda_1}{\tan(\theta-\pi/2)})] - j[|H_b|\sin(\theta)]. \end{cases}$$

The coordinates of B and C are symmetric to the original point, so are those of T and F. Thus, the coordinates of C and F can be easily obtained from B and T so they are omitted due to space limitation.

The BER_{ar_2} in the region $\theta \in [\frac{3\pi}{2}, 2\pi)$ shown in Fig. 4.5(b) can be estimated by

$$\mathrm{BER}_{ar_2} = \Phi(\angle\mathrm{B'TA'}, \angle\mathrm{A'B'T}, \frac{D_{TG}}{2}) + \Phi(\angle\mathrm{EA'T}, 0, |H_a|\sqrt{\frac{{\lambda_1}^2}{1+{\lambda_1}^2}}), \tag{4.11}$$

where $|H_a|\sqrt{\frac{{\lambda_1}^2}{1+{\lambda_1}^2}}$ is the Euclidean distance from T to the decision boundary A′E. The coordinates of A′ and B′ are

$$\begin{cases} A' = [\frac{|H_b|\sin(\theta)}{\tan(\theta-3\pi/2)} + |H_a|\sqrt{\frac{1}{1+{\lambda_1}^2}}(\frac{\lambda_1}{\tan(\theta-3\pi/2)} + 1)] + j[|H_b|\sin(\theta)], \\ B' = [|H_b|\cos(\theta)] + j[|H_b|\cos(\theta)\frac{|H_a|\sqrt{1/(1+{\lambda_1}^2)}-|H_b|\cos(\theta)}{|H_a|\sqrt{{\lambda_1}^2/(1+{\lambda_1}^2)}+|H_b|\sin(\theta)}]. \end{cases}$$

For the region of $\theta \in [0, \pi)$, the Euclidean distance between the target T and the decision boundaries are much larger than that of the cases of $\theta \in [\pi, 2\pi)$, so the error

rate can be neglected. Thus, BER_{ar} considering $\theta \in [0, 2\pi)$ can be expressed as

$$\mathrm{BER}_{ar} = \Pr\{\theta \in (\pi, \frac{3\pi}{2})\}\mathrm{BER}_{ar_1} + \Pr\{\theta \in [\frac{3\pi}{2}, 2\pi)\}\mathrm{BER}_{ar_2} = \frac{\mathrm{BER}_{ar_1} + \mathrm{BER}_{ar_2}}{4}, \tag{4.12}$$

where $\Pr\{.\}$ denotes probability.

BER_{ra} is the bit error rate from relay R to source A in the BC stage. Relay R uses a hierarchical constellation to broadcast the network-coded symbol S_n, which is superimposed by S_{ra} as the enhancement layer shown in Fig. 4.2(b). With $Q[.]$ function, BER_{ra} can be obtained by

$$\mathrm{BER}_{ra} = Q[\frac{|H_a|\sqrt{\frac{1}{1+{\lambda_2}^2}}}{\sigma}]. \tag{4.13}$$

4.5.2 Derivations of BER_{ab} and BER_{ba}

The information exchange between sources A and B takes two-stage transmissions. BER_{ab} and BER_{ba} can be obtained similarly. BER_{ab} can be obtained by

$$\mathrm{BER}_{ab} = \mathrm{BER}_r(1 - \mathrm{BER}_{rb}) + (1 - \mathrm{BER}_r)\mathrm{BER}_{rb}, \tag{4.14}$$

where BER_{rb} denotes the error rate of broadcasting the network-coded symbol S_n from relay R to source B in the BC stage over link L_{br}.

BER_r

We first study how to estimate BER_r. Similar to the analysis to obtain BER_{ar}, we still consider the target symbol pair $(00, 0)$, and traverse the phase shift difference $\theta \in [0, 2\pi)$. The expected received constellation at relay R with different regions of θ are shown in Fig. 4.7.

We use Fig. 4.7(a) as an example to show how to calculate BER_r. The decision boundaries for the network-coded symbol S_n are shown by the red curves[6]. Denote the relay mapping error rate in the region $\theta \in (0, \frac{\pi}{4})$ as BER_{r1}, which can be expressed

[6]The red solid curves stand for the decision boundaries we calculated, and the red dashed curves stand for the decision boundaries with a typically much larger Euclidean distance from the target point T and they are neglected in our calculation.

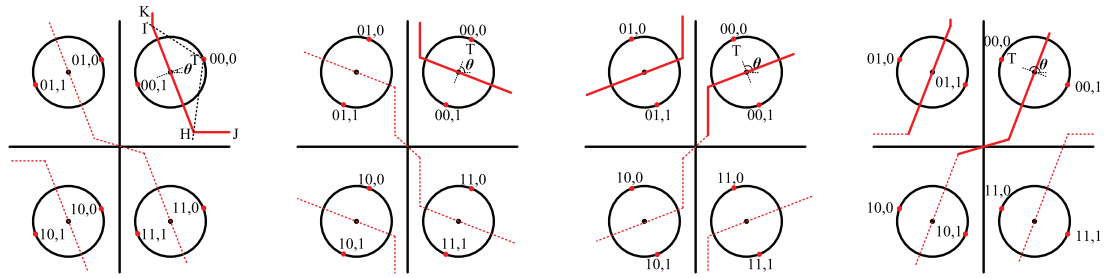

(a) $\theta \in (0, \frac{\pi}{4})$. (b) $\theta \in (\frac{\pi}{4}, \frac{\pi}{2})$. (c) $\theta \in (\frac{\pi}{2}, \frac{3\pi}{4})$. (d) $\theta \in (\frac{3\pi}{4}, \pi)$.

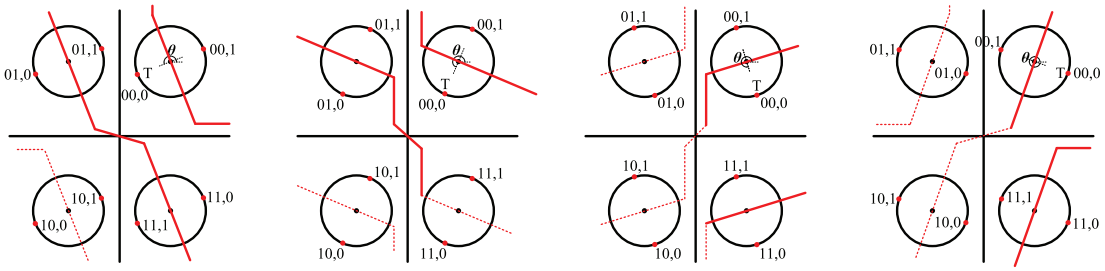

(e) $\theta \in (\pi, \frac{5\pi}{4})$. (f) $\theta \in (\frac{5\pi}{4}, \frac{3\pi}{2})$. (g) $\theta \in (\frac{3\pi}{2}, \frac{7\pi}{4})$. (h) $\theta \in (\frac{7\pi}{4}, 2\pi)$.

Figure 4.7: Decision boundaries of BER_r.

as

$$\begin{aligned}\mathrm{BER}_{r1} = \Phi(\angle\mathrm{HTI}, \angle\mathrm{TIH}, |H_b|) + \Phi(\angle\mathrm{JHT}, 0, |H_a|\sqrt{\frac{{\lambda_1}^2}{1+{\lambda_1}^2}}) \\ + \Phi(\pi - \angle\mathrm{TIK}, 0, |H_a|\sqrt{\frac{1}{1+{\lambda_1}^2}}).\end{aligned} \tag{4.15}$$

Thus, combining all the BER_{ri} of cases $i \in \{1, \cdots, 8\}$ results in an overall BER_r as

$$\mathrm{BER}_r = \frac{1}{8}\sum_{i=1}^{8} \mathrm{BER}_{ri}. \tag{4.16}$$

$\mathbf{BER}_{ab}$ and $\mathbf{BER}_{ba}$

BER_{rb} denotes the BER of base layer of the hierarchical constellation at relay R shown in Fig. 4.2(b). We can easily obtain $\mathrm{BER}_{rb} = Q[\frac{|H_b|\sqrt{\frac{{\lambda_2}^2}{1+{\lambda_2}^2}}}{\sigma}]$. Thus, substituting BER_{rb} into (4.14), we can obtain

$$\mathrm{BER}_{ab} = \mathrm{BER}_r(1 - Q[\frac{|H_b|\sqrt{\frac{{\lambda_2}^2}{1+{\lambda_2}^2}}}{\sigma}]) + (1 - \mathrm{BER}_r)Q[\frac{|H_b|\sqrt{\frac{{\lambda_2}^2}{1+{\lambda_2}^2}}}{\sigma}]. \tag{4.17}$$

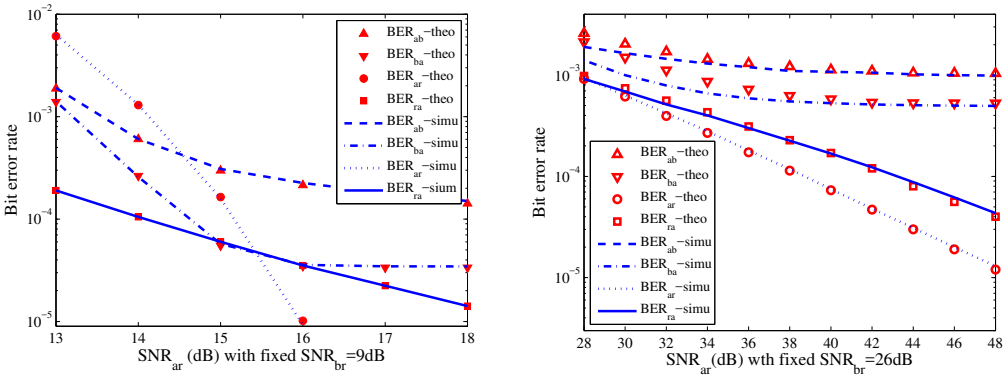

(a) AWGN channel. (b) Rayleigh fading channel.

Figure 4.8: Theoretical results vs simulation results.

Similarly, BER_{ba} can be obtained by

$$\text{BER}_{ba} = \text{BER}_r(1 - Q[\frac{|H_a|\sqrt{\frac{{\lambda_2}^2}{1+{\lambda_2}^2}}}{\sigma}]) + (1 - \text{BER}_r)Q[\frac{|H_a|\sqrt{\frac{{\lambda_2}^2}{1+{\lambda_2}^2}}}{\sigma}]. \tag{4.18}$$

To summarize, BER_{ar}, BER_{ra}, BER_{ab} and BER_{ba} can be obtained by (4.12), (4.13), (4.17) and (4.18). The optimal λ_1 and λ_2 in (4.5) and (4.6) can be obtained. Fig. 4.8(a) shows that the theoretical results match the simulation results, where we fix $\text{SNR}_{br} = 9$ dB and gradually increase SNR_{ar}. When SNR_{ar} is sufficiently large, e.g., larger than 16 dB, the link between source B and relay R, L_{br}, with $\text{SNR}_{br} = 9$ dB is the bottleneck link of the system. In this case, the bit errors contributed to BER_{ba} are mainly caused by signal superimposing in the MA stage subject to SNR_{br}, and the link L_{ar} can forward bits from relay R to source A with a high SNR_{ar}. Thus, when SNR_{ar} is large enough, BER_{ba} will converge to a value (about 3e-05) as shown in Fig. 4.8(a) close to but higher than BER of single-hop BPSK with SNR = 9 dB (about 2e-05). Similarly, for BER_{ab}, roughly speaking it suffers from the bottleneck link L_{br} twice, which includes the signal superimposing in the MA stage and the forwarding from relay R to source B. Thus, when SNR_{ar} is sufficiently high, BER_{ab} will converge to a value close to but higher than twice of single-hop BPSK BER.

4.5.3 Error performance analysis under Rayleigh fading channel

We discuss the error performance analysis of QPSK-BPSK H-PNC under Rayleigh fading channels. To obtain the exact BER of PNC-based under fading channels are quite challenging due to the complexity of the received constellation map at the relay specially when the higher-order modulations are applied by the sources. Denote the probability density function (PDF) of Rayleigh distribution as $f(x,\delta) = \frac{x}{\delta^2}\exp(\frac{-x^2}{2\sigma^2})$, with mean value $E(x) = \delta\sqrt{\frac{\pi}{2}}$. Denote the PDF of channel gains $|H_a|$ and $|H_b|$ as $f(|H_a|,\delta_1)$ and $f(|H_b|,\delta_2)$, respectively.

BER_{ar} can be estimated by considering the worst case with $\theta = \frac{\pi}{2}$ or $\frac{3\pi}{2}$ in Fig. 4.5, and we have

$$\text{BER}_{ar} \approx \int_0^\infty \int_0^\infty f(|H_a|,\delta_1) f(|H_b|,\delta_2) Q[\frac{|H_a|\sqrt{\frac{\lambda_1^2}{1+\lambda_1^2}} - |H_b|}{\sigma}]\text{d}|H_a|\text{d}|H_b|. \quad (4.19)$$

From (4.13), the error performance of BER_{ra} can be obtained by

$$\text{BER}_{ra} = \int_0^\infty f(|H_a|,\delta_1) Q[\frac{|H_a|\sqrt{\frac{1}{1+\lambda_1}}}{\sigma}]\text{d}|H_a|. \quad (4.20)$$

From (4.15) and (4.16), the BER_r can be approximated by

$$\text{BER}_r = \int_0^\infty f(|H_b|,\delta_2) Q[\frac{|H_b|}{\sigma}]\text{d}|H_b|, \quad (4.21)$$

where only the closest decision boundaries in Fig. 4.7 are considered.

BER_{ab} and BER_{ba} are obtained by replacing $Q[\frac{|H_a|\sqrt{\lambda_2^2/(1+\lambda_2^2)}}{\sigma}]$ and $Q[\frac{|H_b|\sqrt{\lambda_2^2/(1+\lambda_2^2)}}{\sigma}]$ by $\int_0^\infty f(|H_a|,\delta_1) Q[\frac{|H_a|\sqrt{\lambda_2^2/(1+\lambda_2^2)}}{\sigma}]\text{d}|H_a|$ and $\int_0^\infty f(|H_b|,\delta_2) Q[\frac{|H_b|\sqrt{\lambda_2^2/(1+\lambda_2^2)}}{\sigma}]\text{d}|H_b|$ from (4.17) and (4.18), respectively.

In Fig. 4.8(b), we compare the theoretical and simulation results under Rayleigh fading channels. Note that we set SNR_{br} = 9 dB and 26 dB under AWGN and Rayleigh fading channels to maintain the overall BER performance around 10e-03. It can be observed that the theoretical results match well with the simulation results for BER_{ar} and BER_{ra}. The small gap between the theoretical and simulation results for BER_{ab} and BER_{ba} are due to the approximation in (4.21) where only the closest Euclidean boundaries are considered. According to the algorithms in Section 4.4.3,

values of λ_1 and λ_2 from 13 dB to 18 dB in Fig. 4.8(a) are 1.75, 1.77, 1.78, 1.78, 1.78, 1.78 and 1.47, 1.63, 1.81, 2.01, 2.24, 2.49, respectively. In Fig. 4.8(b), $\lambda_1 = 1.45$ and λ_2 are 1.4, 1.6, 1.8, 2.1, 2.4, 2.6, 2.8, 3.0, 3.2, 3.4, 3.6, respectively, for ranging from 28 dB to 48 dB with a 2 dB interval.

4.6 Performance Evaluation

In this section, the performance of H-PNC is evaluated under the asymmetric TWRC scenario. We studied a generalized physical-layer design without specifying any wireless communication system, and we consider that in any slot only one symbol is transmitted from any node. We first fix SNR_{br} and gradually increase SNR_{ar}, aiming to study how source-relay channels influence the constellation design and system performance under both AWGN and Rayleigh fading channels. Second, the throughput[7] and the throughput upper bound[8] performance of different H-PNC schemes are studied, aiming to study how to select H-PNC schemes with different channel conditions and various data exchange requirements. Let all nodes transmit signals with the same symbol energy E_s, and the average received SNR of all links are proportional to link distance to the power of path-loss component ($\alpha = 3$). Phase shift difference θ is uniformly distributed between $[0, 2\pi)$.

4.6.1 BER performance with fixed SNR_{br}

The error performance of three H-PNC schemes under AWGN channel are shown in Figs. 4.9 and 4.10, where we fix $\text{SNR}_{br} = 8$ dB and gradually increase SNR_{ar}. Fig. 4.9 shows the error performance of QPSK-BPSK H-PNC. The red curves show error performance with the optimal λ_1 and λ_2 obtained from (4.5) and (4.6), respectively. The blue curves are with symmetric constellation setting in the MA stage, where $\lambda_1 = 1$ and λ_2 is set to its optimal value. From the results, without hierarchical constellation design in the MA stage, BER_{ar} is much worse than BER_r (BER_r overlaps with BER_{ba} and thus is omitted in Fig. 4.9), which implies the necessity of hierarchical constellation design. Considering the red curves, given SNR_{br} and when SNR_{ar} is large, $\gamma = |H_b|/|H_a| = 10^{(\text{SNR}_{br}(\text{dB}) - \text{SNR}_{ar}(\text{dB}))/20}$ is small. Thus, BER_r is dominated by the errors within one BPSK circle and the error over link L_{ar} in the BC stage can

[7] Throughput (bits/slot) is defined as the successfully received bits per slot by all the destinations.

[8] Throughput upper bound (bits/slot) is defined as the theoretical maximal throughput without considering the channel noise.

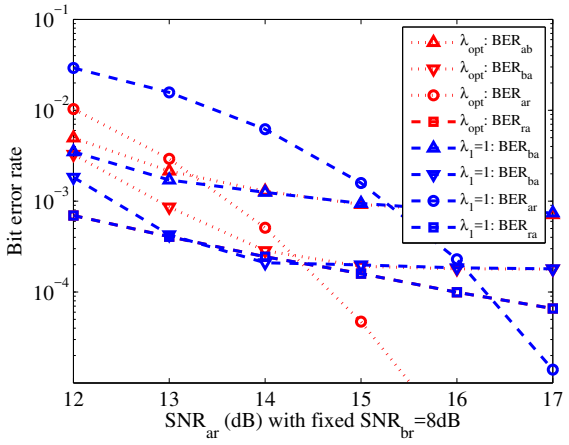

Figure 4.9: QPSK-BPSK H-PNC with fixed $\text{SNR}_{br} = 26$ dB under AWGN channels.

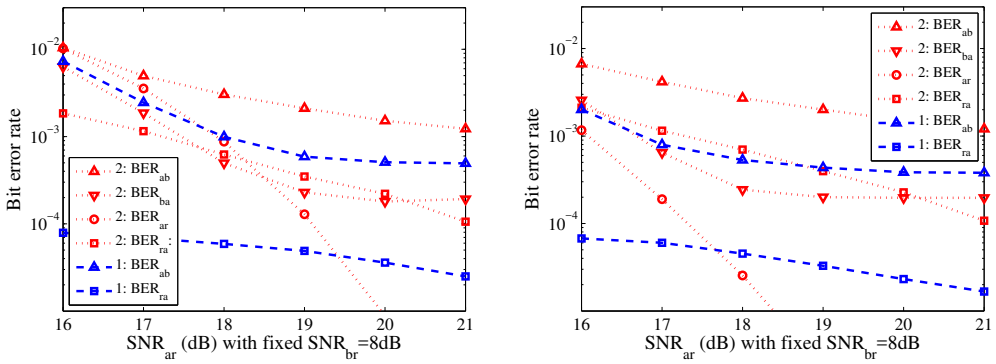

(a) 8QAM-BPSK H-PNC case 1.

(b) 8QAM-BPSK H-PNC case 2.

Figure 4.10: 8QAM-BPSK H-PNC with fixed $\text{SNR}_{br} = 8$ dB under AWGN channels.

be ignored, and that is also why BER_r overlaps with BER_{ba}. Thus, both BER_r and BER_{ba} converge to the error performance of single hop BPSK with SNR = 8 dB under AWGN channels. BER_{ar} and BER_{ra} reduce with the increase of SNR_{ar} monotonously. The solid red and solid black curves are sum $\frac{\text{BERs}}{4}$ (we divide sum BERs by 4 in order to fit in the same figure) performance of QPSK-BPSK H-PNC with or without optimized constellation design, respectively.

Figs. 4.10(a) and 4.10(b) show the error performance of 8QAM-BPSK case 1 and case 2, respectively. The optimal constellation setting are applied for both transmit constellation at source A and broadcast constellation at relay R obtained from (4.5), (4.7) and (4.8). The red and blue curves denote that two bits and one bit of S_{ra} are superimposed on S_n in the BC stage, respectively. For the case that one bit of

S_{ra} is superimposed, BER_{ar} and BER_{ba} are omitted, because BER_{ar} is not affected and BER_{ba} overlaps with that of the scenario where two bits of S_{ra} are superimposed. From the red curves in Figs. 4.10(a) and 4.10(b), BER_{ab} has the worse error performance because the information delivery from source A to source B is under bottleneck link L_{br} twice. Superimposing one bit of S_{ra} only improves BER_{ab} because of the constellation modification in the BC stage. However, the throughput will be reduced accordingly. Thus, there is a tradeoff between the error performance and throughput. How many bits are superimposed in the BC stage are dependent on the data exchange ratio and the error rate requirements.

Figs. 4.11 and 4.12 show the error performance of three H-PNC schemes under Rayleigh fading channels, where we fix $\text{SNR}_{br} = 26$ dB and gradually increase SNR_{ar}. In Fig. 4.11, when SNR_{ar} is large, BER_r is determined by BPSK error performance with SNR = 26 dB under Rayleigh fading channels. Thus, BER_{ba} converges to BER_r as errors over L_{ar} are negligible, and BER_{ab} converges to twice BER_{ba} as the data from A to B are transmitted over bottleneck link L_{br} twice. Figs. 4.12(a) and 4.12(b) are for 8QAM-BPSK H-PNC case 1 and case 2, respectively. The red curves are for the case that two bits of S_{ra} are superimposed in the BC stages, and the blue curves are for the case that only one bit of S_{ra} is superimposed. From the results, superimposing one bit of S_{ra} will improve BER_{ab} and BER_{ra} with a loss of throughput gain. The solid black curves are the end-to-end error performance, i.e., $\frac{\text{BER}_{ab}+\text{BER}_{ba}}{2}$, of BPSK-BPSK PNC. Given $\text{SNR}_{br} = 26$ dB, when SNR_{ar} is large enough, BER_r for QPSK-BPSK H-PNC and 8QAM-BPSK H-PNC is close to that of BPSK-BPSK PNC as the closest Euclidean distance on the received constellation map at the relay, i.e., $|H_b|$, will dominate the BER_r performance. For the end-to-end BER performance, BPSK-BPSK PNC outperforms QPSK-BPSK H-PNC as expected, given a lower-order modulation. However, the system throughput for BPSK-BPSK PNC, 1 bit/slot, is only half of that for QPSK-BPSK H-PNC. Combining both of the throughput and error performance, the system throughput of QPSK-BPSK H-PNC is much higher than that of BPSK-BPSK PNC, and more comparisons on throughput will be presented in Sec. 4.6.3.

4.6.2 Throughput upper bound comparison

H-PNC achieves four flow information exchange not only between the sources but also between the source with the better source-relay channel condition and the relay. The

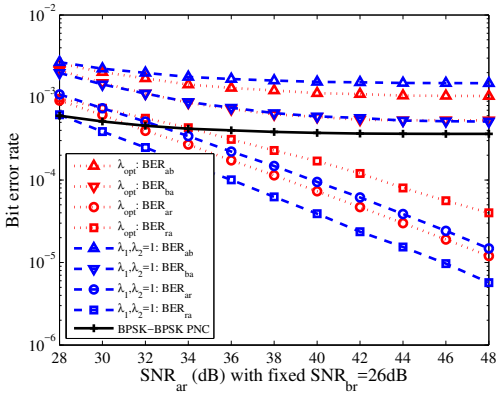

Figure 4.11: QPSK-BPSK H-PNC with fixed $\text{SNR}_{br} = 26$ dB under Rayleigh fading channels.

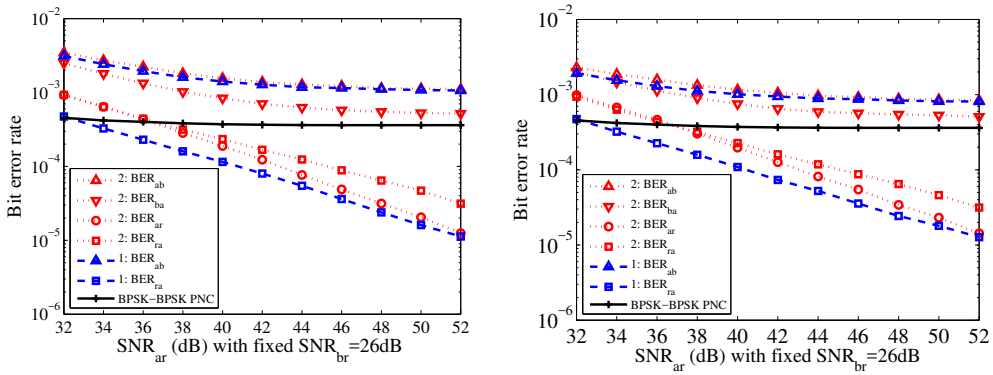

(a) 8QAM-BPSK H-PNC case 1.

(b) 8QAM-BPSK H-PNC case 2.

Figure 4.12: 8QAM-BPSK H-PNC with fixed $\text{SNR}_{br} = 26$ dB under Rayleigh fading channels.

data exchange requirements between these four flows impact on the system throughput of H-PNC. The throughput upper bound of proposed H-PNC, traditional symmetric PNC[9] and single-hop transmission are compared in Fig. 4.13. The throughput upper bound takes a summation of all the links with the unit of bits/slot. If a part of bits cannot be transmitted by H-PNC or symmetric PNC, the leftover bits are transmitted by point-to-point transmissions hop-by-hop with the highest modulation-order supported by each hop. Denote the amount of data delivered by S_{ar}, S_{ra}, S_{ab} and S_{ba} as μ_{ar}, μ_{ra}, μ_{ab} and μ_{ba}, respectively. For QPSK-BPSK and 8QAM-BPSK H-PNC case 1, which are both suitable to transmit data amount of $\mu_{ar} = \mu_{ra}$ and $\mu_{ab} = \mu_{ba}$.

[9]Only BPSK-BPSK PNC can be applied as the symmetric PNC, due to that the bottleneck link L_{br} can only support BPSK.

So is for symmetric PNC, which is suitable to exchange data amount $\mu_{ab}=\mu_{ba}$. Thus, denote $\beta_1 = \frac{\mu_{ar}}{\mu_{ab}}$, where $\mu_{ar} = \mu_{ra}$ and $\mu_{ab} = \mu_{ba}$. β_1 denotes the data amount between source A and relay R over that between sources A and B. For example, when $\beta_1=0$, H-PNC deteriorates to HePNC [68], and when β_1 goes to infinity, H-PNC deteriorates to the single-hop transmission from source A to relay R. Fig. 4.13(a) shows the throughput upper bound comparison of QPSK-BPSK H-PNC, BPSK-BPSK PNC and the single hop transmission. We can observe that QPSK-BPSK H-PNC is most suitable to support the data exchange ratio $\beta_1 = 1$, where 4 bits can be delivered in 2 slots. The maximum throughput gain compared to BPSK-BPSK PNC is 50%. For BPSK-BPSK PNC and the single hop transmission, throughput upper bound increases with the increase of β_1. In Fig. 4.13(b), 8QAM-BPSK H-PNC case 1 achieves the highest throughput upper bound when $\beta_1 = 2$, where totally 6 bits can be delivered by 2 slots. The maximum throughput gain compared to BPSK-BPSK PNC is 66.7%.

For 8QAM-BPSK H-PNC case 2, the data exchange ratio between sources A and B, and that between source A and relay R, is asymmetric. Denote $\beta_2 = \frac{\mu_{ar}}{\mu_{ba}}$ with $\mu_{ab} = 2\mu_{ba}$ and $\mu_{ra} = 2\mu_{ar}$[10]. In Fig. 4.13(c), all throughput upper bounds of three transmission schemes are proportional to β_2, and finally converges to 3 bits/slot, i.e., the majority bits are transmitted over link L_{ar} by 8QAM. When $\beta_2=1$, the maximum throughput gain compared to BPSK-BPSK PNC is 44%.

4.6.3 Discussion on H-PNC scheme selection.

In this subsection, we discuss the guide of H-PNC selection. In Fig. 4.14, by fixing SNR_{br} = 26 dB and adjusting SNR_{ar} in a large range from 28 dB to 52 dB, the throughput performance under Rayleigh fading channels by selecting different H-PNC schemes can be easily compared. We consider that one block contains 256 bits, and a block is successfully received if all bits are correctly received; otherwise, the block is dropped and bits in the erroneous block are not counted in throughput. Figs. 4.14(a), 4.14(b), 4.14(c) and 4.14(d) compare the throughput over different flows given source-relay channels by selecting different H-PNC schemes.

We should select the suitable H-PNC scheme by jointly considering the data exchange requirements among sources A and B and source A and relay R, two source-

[10]Note that, up to 2 bit of S_{ra} can be superimposed, which cause more asymmetric but a higher throughput gain. For a fair comparison, Fig. 4.13(c) only considers 1 bit of S_{ra} is superimposed.

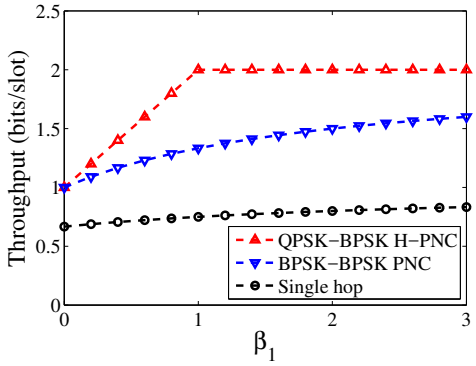

(a) QPSK-BPSK H-PNC.

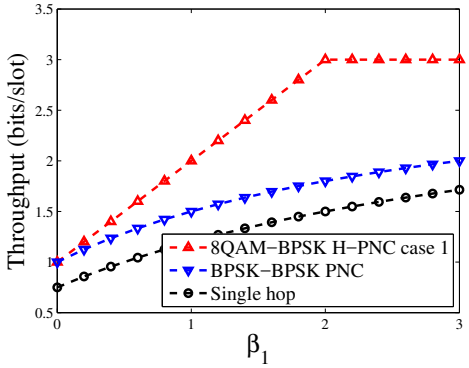

(b) 8QAM-BPSK H-PNC case 1.

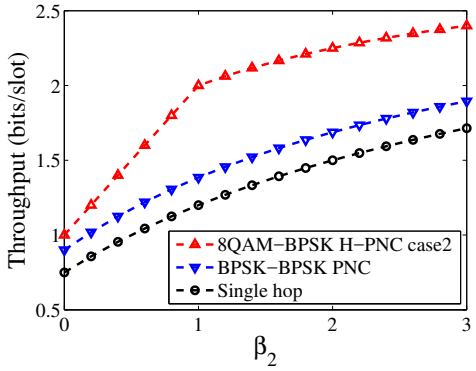

(c) 8QAM-BPSK H-PNC case 2.

Figure 4.13: Throughput upper bound of different transmission schemes.

relay channel conditions and the BER requirement of each flow. For example, if sources A and B, and source A and relay R exchange the same amount of data, QPSK-BPSK H-PNC is suggested and we can observe throughput performance under different two source-relay channel conditions in Fig. 4.14. QPSK-BPSK H-PNC

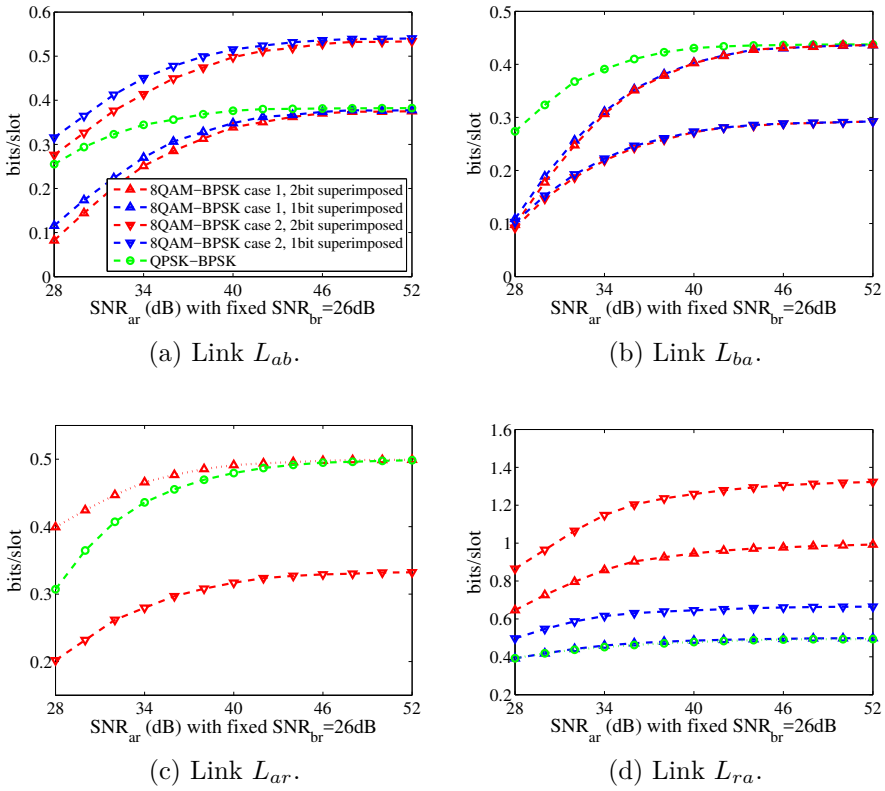

(a) Link L_{ab}. (b) Link L_{ba}.

(c) Link L_{ar}. (d) Link L_{ra}.

Figure 4.14: Throughput under Rayleigh fading channels.

achieves the best data rate for flow from B to A compared to 8QAM-BPSK H-PNC as shown in Fig. 4.14(b), however, it achieves a relatively lower data rate for flow R to A as shown in Fig. 4.14(d). 8QAM-BPSK H-PNC achieves better BER_{ar} compared to QPSK-BPSK H-PNC as shown in Fig. 4.14(c), but a relatively lower data rate for flow from A to B as shown in Fig. 4.14(a). Thus, there is a tradeoff to select and configure H-PNC.

Chapter 5

Design of Multi-hop Physical Layer Network Coding

5.1 Overview

In the last three chapters, we focus on designs where only one relay is required to forward message between two sources. In this chapter, we investigate multi-hop PNC, where multiple relays located in a linear topology are scheduled to exchange the message between two end sources. In multi-hop PNC design, the impact of error propagation and mutual-interference should be carefully addressed. In this chapter, we propose two multi-hop PNC design, D-MPNC and S-MPNC, which target for simple implementation and the optimal end-to-end BER, respectively. The error propagation impact is carefully controlled and theoretical end-to-end BER is obtained. Performance evaluations in terms of end-to-end BER and throughput[1] are further conducted under both AWGN and Rayleigh fading channels.

5.2 Related Work

Traditional PNC has been extensively studied from theory [3, 5, 13, 37, 54, 55] to implementation [56]. [62] generalized the PNC design with a star topology, where the information exchange of four nodes with help of one relay was considered. [63] further generalized the star-topology design with an arbitrary number of sources.

[1]Throughput (symbols/slot) is defined the successfully received symbols per slot by all the destinations.

The design of multi-hop PNC has received less attention. [34] proposed a directional multi-hop PNC design. [4] provided specific PNC designs with a given number of relays. [64–66] generalized design of multi-hop analog network coding (ANC) in a linear topology with outage probability analysis. The design in [64] can outperform non-PNC scheme with a small number of relays, while the design in [65] can outperform non-PNC scheme with a large number of nodes. [66] further extended [64] and [65], and its end-to-end throughput upper bound decreases with the increase of the number of relays. An inspiring generalization of multi-hop PNC was proposed in [1], which achieved the end-to-end throughput upper bound of one symbol per symbol duration. However, the error propagation effect is not addressed, which may result in a serious error propagation problem as discussed in Sec. 5.3.3. Also, the mutual-interference from other transmitting nodes are not addressed in the existing multi-hop PNC and ANC designs.

In this chapter, the impact of error propagation and mutual-interference in multi-hop PNC are addressed. We propose two multi-hop PNC designs targeting on simple-implementation and the optimal end-to-end BER, respectively. The tradeoff between these two designs is discussed in Sec. 5.5.4. Both designs can achieve the maximum end-to-end throughput upper bound of one symbol per symbol duration, which is the same as that of traditional PNC with a single relay.

5.3 Design Criterion of Multi-hop PNC

5.3.1 System model

Consider a multi-hop TWRC network where sources A and B want to exchange information with the help of multiple relays arranged in a linear topology. In this chapter, each node uses BPSK modulation for transmission. Each node is equipped with one antenna and works in the half-duplex mode. We assume symbol-level synchronization at the relays and perfect channel estimation at the receivers.

All the nodes, including the sources and the relays, follow a transmitting-and-receiving pattern, i.e., to alternate between the transmission mode and receiving mode, and to stay in each mode for one slot duration. In order to achieve the end-to-end throughput of one symbol per symbol duration, i.e., the same as that of traditional PNC with a single relay, there cannot exist any idle slot except the constant

initialization slots[2]. We consider that at any slot only one symbol is transmitted from any node and slot duration equals symbol duration. Depending on how many useful signals are received at the receiver, transmissions of multi-hop PNC can be divided into two categories, multiple-access transmission and single-hop transmission. The multiple-access transmission refers to that two useful signals transmitted from neighboring nodes are superimposed at a relay, and the single-hop transmission refers to that a relay transmits a signal to a destination. Note that in multi-hop PNC, all the nodes not only receive useful signals, but also the mutual-interference from all other transmitting nodes, which is explained in Sec. 5.3.4 and considered in Sec. 5.4 and Sec. 5.5.

5.3.2 Procedure of the proposed multi-hop PNC

Denote the indexes of time-slot and relay as i and j, respectively, where $i \in \{1, 2, \cdots\}$, $j \in \{1, 2, \cdots, N\}$ and N is the total number of the relays in the multi-hop PNC. For multiple-access transmission, the received symbol of the j-th relay in the i-th slot is

$$Y_{r_{j,i}} = H_{r_{j-1,i}}(1 - 2S_{r_{j-1,i}}) + H_{r_{j+1,i}}(1 - 2S_{r_{j+1,i}}) + N_j, \tag{5.1}$$

where $H_{r_{j-1,i}}$ and $H_{r_{j+1,i}}$ are the channel gains of the links between the $(j-1)$-th and the j-th node, and that between the j-th and the $(j+1)$-th node, respectively. N_j is the sum of complex Gaussian noise with variance $2\sigma^2$ and the mutual-interference from all other transmitting nodes. $S_{r_{j-1,i}}$ and $S_{r_{j+1,i}} \in \{0, 1\}$ are the symbols transmitted from the $(j-1)$-th node and the $(j+1)$-th node, respectively. The network-coded symbol obtained by the j-th relay is

$$S_{r\_xor_{j,i}} = \hat{S}_{r_{j-1,i}} \oplus \hat{S}_{r_{j+1,i}}, \tag{5.2}$$

where $\hat{S}_{r_{j-1,i}}$ and $\hat{S}_{r_{j+1,i}}$ are the estimations of the superimposed symbols from neighboring relays, which can be obtained by

$$(\hat{S}_{r_{j-1,i}}, \hat{S}_{r_{j+1,i}}) = \underset{s_{r_{j-1,i}}, s_{r_{j+1,i}} \in \{0,1\}}{\operatorname{argmin}} |Y_{r_{j,i}} - H_{r_{j-1,i}}(1 - 2s_{r_{j-1,i}}) - H_{r_{j+1,i}}(1 - 2s_{r_{j+1,i}})|^2. \tag{5.3}$$

Note that for the j-th relay, it may not directly transmit the network-coded symbol

[2]When the number of the transmission slots goes to infinity, the impact of the constant number of initialization slots to end-to-end throughput can be neglected.

$S_{r\_xor_{j,i}}$ in (5.2) in the following slot, as the received information in the previous slots may be positively applied and combined with $S_{r\_xor_{j,i}}$. Similarly, the sources may not simply transmit X_i and Y_i at the transmitting slots, where i is the index of the source data, as the received information in the previous slots can also be positively applied. These issues are discussed in Sec. 5.3 by an example, and in Sec. 5.4 and Sec. 5.5 in detail.

For the single-hop transmission from the source neighboring relays to the sources, at the i-th slot, $i \in \{2, 4, \cdots\}$, the received signal at source A from the first relay is

$$Y_{a_i} = H_{a_i}(1 - 2S_{r_{1,i}}) + N_a, \tag{5.4}$$

where H_{a_i} is the channel gain of the link between source A and the first relay and N_a is the summation of Gaussian noise and mutual-interference from all other transmitting nodes. The estimation of $S_{r_{1,i}}$ can be obtained by

$$\hat{S}_{r_{1,i}} = \underset{s_{r_{1,i}} \in \{0,1\}}{\operatorname{argmin}} |Y_{a_i} - H_{a_i}(1 - 2s_{r_{1,i}})|^2. \tag{5.5}$$

The detection at source B can be obtained similarly to (5.4) and (5.5). Note that different from traditional PNC with a single relay, in multi-hop PNC, source A may not directly obtain target information from $\hat{S}_{r_{1,i}}$, as $\hat{S}_{r_{1,i}}$ may be an XOR result of multiple symbols. How to obtain the target information from $\hat{S}_{r_{1,i}}$ is explained in Sec. 5.3.3 by an example and explained in Sec. 5.4.2 and Sec. 5.5.2 in detail.

The transmission protocol design of multi-hop PNC is challenging. How to apply the received information in the previous slots at all nodes is a tricky issue, and improperly applying the previously received information may result in serious error propagation as shown in Sec. 5.3.3. Also, different strategies of applying these information will result in different symbol combination patterns at the relays, which further challenges the sources how to identify the received symbol combinations varied in different slots and how to extract the target information from the symbol combinations by a generalized decoding algorithm.

5.3.3 Error propagation in multi-hop PNC

Error propagation is an important issue in multi-hop PNC and improper design may result in serious error propagation. We use the multi-hop PNC with three relays in [1]

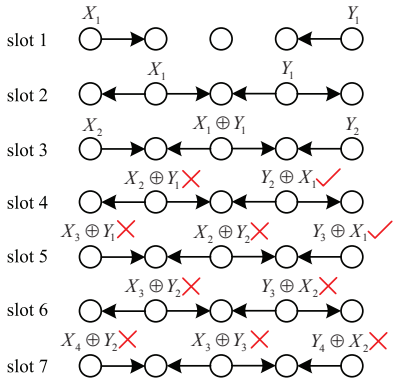

Figure 5.1: Impact of error propagation in multi-hop PNC.

as shown in Fig. 5.1 to explain the impact of error propagation. By the scheduling introduced in [1], at the i-th slot, $i \in \{5, 7, \cdots\}$, the source A (B) transmits the XOR result of $X_{\frac{i+1}{2}}$ ($Y_{\frac{i+1}{2}}$) and the estimated $\hat{Y}_{\frac{i-3}{2}}$ ($\hat{X}_{\frac{i-3}{2}}$) in the last slot. For example, at the fifth slot, source A transmits XOR result of X_3 and $\hat{Y}_1$ obtained in the fourth slot. The relays transmit XOR results of the two network-coded symbols obtained in the last slot and the last three slots. For example, at the fifth slot, the second relay transmits $X_2 \oplus Y_2$, which is the XOR result of the network-coded symbol $X_2 \oplus Y_1 \oplus Y_2 \oplus X_1$ obtained in the fourth slot and that $X_1 \oplus Y_1$ obtained in the second slot.

The above scheduling may result in infinite end-to-end estimation errors. In Fig. 5.1, consider the case that the estimation of $X_2 \oplus Y_1$ is erroneous at the first relay at the third slot. The transmitted symbol from the first relay at the fourth slot, i.e., $X_2 \oplus Y_1$, is erroneous accordingly. The impact on the following slots are marked in the figure, where the check and cross mark means the corresponding symbol is correct or in error, respectively. Note that, although at the fifth slot the binary results of $X_3 \oplus Y_1$ and $X_2 \oplus Y_2$ are both erroneous at the first relay and the second relay, respectively, the resulting network-coded symbol $X_3 \oplus Y_2$ at the second relay at the sixth slot is still erroneous by XOR the previous erroneous network-coded symbol $X_2 \oplus Y_1$. We can easily find that all the end-to-end estimations of Y_i, $i \in \{1, 2, \cdots\}$ and X_i, $i \in \{2, 3, \cdots\}$ at the sources are erroneous. Thus, improperly utilizing received information in the previous slots can result in serious error propagation. How to control and minimize error propagation is an important issue in multi-hop PNC, which directly determines the end-to-end throughput.

5.3.4 Mutual-interference in multi-hop PNC

Different from the traditional PNC with a single relay, in multi-hop, the received signals at any node not only contain useful information from neighboring nodes, but also possible mutual-interference from all other transmitting nodes depending on scheduling [106, 107]. For example, consider the multi-hop PNC with three relays as shown in Fig. 5.1. When the first relay receives two useful signals from source A and the second relay, it also suffers from mutual-interference from source B. Similar mutual-interferences exist for other nodes. With the increase of the number of relays, one receiver may suffer from the mutual-interference from more than one node.

In this chapter, for a fair comparison, the total transmission power at all the nodes in any two continuous slots are fixed and denoted as $2E_b$. The distance between sources A and B is d (m) and the path-loss exponent is α. The end-to-end SNR (dB), i.e., SNR_{ab}, is defined as the single-hop SNR considering the direct transmission without PNC, which can be expressed as

$$\text{SNR}_{ab}(\text{dB}) = 10\log_{10}(\frac{E_b d^{-\alpha}}{2\sigma^2}), \tag{5.6}$$

where $\text{SNR}_{ab}(\text{dB})$ denotes the direct transmission from the two sources without PNC with transmission power E_b. For multi-hop PNC with N relays, the transmission power for each node is $\frac{2E_b}{N+2}$, and hop-distance between any two nodes is $\frac{d}{N+1}$ equally[3]. Different from traditional PNC with a single relay, in multi-hop PNC, due to the mutual-interference, SINR should be considered for any node instead of SNR. The SINR (dB) for the k-th node, $k \in \{1, 2, \cdots, N+2\}$, is

$$\text{SINR}_k(\text{dB}) = 10\log_{10}\frac{\frac{2E_b}{N+2}(\frac{d}{N+1})^{-\alpha}}{2\sigma^2 + \sum_{i=1}^{\lfloor\frac{k-1}{3}\rfloor}\frac{2E_b}{N+2}(\frac{(2i+1)d}{N+1})^{-\alpha} + \sum_{j=1}^{\lfloor\frac{N+2-k}{3}\rfloor}\frac{2E_b}{N+2}(\frac{(2j+1)d}{N+1})^{-\alpha}}, \tag{5.7}$$

where $\sum_{i=1}^{0}(\cdot) = 0$, $\sum_{i=1}^{\lfloor\frac{k-1}{3}\rfloor}\frac{2E_b}{N+2}(\frac{(2i+1)d}{N+1})^{-\alpha}$ and $\sum_{j=1}^{\lfloor\frac{N+2-k}{3}\rfloor}\frac{2E_b}{N+2}(\frac{(2j+1)d}{N+1})^{-\alpha}$ are the sum of the interference from the nodes on the left-side and the right-side of the k-th node, respectively. From (5.6) and (5.7), when the end-to-end SNR_{ab} (dB) is sufficiently large, it is easy to find that $\text{SINR}_k(\text{dB})$ will be upper bounded by $10\alpha\log_{10}(3)$, where 3 is determined by the distance ratio of the closest interference node, i.e., 3 hop-distance away, and the neighboring node.

[3]The impact when the relays are not equally located are studied in Sec. 5.6.3.

5.3.5 Proposed multi-hop PNC designs

In this chapter, depending on the operations of the sources and the relays, we propose two multi-hop PNC designs, D-MPNC and S-MPNC. The error propagation and mutual-interference issues are well addressed in both designs. In D-MPNC, the operations of relays are the same as that in the traditional PNC with a single relay, i.e., to demodulate the superimposed symbols from neighboring nodes and directly broadcast network-coded symbol constructed from demodulation results. In other words, previously received information are not utilized by the relays in D-MPNC. In S-MPNC, we target to obtain and generalize multi-hop PNC design in terms of the optimal end-to-end BER. All of the sources and relays are able to apply the previously received information in S-MPNC. The key issues in the D-MPNC design include how the sources identify received symbol combination from neighboring relays and how to design a generalized decoding algorithm for the sources as received symbol combination varies with slots. The key issues in the S-MPNC design include how to properly apply previously received information to minimize the error propagation impact, how to design the generalized decoding algorithm at the sources, how to minimize end-to-end BER and maximize end-to-end throughput and how to generalize S-MPNC with an arbitrary number of relays. We elaborate the designs of D-MPNC and S-MPNC in Sec. 5.4 and Sec. 5.5, respectively.

5.4 Design of D-MPNC

In this section, we provide the design of D-MPNC. D-MPNC benefits from simple implementation, as the functions of relays are the same as that of traditional PNC with a single relay, i.e., to receive superimposed signals and broadcast network-coded symbol directly. We illustrate the design of D-MPNC and obtain the bound of end-to-end BER for D-MPNC.

5.4.1 Procedure of D-MPNC

The procedure of D-MPNC with an odd number of relays can be summarized as follows:

1) The sources and the even-index relays transmit at the i-th slot, $i \in \{1, 3, \cdots\}$ and receive at the $(i+1)$-th slot. The odd-index relays transmit at the $(i+1)$-th slot and receive at the i-th slot.

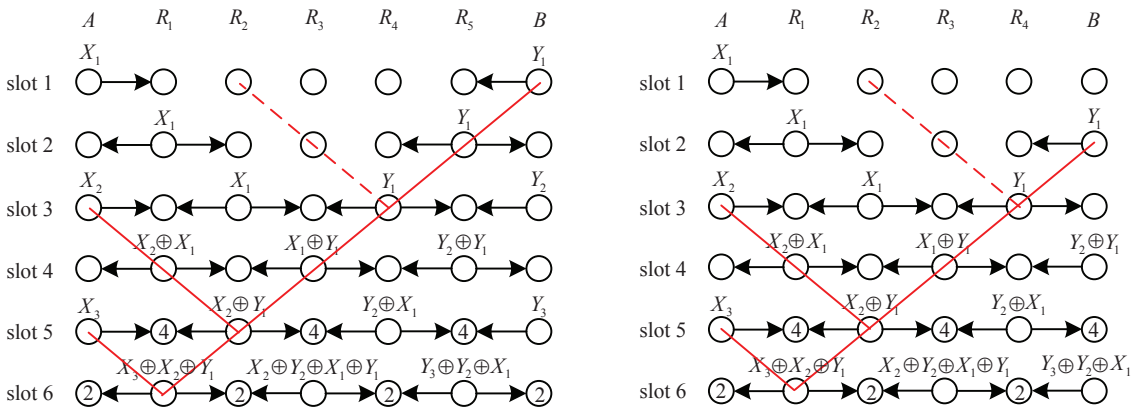

(a) D-MPNC with $N = 5$. (b) D-MPNC with $N = 4$.

Figure 5.2: Transmission graph of D-MPNC.

2) The source A and B transmit $X_{\frac{i+1}{2}}$ and $Y_{\frac{i+1}{2}}$, respectively, at the i-th slot, $i \in \{1, 3, \cdots\}$.

3) All the relays directly transmit the network-coded symbol obtained in (5.2) at the transmitting slots, which is the same as that of traditional PNC with a single relay.

The D-MPNC with even-number N relays can be extrapolated from the D-MPNC with N+1 relays by letting source B transmit XOR result of $Y_{\frac{i}{2}}$, $i \in \{2, 4, \cdots\}$ and the last received binary information, where N is number of the relays. We use Figs. 5.2(a) and 5.2(b) as two examples to explain the procedure of D-MPNC, which show the transmission graph of D-MPNC with $N = 5$ and $N = 4$, respectively. In Fig. 5.2(a), the first four slots are initializing slots, as the first two target information X_1 and Y_1 have not been delivered to the other source. From the fifth slot, two sources can exchange two packets end-to-end by every two slots. Thus, when the number of transmission slots is sufficiently large, the end-to-end throughput upper bound is one symbol per symbol duration as two packets are delivered in any two slots. In Fig. 5.2(b), it shows that D-MPNC with $N = 4$ can be extrapolated from D-MPNC with $N = 5$ by letting source B transmit the XOR result of $Y_{\frac{i}{2}}$, $i \in \{2, 4, \cdots\}$ and the last received binary information. For example, at the 4-th slot, source B transmits $Y_2 \oplus Y_1$.

From Fig. 5.2, we can see that with the increase of transmission slots, the transmitting symbol at the relay may be an XOR result of a symbol combination containing more and more symbols. However, it is unnecessary for the relay to identify any bit in the symbol combination. For the relay perspective, it simply receives two superimposed signals from the neighboring nodes and broadcasts the network-coded symbol

obtained by (5.2) without knowing the details of symbol combination. Note that the challenge part is that how the sources identify symbol combination from neighboring relays in (5.5) and then extract the target information from the other source, which is discussed in the next subsection.

5.4.2 Design of the decoding algorithm for D-MPNC

The generalized decoding algorithm for D-MPNC is provided in this subsection, which specifies the iteration algorithm for the sources to extract the target information of the other source from the obtained symbol combinations. The first step for the source is to identify the received symbol combination from neighboring relay, which varies with slots. The second step is to extract the target information from the identified symbol combination by a generalized algorithm. We use D-MPNC with $N = 5$ in Fig. 5.2(a) as an example to illustrate, followed by concluding D-MPNC designs with other numbers of relays.

Identifying the received symbol combination

At the i-slot, $i \in \{2, 4, \cdots\}$, for source A, the target symbol to be estimated from source B is $Y_{\frac{i-N+1}{2}}$, because symbol $Y_{\frac{i-N+1}{2}}$ takes $N + 1$ slots to be delivered from source B to source A. The precondition for source A to extract the target information $Y_{\frac{i-N+1}{2}}$ is to identify the symbol combination of $S_{r_{1,i}}$ in (5.5). For D-MPNC, the sources can identify the received symbol combination of $S_{r_{1,i}}$ according to a graph-based algorithm. Considering D-MPNC with $N = 5$ as shown in Fig. 5.2(a), the graph-based algorithm is described as follows:

1) Generate a tree with the root of relay R_1 at the i-th slot, $i \in \{6, 8, \cdots\}$.

2) Visit the two neighboring nodes of all the roots at the $(i-1)$-th slot. If any node is not a source node nor it is visited twice, update it as a new root.

3) Generate edges connecting root R_1 at the i-th slot with the new root and the visited source at the $(i-1)$-th slot.

4) Repeat steps 2) and 3) until the first slot is considered.

5) The received symbol combination at source A at the i-th slot, i.e., $S_{r_{1,i}}$, is the XOR combination result of all the symbols at the source nodes visited.

We provide an example to explain the above graph-based algorithm. In Fig. 5.2(a), the received symbol combination at source A at the sixth slot can be obtained by selecting the relay R_1 at the sixth slot as the root in step 1). In step 2), visit source

A and relay R_2 at the fifth slot. Update R_2 as a new root as it is only visited once. In step 3), generate two edges connecting root R_1 at the sixth slot with source A and R_2 at the fifth slot, respectively. In step 4), steps 2) and 3) are repeated until the first slot is visited. In step 5), the symbol combination of $S_{r_{1,6}}$ at the sixth slot can be expressed by XOR all the symbols at the source nodes visited, i.e., $S_{r_{1,6}} = X_3 \oplus X_2 \oplus Y_1$. By observing the tree generated in the graph presented in the red edges, we can easily find that the received symbol combination $S_{r_{1,i}}$ at source A follows a pattern of $X_i \oplus X_{i-1} \oplus Y_{i-2} \oplus X_{i-3} \oplus Y_{i-4} \cdots$ until the index is 1.

Generalizing the iteration decoding algorithm

The graph-based algorithm identifies the received symbol combination at the sources from neighboring relays. We target on generalizing the decoding algorithm for D-MPNC by the help of the pattern obtained from the graph-based algorithm. We use D-MPNC with $N = 5$ as an example, where source A (B) can extract the target information from the received symbol combination by an iteration decoding algorithm summarized as follows:

1) Maintain two buffers denoted as B_1 and B_2, which are initialized as $B_1 = 0$ and $B_2 = X_1$ at source A (B).

2) At the i-th slot, $i \in \{6, 10, 14, \cdots\}$[4], obtain $\hat{S}_{r_{1,i}}$ by (5.5). Extract $\hat{Y}_j = \hat{S}_{r_{1,i}} \oplus X_{j+2} \oplus X_{j+1} \oplus B_1$, $j = \frac{i}{2} - 2$. Update $B_1 = X_{j+2} \oplus \hat{S}_{r_{1,i}}$.

3) At the i-slot, $i \in \{8, 12, 16, \cdots\}$, obtain $\hat{S}_{r_{1,i}}$ by (5.5). Extract $\hat{Y}_j = \hat{S}_{r_{1,i}} \oplus X_{j+2} \oplus X_{j+1} \oplus B_2$, $j = \frac{i}{2} - 2$. Update $B_2 = X_{j+2} \oplus \hat{S}_{r_{1,i}}$.

For example, at the sixth slot, $\hat{Y}_1$ can be obtained by $\hat{Y}_1 = \hat{S}_{r_{1,6}} \oplus X_3 \oplus X_2 \oplus B_1$, where $\hat{S}_{r_{1,6}} = X_3 \oplus X_2 \oplus \hat{Y}_1$ and $B_1 = 0$ by step 1), and then B_1 is updated to be $X_2 \oplus \hat{Y}_1$. At the tenth slot, $\hat{Y}_3$ can be obtained by $\hat{Y}_3 = \hat{S}_{r_{1,10}} \oplus X_5 \oplus X_4 \oplus B_1$, where $\hat{S}_{r_{1,10}} = X_5 \oplus X_4 \oplus \hat{Y}_3 \oplus X_2 \oplus \hat{Y}_1$, and then B_1 is updated to be $X_4 \oplus \hat{Y}_3 \oplus X_2 \oplus \hat{Y}_1$. Note that by the above iteration decoding algorithm, although $S_{r_{1,i}}$, B_1 and B_2 are the XOR combination of multiple symbols, the sources only need to maintain two binary results in buffers B_1 and B_2 without identifying any individual symbol in the symbol combinations.

[4]The sixth slot is the first slot that the target information Y_1 is delivered from source B to source A.

5.4.3 Decoding algorithm of D-MPNC with other numbers of relays

When $N=1$, D-MPNC deteriorates to the traditional PNC with a single relay. The traditional PNC decoding algorithm can be directly applied.

When $N=3$, the received symbol pattern can be obtained according to the graph-based algorithm described in Sec. 5.4.2, i.e., at the i-th slot, $i \in \{4, 6, \cdots\}$, the received symbol combination at source A is $X_{\frac{i}{2}} \oplus X_{\frac{i}{2}-1} \oplus \hat{Y}_{\frac{i}{2}-1}$. Thus, the iteration decoding algorithm applied at source A is to extract $\hat{Y}_{\frac{i}{2}-1} = \hat{S}_{r_{1,i}} \oplus B$ by maintaining one buffer initialized with $B = X_2 \oplus X_1$ and updated by $B = X_{\frac{i}{2}} \oplus X_{\frac{i}{2}-1}$.

When $N = 7$, according to the graph-based algorithm, at the i-th slot, $i \in \{8, 10, \cdots\}$, the received symbol combination at source A is $X_{\frac{i}{2}} \oplus X_{\frac{i}{2}-1} \oplus X_{\frac{i}{2}} \oplus \hat{Y}_{\frac{i}{2}-1}$. Thus, the iteration decoding algorithm applied at the source A is to extract $\hat{Y}_{\frac{i}{2}-3} = \hat{S}_{r_{1,i}} \oplus B$ by maintaining one buffer initialized with $B = X_4 \oplus X_3 \oplus X_1$ and updated by $B = X_{\frac{i}{2}} \oplus X_{\frac{i}{2}-1} \oplus X_{\frac{i}{2}-3}$.

The design of D-MPNC with even-number N can be extrapolated from D-MPNC with N+1 relays. To generalize D-MPNC with an arbitrary number of N is challenging, because the transmission patterns of D-MPNC with different N are dynamic. For D-MPNC with $N > 7$, we can first design the case when N is an odd number and then obtain D-MPNC with $(N-1)$ by extrapolating from D-MPNC with N. To design the iteration algorithm for D-MPNC given N, we first need to identify the received symbol combination at the sources according to the graph-based algorithm described in Sec. 5.4.2, and then generalize the pattern of received symbol combination, followed by designing the iteration decoding algorithm with the help of the symbol combination pattern.

5.4.4 End-to-end BER analysis of D-MPNC

One of the main concern for multi-hop PNC design is the error propagation issue. In this section, we analyze the end-to-end BER performance of MPNC, which is defined as

$$\mathrm{P}_{e2e} = (\mathrm{P}\{\hat{X} \neq X\} + \mathrm{P}\{\hat{Y} \neq Y\})/2. \tag{5.8}$$

For the multi-hop path with N relays, the per-hop distance is assumed the same. The transmission procedure of MPNC includes multi-access and single-hop transmissions, which should be studied separately. We first obtain relay mapping error rate

(P_{xor}) of the multi-access transmission and single-hop transmission error rates ($\mathrm{P}_{a,r}$ and $\mathrm{P}_{b,r}$) for the traditional PNC with a single relay, and then study the end-to-end BER for PNC with multiple relays.

Traditional PNC with a single relay

We first provide the end-to-end error performance of traditional PNC with a single relay. Denote the channel gain over source-relay link between source A and the relay and between source B and the relay as H_a and H_b, respectively, where H_a and H_b are complex numbers. According to [94, 108], for the AWGN channels, the error performance of the multiple-access transmission can be estimated by

$$\mathrm{P}_{xor} = 2\mathrm{P}_{\theta\in(0,\frac{\pi}{2})} + 2\mathrm{P}_{\theta\in(\frac{\pi}{2},\pi)}, \tag{5.9}$$

where $\mathrm{P}_{\theta\in\{0,\frac{\pi}{2}\}} = \mathrm{P}_{\theta\in\{\frac{3\pi}{2},2\pi\}}$ and $\mathrm{P}_{\theta\in\{\frac{\pi}{2},\pi\}} = \mathrm{P}_{\theta\in\{\pi,\frac{3\pi}{2}\}}$ due to the symmetry of the received constellation map at the relay. Define amplitude ratio and phase shift difference between H_a and H_b as γ and θ, respectively, where $H_a = H_b\gamma\exp(j\theta)$. Define

$$G(\phi, L) = \frac{1}{2\pi}\int_0^{\phi} \exp(-\frac{L^2}{2\sigma^2\sin^2(\theta')})\mathrm{d}\theta', \tag{5.10}$$

we have

$$\begin{aligned}\mathrm{P}_{\theta\in(0,\frac{\pi}{2})} = \frac{\frac{\pi}{2}-0}{2\pi}\frac{1}{2\pi}\int_0^{\frac{\pi}{2}} \{&G(\frac{\pi}{2}+\tan^{-1}(\frac{1-\gamma\cos(\theta)}{\gamma\sin(\theta)}), H_b^2) \\ &+ G(\frac{\pi}{2}+\tan^{-1}(\frac{\gamma-\cos(\theta)}{\sin(\theta)}), H_a^2)\}\mathrm{d}\theta,\end{aligned} \tag{5.11}$$

$$\mathrm{P}_{\theta\in(\frac{\pi}{2},\pi)} \approx \frac{\pi-\frac{\pi}{2}}{2\pi}G(\pi, H_b^2) + \frac{\pi-\frac{\pi}{2}}{2\pi}G(\pi, H_a^2). \tag{5.12}$$

Note that (5.11) is valid for the case of $\gamma \leq 1$. When $\gamma > 1$, we need to swap H_a and H_b in (5.11). The error performance of multiple-access transmission P_{xor} can be obtained by substituting (5.11) and (5.12) into (5.9).

The BER of single-hop transmission $\mathrm{P}_{i,r}$ over link between source $i \in \{a, b\}$ and the relay can be obtained by

$$\mathrm{P}_{i,r} = \frac{1}{2\pi}\int_0^{\pi} \exp(\frac{H_i^2}{2\sigma^2\sin^2(\theta')})\mathrm{d}\theta', \tag{5.13}$$

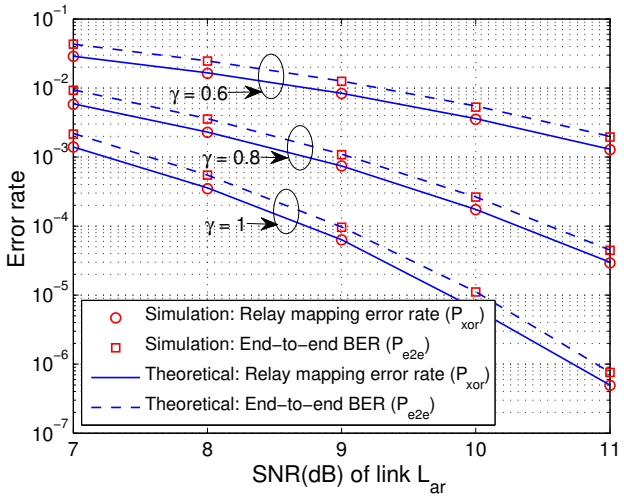

Figure 5.3: Theoretical vs simulation.

where $i \in \{a, b\}$. Thus, end-to-end BER performance can be obtained by

$$\mathrm{P}_{e2e} = \frac{\mathrm{P}_{xor}(2-\mathrm{P}_{a,r}-\mathrm{P}_{b,r})+(1-\mathrm{P}_{xor})(\mathrm{P}_{a,r}+\mathrm{P}_{b,r})}{2}. \tag{5.14}$$

The theoretical and simulation comparison is shown in Fig. 5.3, we can see that (5.9) and (5.14) match the simulation results well.

End-to-end BER bound of D-MPNC

We first study the error propagation impact in D-MPNC, we will show that the error propagation caused by a single estimation error at the relay can be bounded by constant bits, and the end-to-end BER can be bounded by the sum of the individual effect of the multi-access and single-hop transmission errors. We use the case of D-MPNC with $N=5$ as shown in Fig. 5.4 to explain.

Consider the case that if and only if the superimposed symbol at R_1 at the fifth slot is in error as shown in Fig. 5.4. The received symbol combinations at A in the sixth and eighth slots are in error, which result in the erroneous estimations of Y_1 and Y_2, respectively. Similarly, the estimation of X_3 in the tenth slot at B is erroneous. Note that in the seventh slot, the superimposed symbol at R_1 is erroneous, as it is superimposed by the correct symbol from A and the erroneous symbol from R_2. In the tenth slot at A, although the received symbol combination, i.e., $X_5 \oplus X_4 \oplus Y_3 \oplus X_2 \oplus Y_1$, is correct, the estimation of Y_3 is still erroneous as the previous estimation of Y_1 is

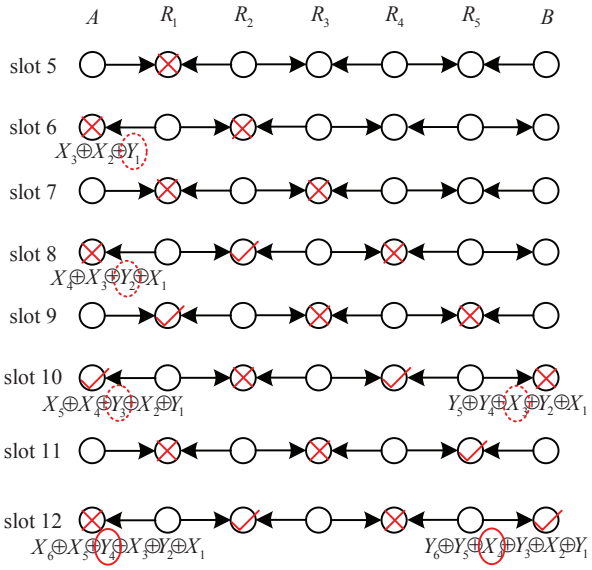

Figure 5.4: Bounded error propagation in D-MPNC.

erroneous. After the tenth slot, all the estimations of the following bits are correct at both A and B. In other words, the error propagation effects are bounded by four bits in error, i.e., Y_1, Y_2, Y_3, X_3, which is briefly proved below.

From Fig. 5.4, we observe that the pattern from slot 12 to slot 15 is the same as that from slot 8 to slot 11, and repeats in a four-slot period. We first consider the bits received by source A. In the i-th slot, $i \in \{12, 16, \cdots\}$, the received symbol combination by A, $X_{\frac{i}{2}} \oplus X_{\frac{i}{2}-1} \oplus Y_{\frac{i}{2}-2} \cdots Y_2 \oplus X_1$, is erroneous. However, each of them contains one erroneous estimation on Y_2. Thus, all the estimations of $Y_4, Y_6, \cdots$ are correct. In the j-th slot, where $j \in \{14, 18, \cdots\}$, the received symbol combination $X_{\frac{j}{2}} \oplus X_{\frac{j}{2}-1} \oplus Y_{\frac{j}{2}-2} \cdots Y_3 \oplus X_2 \oplus Y_1$ is correct. Each of them contains two erroneous estimations Y_3 and Y_1, which results in a correct XOR result. Thus, the estimations of $Y_5, Y_7, \cdots$ are correct. For B, at the i-th slot, $i \in \{12, 16, \cdots\}$, the received symbol combination $Y_{\frac{i}{2}} \oplus Y_{\frac{i}{2}-1} \oplus X_{\frac{i}{2}-2} \cdots X_2 \oplus Y_1$ is correct, and each of them contains the correct information only. Thus, the estimations of $X_4, X_6, \cdots$ are correct. In the j-th slot, where $j \in \{14, 18, \cdots\}$, the received symbol combination $Y_{\frac{j}{2}} \oplus Y_{\frac{j}{2}-1} \oplus X_{\frac{j}{2}-2} \cdots X_3 \oplus Y_2 \oplus X_1$ is erroneous, and each of them contains one erroneous estimation X_3 only. Thus, the estimations of $X_5, X_7, \cdots$ are correct. In summary, the estimations after the tenth slot are no longer affected by the error at R_1 in the fifth slot.

In general, if and only if single multi-access estimation error happens at relays R_1, R_2, R_3, R_4 and R_5, it will result in 4, 2, 4, 2 and 4 bits end-to-end estimation errors,

Table 5.1: End-to-end BER bound of D-MPNC

N	End-to-end BER bound
$N=2$	$\frac{3}{2}\mathrm{P}_{xor\_R_1}+\mathrm{P}_{xor\_R_2}+\frac{1}{2}\mathrm{P}_{a,r}+\frac{3}{2}\mathrm{P}_{b,r}$
$N=3$	$\frac{3}{2}\mathrm{P}_{xor\_R_1}+\mathrm{P}_{xor\_R_2}+\frac{3}{2}\mathrm{P}_{xor\_R_3}+\frac{1}{2}\mathrm{P}_{a,r}+\frac{1}{2}\mathrm{P}_{b,r}$
$N=4$	$2\mathrm{P}_{xor\_R_1}+\mathrm{P}_{xor\_R_2}+2\mathrm{P}_{xor\_R_3}+\mathrm{P}_{xor\_R_4}+\mathrm{P}_{a,r}+2\mathrm{P}_{b,r}$
$N=5$	$2\mathrm{P}_{xor\_R_1}+\mathrm{P}_{xor\_R_2}+2\mathrm{P}_{xor\_R_3}+\mathrm{P}_{xor\_R_4}+2\mathrm{P}_{xor\_R_5}+\mathrm{P}_{a,r}+\mathrm{P}_{b,r}$
$N=6$	$2\mathrm{P}_{xor\_R_1}+\frac{3}{2}\mathrm{P}_{xor\_R_2}+\frac{5}{2}\mathrm{P}_{xor\_R_3}+\mathrm{P}_{xor\_R_4}+\frac{5}{2}\mathrm{P}_{xor\_R_5}+\frac{3}{2}\mathrm{P}_{xor\_R_6}+\frac{1}{2}\mathrm{P}_{a,r}+2\mathrm{P}_{b,r}$
$N=7$	$2\mathrm{P}_{xor\_R_1}+\frac{3}{2}\mathrm{P}_{xor\_R_2}+\frac{5}{2}\mathrm{P}_{xor\_R_3}+\mathrm{P}_{xor\_R_4}+\frac{5}{2}\mathrm{P}_{xor\_R_5}+$ $\frac{3}{2}\mathrm{P}_{xor\_R_6}+2\mathrm{P}_{xor\_R_7}+\frac{1}{2}\mathrm{P}_{a,r}+\frac{1}{2}\mathrm{P}_{b,r}$

respectively. Similarly, if and only if single-hop transmission error from R_1 (R_5) to source A (B), it will result in two bits in error. Note that when there are more than one multi-access and single-hop errors, the impact of multiple errors can be partly canceled. For example, if both of the multi-access errors happen at R_1 and R_3 at the fifth slot, it will result in 2 bits in errors, i.e., only $\hat{X}_2$ and $\hat{Y}_1$ are in error, instead of 8 bits in error. Thus, the end-to-end BER can be bounded by summing the impacted bits of single multi-access and single-hop transmission error. The end-to-end BER bound of D-MPNC with $N=5$ can be obtained by

$$\mathrm{P}_{e2e}=\frac{\sum_{i=1}^{5}w_i\mathrm{P}_{xor\_R_i}+2\mathrm{P}_{a,r}+2\mathrm{P}_{b,r}}{2}, \tag{5.15}$$

where $\mathrm{P}_{xor\_R_i}$ denotes multiple-access error probability at relay R_i and coefficients $w_i=\{4,2,4,2,4\}$ denotes numbers of end-to-end bit estimation errors impacted by error propagation. Different from traditional PNC with a single relay, in multi-hop PNC, the impact of the mutual-interference should be considered. For each receiver, SINR should be considered instead of SNR. Thus, in (5.15), to calculate $\mathrm{P}_{xor\_R_i}$, $\mathrm{P}_{a,r}$ and $\mathrm{P}_{b,r}$, the noise spectral density $2\sigma^2$ in (5.9)-(5.13) should be updated as

$$2\sigma^2+\sum_{i=1}^{\lfloor\frac{k-1}{3}\rfloor}\frac{2E_b}{N+2}(\frac{(2i+1)d}{N+1})^{-\alpha}+\sum_{j=1}^{\lfloor\frac{N+2-k}{3}\rfloor}\frac{2E_b}{N+2}(\frac{(2j+1)d}{N+1})^{-\alpha} \tag{5.16}$$

from (5.7) by considering the mutual interference.

For D-MPNC with other N, the end-to-end BER bound can be obtained similarly as the analysis for D-MPNC with $N=5$. The end-to-end BER bound for D-MPNC with N from 2 to 7 are summarized in Table 5.1. Note that when N is even, at source B, if the received symbol from relay R_N is estimated in error, it will further impact on

the correctness of transmitted symbol from source B in the next slot. For example, for D-MPNC with $N = 2$, we have

$$\mathrm{P}_{e2e} = \frac{w_1 \mathrm{P}_{xor\_R_1} + w_2 \mathrm{P}_{xor\_R_2} + \mathrm{P}_{a,r} + (1 + w_2)\mathrm{P}_{b,r}}{2}, \tag{5.17}$$

where $w_1 = 3$ and $w_2 = 2$.

5.5 Design of S-MPNC

In this section, we present the design of S-MPNC, which targets on maximizing the end-to-end throughput and generalizing design of multi-hop PNC with an arbitrary number of relays. The received information in the previous slots are properly applied at the sources and relays in S-MPNC. There is a tradeoff between applications of D-MPNC and S-MPNC as discussed in Sec. 5.5.4.

5.5.1 Generalization of S-MPNC

D-MPNC benefits from simple implementation as the operations of relays remain the same as that of traditional PNC with a single relay. However, in D-MPNC, a single multiple-access error at the relay may result in more than 2-bit end-to-end estimation errors especially when the number of relays is large. By properly applying the previously received information at the relays, we propose and generalize S-MPNC where single multiple-access error at the relay or single-hop transmission error at the source will only result in 2-bit end-to-end estimation errors.

A straightforward explanatory graph of for the generalization of S-MPNC is shown in Fig. 5.5. Note the final generalization of S-MPNC needs slight modification as explained later. In Fig. 5.5, each of the sources and relays maintains a buffer which stores the last received binary result or the network-coded symbol obtained by (5.2), respectively. All the sources and relays transmit the XOR result of the target information, i.e., the source data for the source and network-coded symbol for the relay, and the information stored in the buffer, and then update the buffer by newly received binary result. For example, in Fig. 5.5(a), at the third slot, source A transmits $X_2 \oplus X_1 \oplus Y_1$, where X_2 is the target information and $X_1 \oplus Y_1$ is the last received binary result in the second slot and stored in the buffer. At the fourth slot, the relay broadcasts $X_2 \oplus Y_2 \oplus X_1 \oplus Y_1$, which is the XOR result of the newly obtained network-coded

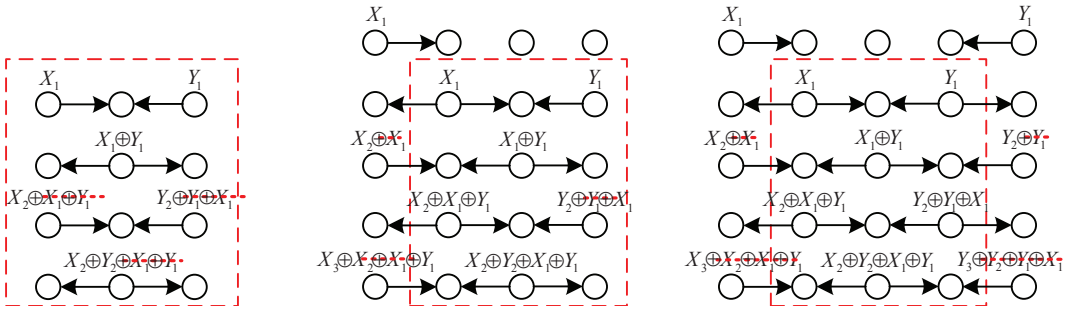

(a) S-MPNC with $N=1$. (b) S-MPNC with $N=2$. (c) S-MPNC with $N=3$.

Figure 5.5: Generalization of S-MPNC.

symbol $X_2 \oplus X_1 \oplus Y_1 \oplus Y_2 \oplus Y_1 \oplus X_1 = X_2 \oplus Y_2$ in the last slot and the network-coded symbol $X_1 \oplus Y_1$ obtained at the first slot and stored in the buffer. Comparing Figs. 5.5(a), 5.5(b) and 5.5(c), we can easily observe that the kernel part marked by the red dashed square is always the same with the increase of relay number. Thus, it can be extended and generalized for an arbitrary relay number N.

Note that the above explanations help to identify the relations of S-MPNC with arbitrary number of relays and prove that S-MPNC can be generalized. However, the final generalization of S-MPNC needs modifications for operations of the sources and source neighboring relays in order to minimize the impact of error propagation. Considering the symbol combinations of the relays that are not source neighbors, the following two operations are equivalent:

1) Operation-1: both sources and their neighboring relays simply transmit the target information, i.e., the same as that of traditional PNC with a single relay.

2) Operation-2: both sources and their neighboring relays transmit the XOR result of the target information and the last binary information or received network-coded symbol, i.e., as that shown in Fig. 5.5 without erasing the bits marked by the red dashed lines.

Note that Operation-1 and Operation-2 refers to erasing or without erasing the bits marked by the red dash lines in Fig. 5.5. Operation-2 is the straightforward explanation introduced above and Operation-1 will lead to the final generalization of S-MPNC.

We give an example to compare these two operations. In Fig. 5.5(c), erasing the bits marked by the red dashed lines, i.e., Operation-1, and remaining these bits, i.e., Operation-2, have the same impact to the symbol combination at the 2-th relay. From

Operation-2, we can easily observe the pattern of the S-MPNC generalization with an arbitrary number of relay. However, considering the error propagation of the single-hop transmission from the sources' neighboring relays to the sources, Operation-1 outperforms Operation-2 in terms of end-to-end BER. Thus, an equivalent transformation from Operation-2 to Operation-1 referring to the symbol combinations at the relays is necessary for the final generalization of S-MPNC.

The generalization of S-MPNC with an odd[5] number of relay N can be summarized as follows:

1) The sources transmit X_i and Y_i at the i-th slot, $i \in \{1, 3, \cdots\}$, respectively.

2) The j-th relay, $j \in \{2, 4, \cdots, N-1\}$ transmits at the i-th slot, $i \in \{1, 3, \cdots\}$ and receives at the $(i+1)$-th slot. The j-th relay, $j \in \{1, 3, \cdots, N\}$, receives at the i-th slot, $i \in \{1, 3, \cdots\}$ and transmits at the $(i+1)$-th slot.

3) The operations of the sources' neighboring relays are the same as that of the traditional PNC with a single relay or D-MPNC. The other relays broadcast the XOR results of the newly received network-coded symbol and the last received network-coded symbol[6].

The transmission graph after erasing the binary bits marked by the red dashed lines in Fig. 5.5 can be obtained by the above generalization. We use an example to explain the generalization of S-MPNC. By criteria 1) and 2), S-MPNC with $N = 1$ deteriorates to the traditional PNC with a single relay as shown in Fig. 5.5(a), where the binary bits marked by the red dashed lines are erased. Criterion 3) can be explained in Fig. 5.5(c), where the operations of the two relays neighboring to the sources are the same as that in traditional PNC with a single relay or D-MPNC. However, the second relay needs to broadcast the XOR result of the newly obtained network-coded symbol and the last obtained network-coded symbol.

Note that criterion 3) can be achieved by maintaining and updating a buffer at each of the relays except the sources' neighboring relay(s). At each transmitting slot i of the relay, the buffer stores the previously obtained network-coded symbol at the $(i-3)$-th slot, and then be updated to store the newly obtained network-coded symbol at the $(i-1)$-th slot.

[5]When N is even, source B needs to transmit with one-slot delay compared to source A as shown in Fig. 5.5(b).

[6]It can be achieved by maintaining a buffer at each of relays.

5.5.2 Generalizing iteration decoding algorithm of S-MPNC

Similarly to the decoding algorithm design of D-MPNC, in S-MPNC, the sources first need to identify the pattern of received symbol combinations from neighboring relays, and then extract the target information from the symbol combinations. We use source A as an example to introduce the decoding algorithm design at the sources and decoding algorithm at source B is similar. At the i-th slot, $i \in \{2, 4, \cdots\}$, the received symbol combination at source A from the first relay can be expressed as

$$\hat{S}_{r_{1i}} = \hat{Y}_{\frac{i-N+1}{2}} \oplus \sum\nolimits_{m=1}^{\frac{i}{2}} X_m \oplus \sum\nolimits_{n=1}^{\frac{i-N-1}{2}} \hat{Y}_n, \tag{5.18}$$

where $\sum_{i=1}^{N} x_i = x_1 \oplus x_2 \cdots \oplus x_N$ defines mod-2 summation and $\hat{Y}_j = 0$ if $j \leq 0$. $\hat{S}_{r_{1i}}$ is estimated binary result from R_1 and the target estimated symbol from source B is $\hat{Y}_{\frac{i-N+1}{2}}$. Note that in (5.18), $\sum_{n=1}^{\frac{i-N-1}{2}} \hat{Y}_n$ denote the summation of mod-2 addition of all previous estimations of Y_j, $j \in \{1, \cdots, \frac{i-N-1}{2}\}$.

Source A needs to apply and update a buffer denoted as B_a by an iteration decoding algorithm. The coding algorithm of S-MPNC at source A can be summarized as follows:

1) At the i-th slot, $i \in \{N+1, N+3, \cdots\}$, obtain symbol combination $\hat{S}_{r_{1i}}$ by (5.5).

2) Extract target information $\hat{Y}_{\frac{i-N+1}{2}}$ from $\hat{S}_{r_{1i}}$ by

$$\hat{Y}_{\frac{i-N+1}{2}} = \hat{S}_{r_{1i}} \oplus B_a \oplus X_{N-1}, \tag{5.19}$$

where buffer B_a is initialized as $X_1 \oplus X_2 \cdots X_{N-2}$ at the $(N+1)$-th slot.

3) Update buffer $B_a = \hat{S}_{r_{1i}}$.

We use an Fig. 5.5(c) as an example to explain the decoding algorithm of S-MPNC. In step 1), at the fourth slot, which is the first slot that source A receives the target information Y_1 from source B. Source A receives and obtains the estimation of symbol combination $\hat{S}_{r_{1,i}}$ by (5.5), which can be expressed as $\hat{S}_{r_{1,i}} = X_2 \oplus X_1 \oplus \hat{Y}_1$ by (5.18). In step 2), source A can extract the target information $\hat{Y}_1 = \hat{S}_{r_{1,i}} \oplus B_a \oplus X_2$, where buffer B_a is initialized as X_1. Finally, buffer B_a is updated to store the received binary result $\hat{S}_{r_{1,i}}$, which will be further applied to detect Y_2 at the sixth slot.

Note that in (5.18), $\sum_{m=1}^{\frac{i}{2}} X_m$ is always correct as it is known by source A. $\hat{S}_{r_{1,i}}$ is the estimation of the received symbol combination from R_1 and $\sum_{n=1}^{\frac{i-N-1}{2}} \hat{Y}_n$ is the summation of all the previous estimations of Y_j, $j \in \{1, \cdots, \frac{i-N-1}{2}\}$. Thus, both of them may be erroneous. However, in the next subsection, we will show that the

error prorogation of the single multiple-access error at the relays or the single-hop transmission from R_1 (R_N) to source A (B) will be 2-bit end-to-end estimation errors. If more than one multiple-access and single-hop errors happen, the end-to-end BER of S-MPNC will be bounded by considering the summation of the individual impact of each error events.

5.5.3 End-to-end BER analysis of S-MPNC

S-MPNC can achieve the end-to-end BER bound expressed as

$$\sum_{i=1}^{N} \mathrm{P}_{xor\_R_i} + \mathrm{P}_{a,r} + \mathrm{P}_{b,r}, \tag{5.20}$$

where $\mathrm{P}_{xor\_R_i}$ is the error rate of the multiple-access transmission at the i-th relay, $i \in \{1, 2, \cdots, N\}$, and $\mathrm{P}_{a,r}$ and $\mathrm{P}_{b,r}$ are the single-hop transmission error rate from relay R_1 (R_N) to source A (B).

Impact of the error propagation

We first consider the single multiple-access error at any of the relays. For the j-th relay, at the i-th slot, if and only if the obtained network-coded symbol $\hat{S}_{r_{j,i}}$ is in error, it will result in 2-bit estimation error at each source, i.e., the estimations of $\hat{Y}_{\frac{i+j-N+1}{2}}$ and $\hat{X}_{\frac{i-j}{2}}$ are erroneous.

Proof: If and only if $\hat{S}_{r_{j,i}}$ is in error, the errors will propagate to the neighbor nodes in the following slots as shown in Fig. 5.6(a). The received or transmitted symbols of the nodes in shadowed region will be erroneous[7]. The binary estimation error starts from $S_{r_{j,i}}$ and propagates to R_1 and R_N in j slots and $(N-j)$ slots, respectively. The first erroneous symbol combination at source A from R_1 is

$$\hat{S}_{r_{1,i+j}} = \hat{Y}_{\frac{i+j-N+1}{2}} \oplus \sum\nolimits_{m=1}^{\frac{i+j}{2}} X_m \oplus \sum\nolimits_{n=1}^{\frac{i+j-N-1}{2}} \hat{Y}_n, \tag{5.21}$$

where $\hat{S}_{r_{1,i+j}}$ is erroneous and $\sum_{m=1}^{\frac{i+j}{2}} X_m \oplus \sum_{n=1}^{\frac{i+j-N-1}{2}} \hat{Y}_n$ is correct. Thus, end-to-end estimation $\hat{Y}_{\frac{i+j-N+1}{2}}$ is erroneous. Similarly, end-to-end estimation $\hat{X}_{\frac{i-j}{2}}$ is erroneous at source B.

[7]The information transmitted from the sources are always correct in S-MPNC as no previously received information is applied in the transmitted signals.

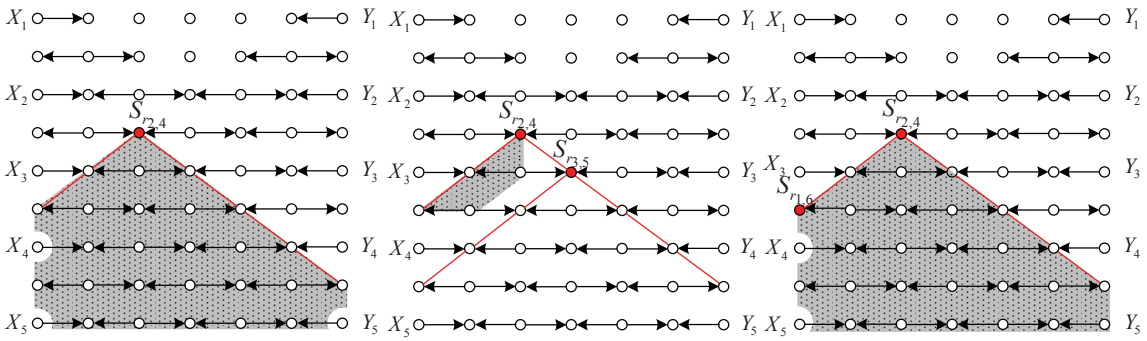

(a) Case 1. (b) Case 2. (c) Case 3.

Figure 5.6: End-to-end BER bound analysis of S-MPNC.

However, we will show that all other end-to-end estimations after $\hat{Y}_{\frac{i+j-N+1}{2}}$ and $\hat{X}_{\frac{i-j}{2}}$ are correct. The estimation of $\hat{Y}_{\frac{i+j-N+3}{2}}$ can be obtained by

$$\hat{S}_{r_{1,i+j+2}} = \hat{Y}_{\frac{i+j-N+3}{2}} \oplus \sum_{m=1}^{\frac{i+j+2}{2}} X_m \oplus \sum_{n=1}^{\frac{i+j-N+1}{2}} \hat{Y}_n, \tag{5.22}$$

where $\hat{S}_{r_{1,i+j+2}}$ and $\sum_{n=1}^{\frac{i+j-N+1}{2}} \hat{Y}_n$ are erroneous and $\sum_{m=1}^{\frac{i+j+2}{2}} X_m$ is correct. Thus, end-to-end estimation $\hat{Y}_{\frac{i+j-N+3}{2}}$ is correct. For any $\hat{Y}_k$, $k > \frac{i+j-N+1}{2}$, as in (5.22), the term on the left-side of '=' and the third term on the right-side of '=' are always erroneous, and the second term on the right-side of '=' is correct. Thus, the target information in the first term on the right-side of '=' is correct. We can similarly obtain that all $\hat{X}_k$, $k > \frac{i-j}{2}$ are correct. Thus, single multiple-access error at any relay will result in 2-bit end-to-end estimation errors.

Second, we study the impact of individual single-hop transmission error from relay R_1 (R_N) to source A (B). If and only if an error happens over the hop from R_1 (R_N) to source A (B), which will result in 2-bit end-to-end estimation errors at source A (B).

Proof: At the i-th slot, $i \in \{N+1, N+3, \cdots\}$, the received symbol combination at source A from the first relay is

$$\hat{S}_{r_{1,i}} = \hat{Y}_{\frac{i-N+1}{2}} \oplus \sum_{m=1}^{\frac{i}{2}} X_m \oplus \sum_{n=1}^{\frac{i-N-1}{2}} \hat{Y}_n. \tag{5.23}$$

The target information $\hat{Y}_{\frac{i-N+1}{2}}$ is erroneous as the estimation of symbol combination $\hat{S}_{r_{1,i}}$ is erroneous. In the $(i+2)$-th slot, $i \in \{N+3, N+5, \cdots\}$, the received symbol

combination is

$$\hat{S}_{r_{1,i+2}} = \hat{Y}_{\frac{i-N+3}{2}} \oplus \sum\nolimits_{m=1}^{\frac{i+2}{2}} X_m \oplus \sum\nolimits_{n=1}^{\frac{i-N+1}{2}} \hat{Y}_n. \tag{5.24}$$

The target information $\hat{Y}_{\frac{i-N+3}{2}}$ is erroneous as the estimation of symbol combination $\hat{S}_{r_{1,i+2}}$ is correct, but $\sum_{n=1}^{\frac{i-N+1}{2}} \hat{Y}_n$ is erroneous due to the erroneous $\hat{Y}_{\frac{i-N+1}{2}}$. However, it is easy to see that any $\hat{Y}_k$, $k > \frac{i-N+3}{2}$ is correct as the errors in $\hat{Y}_{\frac{i-N+3}{2}}$ and $\hat{Y}_{\frac{i-N+1}{2}}$ cancel. Thus, the single-hop transmission error will result in 2-bit end-to-end estimation errors.

Third, we study the cases when there are more than one multiple-access and single-hop transmission errors. When more than one multiple-access and single-hop errors, the total end-to-end estimation errors are smaller than that of summing each error probability individually, as the fact that the impact of multiple errors may cancel each other. We provide two examples as shown in Figs. 5.6(b) and 5.6(c) to explain. In Fig. 5.6(b), the error regions caused by erroneous estimations $\hat{S}_{r_{2,4}}$ and $\hat{S}_{r_{3,5}}$ are canceled, which will result in 2-bit estimation errors, i.e., $\hat{Y}_1$ and $\hat{Y}_2$, instead of 4-bit end-to-end estimation errors. Erroneous $\hat{Y}_2$ is caused by the impact of the erroneous estimation $\hat{Y}_1$. In Fig. 5.6(c), if two multiple-access transmission $\hat{S}_{r_{2,4}}$ and single-hop transmission $\hat{S}_{r_{1,6}}$ are erroneous, which will result in 1-bit end-to-end estimation, i.e., $\hat{X}_2$ is erroneous, instead of 4-bit end-to-end estimation errors. Thus, When more than one multiple-access and single-hop errors happen, the total end-to-end estimation errors are smaller than that of summing the bit errors caused by each of the error event individually. Thus, an end-to-end BER bound in (5.20) can be achieved by S-MPNC.

Impact of the interference from other transmitting nodes

In multi-hop PNC, for each receiver, the mutual-interference from other transmitting nodes should be considered. To calculate $\mathrm{P}_{xor\_R_i}$, $\mathrm{P}_{a,r}$ and $\mathrm{P}_{b,r}$ in (5.20), the noise spectral density $2\sigma^2$ in (5.9)-(5.13) should be updated as (5.16). Note that in multi-hop PNC, the impact of mutual-interference and error propagation are independent. The impact of error propagation are caused by the properties of network-coded and multi-hop topology, which can be optimized by properly applying previously received information and designing the symbol combination pattern. The impact of mutual-interference are caused by physical channels, which can be optimized by enlarging the hop-distance of interference nodes. However, end-to-end throughput will also be negatively affected by enlarging the hop-distance of interference nodes due to the

reduction of overall transmission efficiency.

5.5.4 Comparison between D-MPNC and S-MPNC

In this chapter, we propose two designs with different design purposes. D-MPNC benefits from simple-implementation, as the operations of all relays are exactly the same as that of traditional PNC with a single relay. Also, the sources simply transmit target symbol when the number of relays are odd, which is the same as that of the traditional PNC with a single relay. The key issue is the detection of target symbol from the other sources in the obtained symbol combination as elaborated in Sec. 5.4.2. Thus, in D-MPNC, all the relays remain the same and simple operations. To upgrade from traditional PNC with a single relay to D-MPNC, only the detection algorithm at the sources are required to be upgraded, which can be easily achieved by software upgradation. S-MPNC targets for the optimal end-to-end BER by taking advantage of the previously obtained information. The relays except the source neighboring are equipped with one-buffer to store the previously obtained information and updated these information in every two-slot. In other words, the source neighboring relays and other relays have different operations as discussed in Sec. 5.5.1. At the initializing stage, the sources need signaling to inform the relays whether they are or not the sources' neighboring. The end-to-end BER bound of D-MPNC and S-MPNC are summarized in Table 5.1 and (5.20), respectively, and further compared in Sec. 5.6.1. From the end-to-end BER perspective, S-MPNC outperforms D-MPNC benefiting from the better error propagation control. To summary, there is a tradeoff between D-MPNC and S-MPNC depending on the implementation complexity and throughput gain.

5.6 Performance Evaluation

In this section, the performance of the proposed multi-hop PNC schemes are evaluated. For any PNC scheme, we let the total transmission power in any two continuous slots be $2E_b$, and all the nodes equally share the total transmission power. The nodes are located in a linear topology. The average received SNR of all links are proportional to $d^{-\alpha}$, where d is the transmission distance and α is the path-loss parameter. We studied the performance of D-MPNC and S-MPNC under both AWGN and Rician channels with various parameter settings, and the impact of relay locations in

multi-hop PNC are further studied.

5.6.1 Performance of end-to-end BER under AWGN channels

The end-to-end BER performance of D-MPNC and S-MPNC under AWGN channels are shown in Figs. 5.7 and 5.8. The X axis is the end-to-end SNR_{ab} (dB) by direct transmission in (5.6). For traditional PNC with a single relay or multi-hop PNC with N relay(s), the transmission power for each node is $\frac{2E_b}{N+2}$ and transmission distance of each hop is $\frac{d}{N+1}$. Thus, there is a tradeoff between the transmission power and hop-distance. The path-loss parameter α, which is normally set to be from 2 to 6 [109], has two impact on the performance of multi-hop PNC. Given the end-to-end SNR_{ab} (dB) in (5.6) and the distance d (m) between the sources, the larger α is, the SINR (dB) of each hop in (5.7) is larger by shortening the transmission path. Another impact is that a larger α reduces the impact of the mutual-interference from other transmitting nodes to the receiver due to a larger path loss. The impact of the path-loss parameter α are studied in this section.

The end-to-end BER performance of D-MPNC is shown in Fig. 5.7 with different α. In Fig. 5.7(a), the black curves are the end-to-end BER bound of D-MPNC obtained in Table 5.1 and the red circle curves are the exact end-to-end BER performance. We can see that when the BER is lower, the bound approaches the exact end-to-end BER, because when BER is lower, the probability that more than one multiple-access and single-hop errors happen in the same slot becomes smaller, and individual multiple-access error or single-hop error dominates the end-to-end error performance. Comparing Figs. 5.7(a), 5.7(b) and 5.7(c), we can see that α impacts on the end-to-end BER performance. In Fig. 5.7(a), D-MPNC outperforms the traditional PNC with a single relay significantly due to a relatively larger SINR between the neighboring nodes and a relatively smaller interference impact from other transmitting nodes. In Fig. 5.7(c), the traditional PNC with a single relay outperforms D-MPNC, as a relatively larger mutual-interference from other transmitting nodes to the receivers and a relatively smaller gain from shortening the transmission distance. In Figs. 5.7(b) and 5.7(c), with the increase of end-to-end SNR_{ab} (dB), the end-to-end BER performance converge with a larger relay number N. Because the mutual-interference in multi-hop PNC also increases with the increase of SNR_{ab} (dB), and the SINR of two neighboring node approach to the upper bound. Further in-

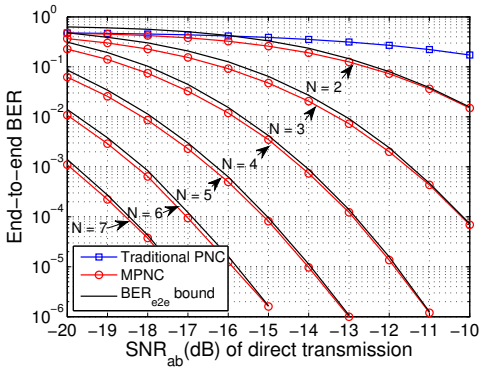

(a) $\alpha = 4$.

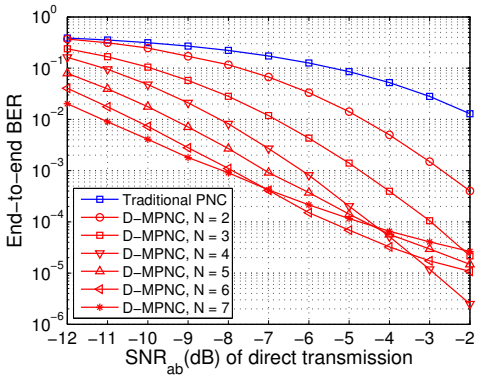

(b) $\alpha = 3$.

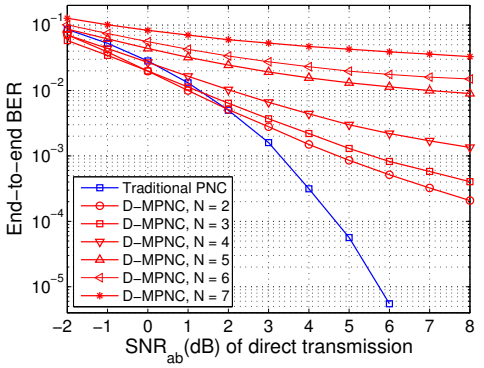

(c) $\alpha = 2$.

Figure 5.7: End-to-end BER performance of D-MPNC under AWGN channel.

crease SNR_{ab} (dB) will not help to improve the end-to-end BER, as the SINR of each hop is upper bounded by $10\alpha \log_{10} 3$ (dB) as explained in Sec. 5.3.4.

Fig. 5.8 compares the end-to-end BER performance of D-MPNC and S-MPNC with different α. S-MPNC outperforms D-MPNC in terms of end-to-end BER, as S-

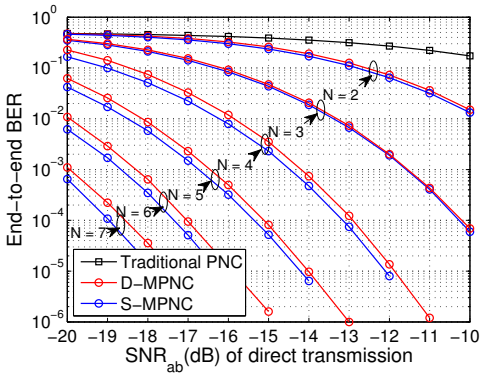

(a) $\alpha = 4$.

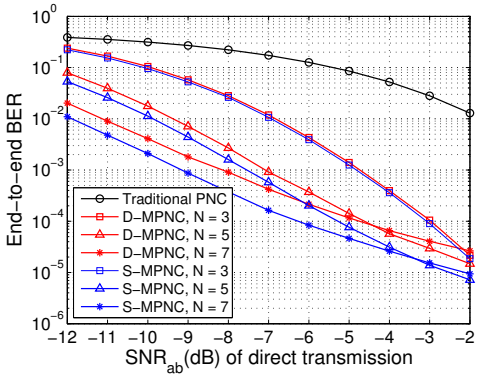

(b) $\alpha = 3$.

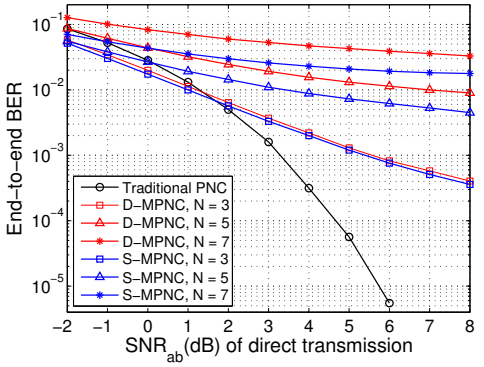

(c) $\alpha = 2$.

Figure 5.8: End-to-end BER performance of S-MPNC under AWGN channel.

MPNC further reduces the error propagation effects by enabling the relays to properly apply the previously received information. Note that the receiver in S-MPNC is also impacted by the interference from other transmitting nodes, which is independent to the impact of the error propagation. However, S-MPNC always outperforms D-

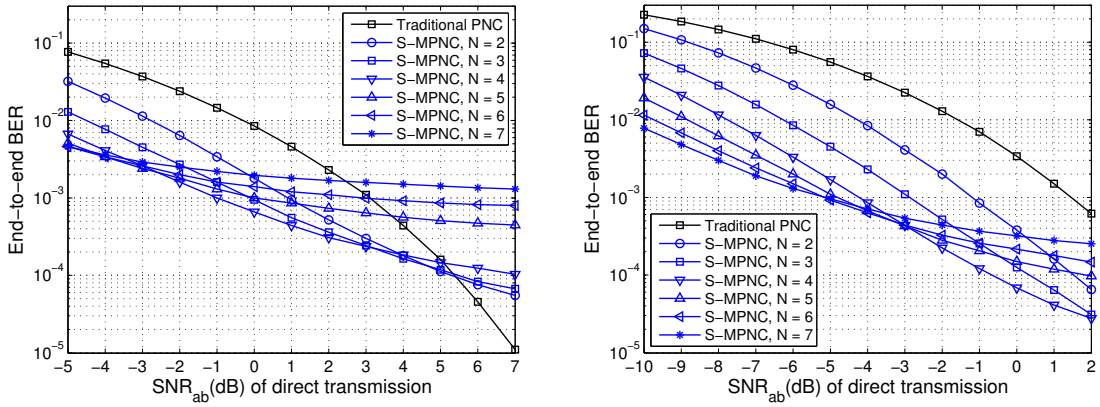

(a) $K_{rician} = 0.2$. (b) $K_{rician} = 0.4$.

Figure 5.9: End-to-end BER performance of S-MPNC under Rician channels with path-loss parameter $\alpha = 3$.

MPNC in terms of end-to-end BER under arbitrary channels due to a smaller error propagation effect. Fig. 5.8 identifies the end-to-end BER performance gap between D-MPNC and S-MPNC, in the following section, we only present the performance of S-MPNC, and the performance of D-MPNC can be easily inferred.

5.6.2 Performance of end-to-end BER under Rician channels

In the subsection, we study the end-to-end BER performance of S-MPNC under Rician channels as shown in Figs. 5.9 and 5.10 with different path-loss parameter α and Rician parameter K_{rician}. K_{rician} is the ratio between the power in the direct path and the power in other scattered paths. Fig. 5.9 shows the end-to-end BER performance of S-MPNC with $\alpha = 3$. In Fig. 5.9(a), when the end-to-end SNR$_{ab}$ is low, e.g., from -5 dB to 2 dB, S-MPNC outperforms the traditional PNC with a single relay. However, the traditional PNC outperforms S-MPNC by further increasing SNR$_{ab}$ (dB) as the increase of the mutual interference. Comparing Figs. 5.9(a) and 5.9(b), we can see that a larger end-to-end SNR$_{ab}$ (dB) is required to maintain the same BER level with a larger K_{rician}.

Fig. 5.10 shows the end-to-end BER performance of S-MPNC with $\alpha = 4$. We can see that with a larger $\alpha = 4$, S-MPNC outperforms the traditional PNC significantly. In Fig. 5.10(a), for S-MPNC with $N = 7$, the end-to-end BER begins to converge at about -8 dB, which implies the end-to-end BER performance will not improve by

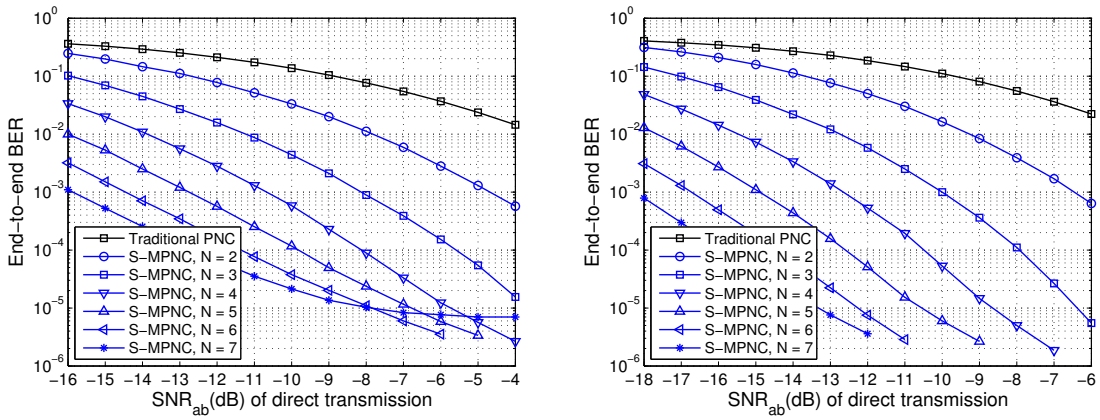

(a) $K_{rician} = 0.2$. (b) $K_{rician} = 0.4$.

Figure 5.10: End-to-end BER performance of S-MPNC under Rician channel with path-loss parameter $\alpha = 4$.

further increasing the number of relays.

5.6.3 Impact of the relay locations

In this subsection, the throughput performance of S-MPNC and the impact of the relay locations are studied. We let each block contains 256 bits, if any bit in the block is estimated in error, the block is dropped without retransmission. The throughput (bits/slot) is defined as the successfully received bits per slot by all the destinations. The blue dotted curves in Figs. 5.11 and 5.12 show the throughput performance of S-MPNC and traditional PNC with a single relay with different path-loss parameter setting, where the relays are equally localized in a linear topology between the sources. From Figs. 5.11 and 5.12, generally speaking, S-MPNC outperforms the traditional PNC with a single relay in the lower end-to-end SNR$_{ab}$ (dB) region, and the larger the path-loss parameter and the smaller the Rician parameter K_{rician} is, the more throughput gain S-MPNC can achieve compared to traditional PNC with a single relay.

We also studied the impact of relay locations on the throughput performance of S-MPNC. Note that for the symbol synchronization in the multi-hop PNC, we can choose one node as the master controller. For example, if the first relay is selected as the master controller, the signals from source A and the second relay will be synchronized at the first relay in the symbol-level, and the transmitting time from

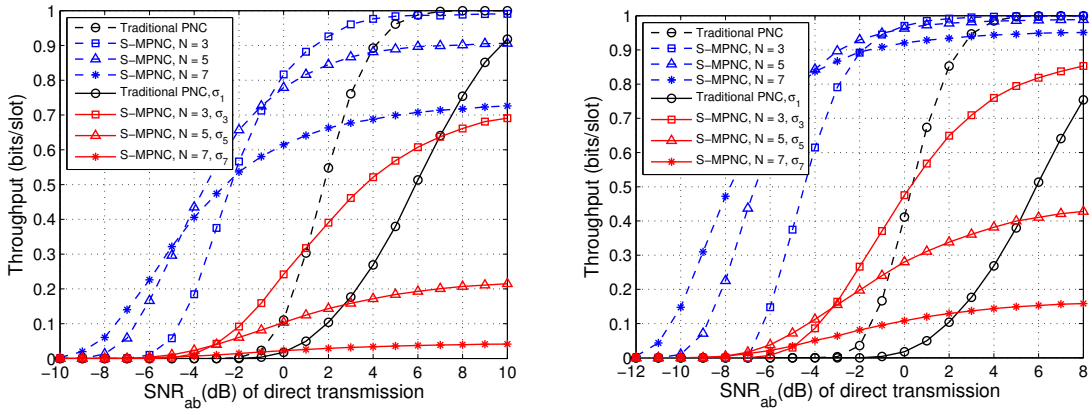

(a) $K_{rician} = 0.2$. (b) $K_{rician} = 0.4$.

Figure 5.11: Impact of non-perfect relay locations with path-loss parameter $\alpha = 3$.

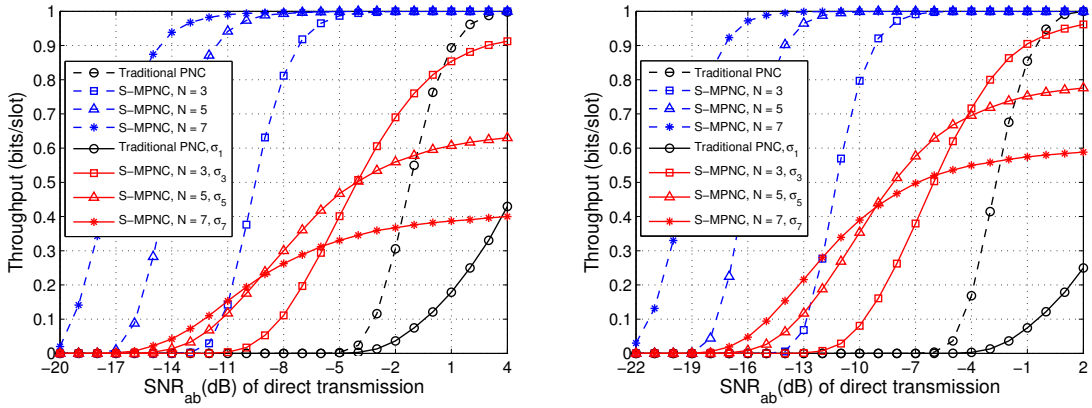

(a) $K_{rician} = 0.2$. (b) $K_{rician} = 0.4$.

Figure 5.12: Impact of non-perfect relay locations with path-loss parameter $\alpha = 4$.

the fourth relay will be adjusted to guarantee that the signals from the second relay and the fourth relay can be synchronized at the third relay. For S-MPNC with N relays, we let the location of the j-th relay, $j \in \{1, 2, \cdots, N\}$, follow a uniformed distribution with mean $\frac{d}{N+1}$ and standard variance $\sigma_N = \frac{(\frac{d}{N+1})}{\sqrt{12}}$. Note that $\sigma_N = \frac{(\frac{d}{N+1})}{\sqrt{12}}$ is the largest standard variance to guarantee that two neighboring relays will not overlap. Thus, the red solid curves in Figs. 5.11 and 5.12 show the lower bound of the throughput performance of S-MPNC with different maximal standard variance σ_i, $i \in \{1, 3, 5, 7\}$. We can see that the relay locations in multi-hop PNC also affect the throughput performance due to the impact of the mutual-interference. The worst

case is that the locations of three neighboring nodes, labelled as node-1, node-2 and node-3, may be too close. In this case when the left-side node of node-1, labelled as node-0, is the receiver, the interference from node-3 to node-0 would be larger enough to impact the useful signals from the node-1. The hop between node-0 and node-1 will be the bottleneck of the multi-hop transmission, which domains the end-to-end throughput performance of multi-hop PNC.

Chapter 6

Conclusions and Future Work

6.1 Conclusion

In this dissertation, we have investigated the applications of PNC under the asymmetric TWRC scenario, and further extended and generalized the single-relay PNC to multiple-relay PNC.

In Chapter 2, based on the fact that the channel conditions of two source-relay links in TWRC may not be similar, and the amount of the data exchange between the sources may not be equal, we proposed the HePNC design. When the sources use the same signal power to transmit, HePNC is favorable in the asymmetric TWRC scenario, where the channel conditions of the two source-relay links are asymmetric, and different modulations are selected by the sources. Note that HePNC can also be applied in the symmetric TWRC scenario with a proper power control. Thus, the HePNC design can extend the traditional PNC from the equal data exchange ratio only to the flexible data exchange ratio determined by the modulation configurations. The key issue in the HePNC design is to optimize the mapping functions at the relay, which map the superimposed signals to the network-coded symbols. Under the symbol-level synchronization, the optimal mapping functions can be obtained according to the CSI of the two source-relay channels. We obtained and presented the optimal mapping functions for several HePNC sample designs, and also presented the guidelines of how to obtain the optimal mapping functions for other higher-order modulation HePNC. In addition, we studied the end-to-end BER performance under both AWGN and Rayleigh fading channels, and the performance of HePNC are also conducted under extensive simulations.

In Chapter 3, we studied how to integrate the channel error control coding into the proposed HePNC design with link-to-link coding. The key issue when integrating channel coding into the PNC-based scheme is the design of decoding algorithm at the relay. We integrated the repeat accumulate codes into the symbol-level HePNC proposed in Chapter 2 with link-to-link coding, where the relay tries to decode the superimposed codewords transmitted from the sources. We proposed a full-state sum-product decoding algorithm, where the input of the tanner-graph is the full-state information of the superimposed signals, and the output is the network-coded symbol optimized by the bit-level mapping. The proposed decoding algorithm outperforms the existing ones for QPSK-BPSK HePNC in terms of the end-to-end BER.

In Chapter 4, motivated by the fact that under the asymmetric TWRC, the channel of the better source-relay link is not fully utilized in the BC stage of HePNC, we proposed the design of hierarchical modulation physical layer network coding (H-PNC). H-PNC achieves an additional data exchange between the relay and the source with a relatively better source-relay channel by superimposing the additional data flow on the PNC transmission. The channel of the better source-relay link can be fully utilized, and the data exchange ratios between the two data flows are flexible determined by the hierarchical modulation configurations. The design of H-PNC is more challenging compared to HePNC, as in the multiple-access stage, part of the message in the superimposed signals are required to be demodulated explicitly, and part of them are mapped to the network-coded symbol directly. Under the asymmetric TWRC, H-PNC outperforms the existing solutions in terms of the system throughput by fully utilizing the channel of the better source-relay link.

In Chapter 5, we investigated the design and generalization of the multi-hop PNC, where multiple relays located in a linear topology are scheduled to support the data exchange between the two end sources. We proposed two multi-hop PNC designs, the direct multi-hop PNC (D-MPNC) and the stored multi-hop PNC (S-MPNC). In D-MPNC, the operation of each relay is exactly the same as that of the relay in the traditional PNC. Thus, D-MPNC benefits from the simple implementation and can be directly upgraded from the traditional PNC with a single relay. In S-MPNC, the operations for different relays may not be the same, as part of the relays may require to store and apply the previously obtained information. However, a better end-to-end BER can be achieved by S-MPNC compared to D-MPNC by a better error propagation control. The end-to-end BER bounds of both D-MPNC and S-MPNC are obtained, and the throughput upper bound of both designs is 1 symbol per symbol

duration, which is the same as that of the traditional PNC with a single relay. The theoretical analysis and simulation results demonstrate the performance gain of the proposed schemes in terms of the end-to-end BER and throughput.

6.2 Future work

For the future work that plans beyond this dissertation, there are still various open issues of importance.

1. For the topic of channel coded PNC, the existing work mainly focused on the design of symmetric channel coded PNC, i.e., the same channel codes are applied to the sources. How to integrate various channel codes into HePNC is an open issue, as different channel codes applied to the sources will require special decoding algorithm designs at the relay. Also, when different channel codes are applied to the sources, the decoding algorithm design at the relay is more challenging. Integrating the channel coding into H-PNC is also an important research issue, which increases the complexity compared to channel coded HePNC as the decoding output at the relay contains both of the target message from source A to the relay and the network-coded symbol. Thus, how to design the channel coded HePNC and H-PNC schemes with different channel codes at the relay to provide different reliability priority is still an open issue.

2. For the higher-order modulation pair H-PNC, due to the complexity of the superimposing constellation map at the relay, how to generalize the constellation design and bit-symbol labeling for the arbitrary higher-order modulation pairs is worthy of further research. In the multi-user multi-relay PNC scenario, the system groups two sources and one relay to construct a PNC-group. The H-PNC technique introduced in Chapter 4 can be applied to each PNC-group. However, different from the pure multi-user PNC system, the grouping and scheduling algorithm in the multi-user H-PNC scenario should further consider the data amount exchanged between the relay and the BS, which is an interesting topic for further research. Opportunistic scheduling is a link-layer solution, which considers the instantaneous PHY layer channel conditions to schedule users with better channel conditions to transmit, aiming to achieve multi-user diversity gain. H-PNC is a PHY-layer design, which considers the network topology and channel conditions of links between three nodes to achieve overall better end-to-end performance. These two solutions are orthogonal and can be applied together in a practical system. How to apply and optimize both is an interesting issued to be further studied.

3. For the topic of multi-hop PNC, our proposed multi-hop PNC design is BPSK-based, i.e., all the nodes use BPSK modulation. Thus, the design of the mapping function at each relay is unique, i.e., XOR. The design of multi-hop PNC with the higher-order modulation is quite challenging. First, as we know that for the higher-order modulation PNC, adaptive mapping function design is necessary. Otherwise, the impact of SFS will increase the per-hop error rate greatly. Consider the multi-hop PNC, where all the nodes apply QPSK. The network-coded symbol obtained at the multiple-access may require a 5-ary constellation instead of QPSK due to the SFS impact. Thus, how to schedule the transmission with a 4-ary constellation in the multiple-access stage and the 5-ary constellation in the broadcast stage is quite challenging. Similar situations may happen when other higher-order modulations are applied. Thus, how to design the multi-hop PNC with higher-order modulation considering both effectiveness and reliability is an open issue.

Bibliography

[1] S. Zhang, S. C. Liew, and P. P Lam. Hot topic: physical-layer network coding. In *Proc. ACM MOBICOM*, pages 358–365, 2006.

[2] P. Popovski and H. Yomo. The anti-packets can increase the achievable throughput of a wireless multi-hop network. In *Proc. IEEE ICC*, pages 3885–3890, 2006.

[3] S. C. Liew, S. Zhang, and L. Lu. Physical-layer network coding: Tutorial, survey, and beyond. *Physical Communication*, 6:4–42, Mar. 2013.

[4] P. Popovski and H. Yomo. Bi-directional amplification of throughput in a wireless multi-hop network. In *Proc. IEEE VTC*, pages 588–593, 2006.

[5] S. Zhang and S.-C. Liew. Channel coding and decoding in a relay system operated with physical-layer network coding. *IEEE J. Select. Areas Commun.*, 27(5):788–796, Jun. 2009.

[6] B. Nazer and M. Gastpar. Compute-and-forward: Harnessing interference through structured codes. *IEEE Trans. Inf. Theory*, 57(10):6463–6486, Oct. 2011.

[7] S. Katti, S. S. Gollakota, and D. Katabi. Embracing wireless interference: Analog network coding. In *Proc. ACM SIGCOMM*, pages 397–408, 2007.

[8] R. Zhang, Y. C. Liang, C. C. Chai, and S. Cui. Optimal beamforming for two-way multi-antenna relay channel with analogue network coding. *IEEE J. Select. Areas Commun.*, 27(5):699–712, Jun. 2009.

[9] F. Gao, R. Zhang, and Y. C. Liang. Optimal channel estimation and training design for two-way relay networks. *IEEE Trans. on Commun.*, 57(10):3024–3033, Oct. 2009.

[10] B. Jiang, F. Gao, X. Gao, and A. Nallanathan. Channel estimation and training design for two-way relay networks with power allocation. *IEEE Trans. on Wireless Commun.*, 9(6):2022–2032, Jun. 2010.

[11] F. Gao, R. Zhang, and Y. C. Liang. Channel estimation for OFDM modulated two-way relay networks. *IEEE Trans. Signal Process.*, 57(11):4443–4455, Nov. 2009.

[12] H. Gacanin and F. Adachi. Broadband analog network coding. *IEEE Trans. on Wireless Commun.*, 9(5):1577–1583, May 2010.

[13] L. Lu and S. C. Liew. Asynchronous physical-layer network coding. *IEEE Trans. Wireless Commun.*, 11(2):819–831, Feb. 2012.

[14] L. Lu, S. C. Liew, and S. Zhang. Optimal decoding algorithm for asynchronous physical-layer network coding. In *Proc. IEEE ICC*, pages 1–6, 2011.

[15] Q. Yang, S. C. Liew, L. Lu, and Y. Shao. Symbol misalignment estimation in asynchronous physical-layer network coding. *IEEE Trans. Veh. Technol.*, 66(3):2844 – 2852, Jun. 2016.

[16] X. Dang, Q. Li, and X. Yu. Symbol timing estimation for physical-layer network coding. *IEEE Commun. Lett.*, 19(5):755–758, May 2015.

[17] H. Rahul, H. Hassanieh, and D. Katabi. Sourcesync: a distributed wireless architecture for exploiting sender diversity. In *ACM SIGCOMM Computer Communication Review*, volume 40, pages 171–182, 2010.

[18] T. Yang, X. Yuan, P. Li, I. B. Collings, and J. Yuan. A new eigen-direction alignment algorithm for physical-layer network coding in mimo two-way relay channels. In *Proc. IEEE Int. Symp. Inform. Theory*, 2011.

[19] R. Zhou, Z. Li, C. Wu, and C. Williamson. Signal alignment: Enabling physical layer network coding for MIMO networking. *IEEE Trans. Wireless Commun.*, 12(6):3012–3023, Jun. 2013.

[20] Y.-T. Kim, K. Lee, M. Park, K.-J. Lee, and I. Lee. Precoding designs based on minimum distance for two-way relaying MIMO systems with physical network coding. *IEEE Trans. Commun.*, 61(10):4151–4160, Oct. 2013.

[21] H. Gao, T. Lv, S. Zhang, C. Yuen, and S. Yang. Zero-forcing based MIMO two-way relay with relay antenna selection: Transmission scheme and diversity analysis. *IEEE Trans. Wireless Commun.*, 11(12):4426–4437, Dec. 2012.

[22] Z. Zhao, M.Peng, Z. Ding, W. Wang, and H.-H. Chen. Denoise-and-forward network coding for two-way relay MIMO systems. *IEEE Trans. Veh. Technol.*, 63(2):775–788, Feb. 2014.

[23] X. Yuan, T. Yang, and I.B. Collings. Multiple-input multiple-output two-way relaying: A space-division approach. *IEEE Trans. Inf. Theory*, 59(10):6421–6440, Oct. 2013.

[24] R. Cao, T. Lv, H. Gao, S. Yang, and J.M. Cioffi. Achieving full diversity in multi-antenna two-way relay networks via symbol-based physical-layer network coding. *IEEE Trans. Wireless Commun.*, 12(7):3445–3457, Jul. 2013.

[25] T. Yang, X. Yuan, L. Ping, I.B. Collings, and J. Yuan. A new physical-layer network coding scheme with eigen-direction alignment precoding for MIMO two-way relaying. *IEEE Trans. Commun.*, 61(3):973–986, Mar. 2013.

[26] F. Wang, S. C. Liew, and D. Guo. Wireless MIMO switching with zero forcing and network coding. *IEEE J. Sel. Areas Commun.*, 30(8):1452–1463, Sep. 2012.

[27] M. Eslamifar, W. H. Chin, C. Y., and Y. L. Guan. Performance analysis of two-step bi-directional relaying with multiple antennas. *IEEE Trans. Wireless Commun.*, 11(12):4237–4242, Dec. 2012.

[28] S. Zhang, Q.F. Zhou, C. Kai, and W. Zhang. Full diversity physical-layer network coding in two-way relay channels with multiple antennas. *IEEE Trans. Wireless Commun.*, 13(8):4273–4282, Aug. 2014.

[29] F. Rusek, D. Persson, B. K. Lau, E. G. Larsson, T. L. Marzetta, O. Edfors, and F. Tufvesson. Scaling up MIMO: Opportunities and challenges with very large arrays. *IEEE Signal Processing Magazine*, 30(1):40–60, Jan. 2013.

[30] D. Gesbert, M. Shafi, D.-S. Shiu, P. J. Smith, and A. Naguib. From theory to practice: an overview of MIMO space-time coded wireless systems. *IEEE J. Select. Areas Commun.*, 21(3):281–302, Apr. 2003.

[31] J. Guo, T. Yang, J. Yuan, and J. A. Zhang. Linear vector physical-layer network coding for MIMO two-way relay channels: Design and performance analysis. *IEEE Trans. on Commun.*, 63(7):2591–2604, Jul. 2015.

[32] N. A. Kaim Khani, Z. Chen, and F. Yin. MIMO V-BLAST scheme based on physical-layer network coding for data reliability in emerging wireless networks. *Canadian Journal of Electrical and Computer Engineering*, 39(2):103–111, Spring 2016.

[33] Z. Zhang, Z. Ma, Z. Ding, M. Xiao, and G. K. Karagiannidis. Full-duplex two-way and one-way relaying: Average rate, outage probability, and tradeoffs. *IEEE Trans. on Wireless Commun.*, 15(6):3920–3933, Jun. 2016.

[34] F. Wang, L. Guo, S. Wang, Q. Song, and A. Jamalipour. Approaching single-hop performance in multi-hop networks: End-to-end known-interference cancellation (E2E-KIC). *IEEE Trans. Veh. Technol.*, 65(9):7606–7620, Sep. 2015.

[35] H. Lu, P. Hong, and K. Xue. High-throughput cooperative communication with interference cancellation for two-path relay in multi-source system. *IEEE Trans. Wireless Commun.*, 12(10):4840–4851, Oct. 2013.

[36] G. Zheng. Joint beamforming optimization and power control for full-duplex MIMO two-way relay channel. *IEEE Trans. Signal Process.*, 63(3):555–566, Feb. 2015.

[37] T. Koike-Akino, P. Popovski, and V. Tarokh. Optimized constellations for two-way wireless relaying with physical network coding. *IEEE J. Select. Areas Commun.*, 27(5):773–787, Jun. 2009.

[38] V. T. Muralidharan, V. Namboodiri, and B. S. Rajan. Wireless network-coded bidirectional relaying using Latin squares for M-PSK modulation. *IEEE Trans. Inf. Theory*, 59(10):6683–6711, Oct. 2013.

[39] P. Popovski and H. Yomo. Physical network coding in two-way wireless relay channels. In *Proc. IEEE ICC*, pages 707–712, 2007.

[40] D. Wubben and Y. Lang. Generalized sum-product algorithm for joint channel decoding and physical-layer network coding in two-way relay systems. In *Proc. IEEE Globecom*, pages 1–5, Dec. 2010.

[41] A. K. Tanc, T. M. Duman, and C. Tepedelenlioglu. Design of LDPC codes for two-way relay systems with physical-layer network coding. *IEEE Commun, Lett.*, 17(12):2356–2359, Dec. 2013.

[42] P. Chen, Y. Fang, L. Wang, and F. C. M. Lau. Decoding generalized joint channel coding and physical network coding in the LLR domain. *IEEE Signal Processing Lett.*, 20(2):121–124, Feb. 2013.

[43] X. Wu, C. Zhao, and X. You. Joint LDPC and physical-layer network coding for asynchronous bi-directional relaying. *IEEE J. Select. Areas Commun.*, 31(8):1446–1454, Aug. 2013.

[44] T. Huang, T. Yang, J. Yuan, and I. Land. Design of irregular repeat-accumulate coded physical-layer network coding for Gaussian two-way relay channels. *IEEE Trans. on Commun.*, 61(3):897–909, Mar. 2013.

[45] D. To and J. Choi. Convolutional codes in two-way relay networks with physical-layer network coding. *IEEE Trans. Wireless Commun.*, 9(9):2724–2729, Sep. 2010.

[46] U. Bhat and T. M. Duman. Decoding strategies at the relay with physical-layer network coding. *IEEE Trans. on Wireless Commun.*, 11(12):4503–4513, Dec. 2012.

[47] Q. Yang and S. C. Liew. Asynchronous convolutional-coded physical-layer network coding. *IEEE Trans. on Wireless Commun.*, 14(3):1380–1395, Mar. 2015.

[48] D. Wübben. Joint channel decoding and physical-layer network coding in two-way QPSK relay systems by a generalized sum-product algorithm. In *Proc. 7th ISWCS*, pages 576–580, Sep. 2010.

[49] L. Yang, T. Yang, J. Yuan, and J. An. Achieving the near-capacity of two-way relay channels with modulation-coded physical-layer network coding. *IEEE Trans. on Wireless Commun.*, 14(9):5225–5239, Sep. 2015.

[50] B. Rankov and A. Wittneben. Achievable rate regions for the two-way relay channel. In *Proc. IEEE Int. Symposium on Inf. Theory*, pages 1668–1672, 2006.

[51] T.J. Oechtering, C. Schnurr, I. Bjelakovic, and H. Boche. Broadcast capacity region of two-phase bidirectional relaying. *IEEE Trans. Inf. Theory*, 54(1):454–458, Jan. 2008.

[52] W. Nam, S.-Y. Chung, and Y. H. Lee. Capacity of the Gaussian two-way relay channel to within 1/2 bit. *IEEE Trans. Inf. Theory*, 56(11):5488–5494, Nov. 2010.

[53] L. Lu, L. You, and S. C. Liew. Network-coded multiple access. *IEEE Trans. Mobile Comput.*, 13(12):2853–2869, Dec. 2014.

[54] B. Nazer and M. Gastpar. Reliable physical layer network coding. *Proc. IEEE*, 99(3):438–460, Mar. 2011.

[55] S. Zhang, S.-C. Liew, and P. P. Lam. On the synchronization of physical-layer network coding. In *Proc. IEEE Inf. Theory Workshop*, pages 404–408, 2006.

[56] L. Lu, T. Wang, S. C. Liew, and S. Zhang. Implementation of physical-layer network coding. *Physical Commun.*, 6:74–87, Jun. 2013.

[57] S. Katti, H. Rahul, W. Hu, D. Katabi, M. Medard, and J. Crowcroft. XORs in the air: Practical wireless network coding. *IEEE/ACM Trans. Netw.*, 16(3):497–510, Jun. 2008.

[58] P. Pahlevani, H. Khamfroush, D. E. Lucani, M. V. Pedersen, and F. HP Fitzek. Network coding for hop-by-hop communication enhancement in multi-hop networks. *Computer Networks*, pages 138–149, 2016.

[59] J. Zhang, Y. Chen, and I. Marsic. MAC-layer proactive mixing for network coding in multi-hop wireless networks. *Computer Networks*, 54(2):196–207, 2010.

[60] B. Guo, H. Li, C. Zhou, and Y. Cheng. Analysis of general network coding conditions and design of a free-ride-oriented routing metric. *IEEE Trans. Veh. Technol.*, 60(4):1714–1727, Feb. 2011.

[61] M. Alvandi, M. Mehmet-Ali, and J. F. Hayes. Delay optimization and cross-layer design in multihop wireless networks with network coding and successive interference cancelation. *IEEE J. Select. Areas Commun.*, 33(2):295–308, Feb. 2015.

[62] Z. Ning, Q. Song, and Y. Yu. A novel scheduling algorithm for physical-layer network coding under markov model in wireless multi-hop network. *Comput Electr. Eng.*, 39(6):1625–1636, Aug. 2013.

[63] J. He and S. C. Liew. Building blocks of physical-layer network coding. *IEEE Trans. Wireless Commun.*, 14(5):2711–2728, May 2015.

[64] G. Wang, W. Xiang, J. Yuan, and T. Huang. Outage analysis of non-regenerative analog network coding for two-way multi-hop networks. *IEEE Commun. Lett.*, 15(6):662–664, Jun. 2011.

[65] G. Wang, W. Xiang, and J. Yuan. Multihop compute-and-forward for generalised two-way relay channels. *IEEE Trans. Emerging Telecommun. Technol.*, 26(3):448–460, Mar. 2015.

[66] G. Wang, W. Xiang, and J. Yuan. Generalized wireless network coding schemes for multihop two-way relay channels. *IEEE Trans. Wireless Commun.*, 13(9):5132–5147, Sep. 2014.

[67] H. Zhang, L. Zheng, and L. Cai. HePNC: Design of physical layer network coding with heterogeneous modulations. In *Proc. IEEE Globecom*, pages 2684–2689, 2014.

[68] H. Zhang, L. Zheng, and L. Cai. Design and analysis of heterogeneous physical layer network coding. *IEEE Trans. on Wireless Commun.*, 15(4):2484–2497, Apr. 2016.

[69] H. Zhang, L. Zheng, and L. Cai. PiPNC: Piggybacking physical layer network coding for multihop wireless networks. In *Proc. IEEE ICC*, pages 6211–6216, 2015.

[70] R. Ahlswede, N. Cai, S.-Y. R. Li, and R. W. Yeung. Network information flow. *IEEE Trans. Inf. Theory*, 46(4):1204–1216, Jul. 2000.

[71] S.-Y. R. Li, R. W. Yeung, and N. Cai. Linear network coding. *IEEE Trans. Inf. Theory*, 49(2):1204–1216, Feb. 2003.

[72] B. Nazer and M. Gastpar. Computing over multiple-access channels with connections to wireless network coding. In *2006 IEEE International Symposium on Information Theory*, pages 1354–1358, Jul. 2006.

[73] Y. Wu, P. A Chou, S.-Y. Kung, et al. Information exchange in wireless networks with network coding and physical-layer broadcast. Technical report, MSR-TR-2004, 2005.

[74] C. Fragouli, J.-Y. Le Boudec, and J. Widmer. Network coding: an instant primer. *ACM SIGCOMM Computer Communication Review*, 36(1):63–68, 2006.

[75] T. Koike-Akino, P. Popovski, and V. Tarokh. Denoising maps and constellations for wireless network coding in two-way relaying systems. In *Proc. IEEE Globecom*, pages 1–5, 2008.

[76] L. Song, Y. Li, A. Huang, B. Jiao, and A. V. Vasilakos. Differential modulation for bidirectional relaying with analog network coding. *IEEE Trans. Signal Process.*, 58(7):3933–3938, Jul. 2010.

[77] H.-M. Wang, X.-G. Xia, and Q. Yin. A linear analog network coding for asynchronous two-way relay networks. *IEEE Trans. Wireless Commun.*, 9(12):3630–3637, Dec. 2010.

[78] S. Wang, Q. Song, X. Wang, and A. Jamalipour. Rate and power adaptation for analog network coding. *IEEE Trans. Veh. Technol.*, 60(5):2302–2313, Jun. 2011.

[79] Y. Huang, S. Wang, Q. Song, L. Guo, and A. Jamalipour. Synchronous physical-layer network coding: A feasibility study. *IEEE Trans. Wireless Commun.*, 12(8):4048–4057, Aug. 2013.

[80] J. Li, J. Yuan, R. Malaney, M. H. Azmi, and M. Xiao. Network coded LDPC code design for a multi-source relaying system. *IEEE Trans. Wireless Commun.*, 10(5):1538–1551, May 2011.

[81] R. Y. Chang, S.-J. Lin, and W.-H. Chung. Symbol and bit mapping optimization for physical-layer network coding with pulse amplitude modulation. *IEEE Trans. Wireless Commun.*, 12(8):3956–3967, Aug. 2013.

[82] M. Noori and M. Ardakani. On symbol mapping for binary physical-layer network coding with PSK modulation. *IEEE Trans. Wireless Commun.*, 11(1):21–26, Jan. 2012.

[83] S. Wang, Z. Wen, Z. Meng, D. Chen, C. Li, and C. Fan. Coordinated transceiver in MIMO heterogeneous network with physical-layer network coding. In *Proc. IEEE PIMRC*, pages 83–88, 2013.

[84] B. Li, G. Wang, P. H. J. Chong, H. Yang, Y. Guan, and X. Sha. Performance of physical-layer network coding in asymmetric two-way relay channels. *Communications, China*, 10(10):65–73, Oct. 2013.

[85] T. Koike-Akino, P. Popovski, and V. Tarokh. Adaptive modulation and network coding with optimized precoding in two-way relaying. In *Proc. 2009 IEEE Globecom*, pages 1–6.

[86] Z. Chen, H. Liu, and W. Wang. A novel decoding-and-forward scheme with joint modulation for two-way relay channel. *IEEE Commun. Lett.*, 14(12):1149–1151, Dec. 2010.

[87] Z. Chen and H. Liu. Spectrum-efficient coded modulation design for two-way relay channels. *IEEE J. Select. Areas Commun.*, 32(2):251–263, Feb. 2014.

[88] C. Feng, D. Silva, and F. R. Kschischang. An algebraic approach to physical-layer network coding. *IEEE Trans. Inf. Theory*, 59(11):7576–7596, Nov. 2013.

[89] B. Hern and K. Narayanan. Multilevel coding schemes for computeand-forward. In *Proc. IEEE ISIT*, pages 1713–1717, 2011.

[90] T. Yang and I. B. Collings. On the optimal design and performance of linear physical-layer network coding for fading two-way relay channels. *IEEE Trans. Wireless Commun.*, 13(2):956–967, Feb. 2014.

[91] L. Shi, S. C. Liew, and L. Lu. On the subtleties of-pam linear physical-layer network coding. *IEEE Trans. Inf. Theory*, 62(5):2520–2544, May 2016.

[92] H. Zhang and L. Cai. HePNC: a cross-layer design for MIMO networks with asymmetric two-way relay channel. In *Proc. IEEE Globecom*, pages 1–6, 2015.

[93] J. He, P. Cheng, L. Shi, J. Chen, and Y. Sun. Time synchronization in wsns: A maximum-value-based consensus approach. *IEEE Trans. Autom. Control*, 59(3):660–675, Mar. 2014.

[94] J. W. Craig. A new, simple and exact result for calculating the probability of error for two-dimensional signal constellations. In *Proc. IEEE MILCOM*, pages 571–575, 1991.

[95] X. Wang and L. Cai. Proportional fair scheduling in hierarchical modulation aided wireless networks. *IEEE Trans. Wireless Commun.*, 12(4):1584–1593, Apr. 2013.

[96] Z. Yang, L. Cai, Y. Luo, and J. Pan. Topology-aware modulation and error-correction coding for cooperative networks. *IEEE J. Select. Areas Commun.*, 30(2):379–387, Feb. 2012.

[97] Z. Yang, Y. Luo, and L. Cai. Network modulation: A new dimension to enhance wireless network performance. In *Proc. IEEE INFOCOM*, pages 2786–2794, 2011.

[98] Z. Chen, H. Liu, and W. Wang. On the optimization of decode-and-forward schemes for two-way asymmetric relaying. In *Proc. IEEE ICC*, pages 1–5, 2011.

[99] S. Ten Brink and G. Kramer. Design of repeat-accumulate codes for iterative detection and decoding. *IEEE Trans. Signal Process.*, 51(11):2764–2772, Nov. 2003.

[100] D. Divsalar, H. Jin, and R. J. McEliece. Coding theorems for "turbo-like" codes. In *Proc. of the annual Allerton Conference on Communication control and Computing*, pages 201–210, 1998.

[101] F. R. Kschischang, B. J. Frey, and H.-A. Loeliger. Factor graphs and the sum-product algorithm. *IEEE Trans. Inf. Theory*, 47(2):498–519, Feb. 2001.

[102] B. Nazer and M. Gastpar. Computation over multiple-access channels. *IEEE Trans. Inf. Theory*, 53(10):3498–3516, Oct. 2007.

[103] L. Cai, S. Xiang, Y. Luo, and J. Pan. Scalable modulation for video transmission in wireless networks. *IEEE Trans. Veh. Technol.*, 60(9):4314–4323, Nov. 2011.

[104] J. M. Park, S.-L. Kim, and J. Choi. Hierarchically modulated network coding for asymmetric two-way relay systems. *IEEE Trans. Veh. Technol.*, 59(5):2179–2184, Jun. 2010.

[105] A.Y.-C. Peng, S. Yousefi, and I.-M. Kim. On error analysis and distributed phase steering for wireless network coding over fading channels. *IEEE Trans. Wireless Commun.*, 8(11):5639–5649, Nov. 2009.

[106] J. Qiao, L. X. Cai, X. S. Shen, and J. W. Mark. Enabling multi-hop concurrent transmissions in 60 GHz wireless personal area networks. *IEEE Trans. Wireless Commun.*, 10(11):3824–3833, Nov. 2011.

[107] L. X. Cai, L. Cai, X. Shen, J. W. Mark, and Q. Zhang. MAC protocol design and optimization for multi-hop ultra-wideband networks. *IEEE Trans. Wireless Commun.*, 8(8):4056–4065, Aug. 2009.

[108] M. Park, I. Choi, and I. Lee. Exact BER analysis of physical layer network coding for two-way relay channels. In *Proc. IEEE VTC Spring*, pages 1–5, 2011.

[109] A. Goldsmith. *Wireless Communications*. Cambridge University Press, 2005.